THE ANALYSIS OF BIOLOGICAL MATERIALS USING PROTON INDUCED X-RAY EMISSION ANALYSIS

by

OBAIDUR REHMAN KHAN

This thesis is submitted in fulfilment of the requirements for the degree of Master of Philosophy in the Faculty of Science.

Department of Physics,
The University of Aston in Birmingham.

February, 1979.

Analysis of Biological Materials using Proton Induced X-Ray Emission Analysis

Obaidur Rehman Khan

Submitted 1979 for the degree of M.Phil.

ABSTRACT

Proton induced x-ray emission analysis (PIXE) has developed as a useful analytical technique during the last decade. It has provided a successful tool in qualitative and quantitative analysis of trace elements. It is now widely used in various fields to find the unknown constituents and their amount in a sample. Investigation of the quantitative detection of the elements in the biological material is an area of interest, particularly due to the presence of dietary essentials and non-essentials, including toxic elements in body fluids and tissues.

Study of materials of biomedical origin have been reported extensively by this technique. A method of target preparation for biological specimens has been developed and investigated in the present work. The limits of reproducibility and homogeneity of the targets have been examined. A thin target mounting system has been designed to study the reproducibility for metallic foils and biological targets. Doped target deposits of standard material Bovine liver (SRM-1577) issued by the National Bureau of Standards (N.B.S.) have been used to compare the concentration of internal standard, with the amount of trace elements present in the material.

Trace elements in a bio-environmental material "SALAJEET" from Northern Pakistan have been identified and discussed. Other biological materials such as pasteurised milk, human whole blood, sheep's liver and kidney, have also been studied.

The quantitative measurements made for the standard material (NBS-1577), bovine liver, have been compared with the measurements of other workers, and agree well. This justifies the technique for the target preparation and the use of target rotary system.

KEYWORDS

Proton induced x-rays - biological materials.

ACKNOWLEDGEMENTS

I acknowledge the assistance and encouragement of my supervisor, Dr. D. Crumpton. I am very thankful to him, particularly for his long patience and helpful supervision during the work. I am grateful to Dr. P.E. Francois and to Professor S.E. Hunt for their support.

I have received experimental assistance both from the Department of Physics and the Birmingham Radiation Centre. I am indebted to Mr. F. Lane and Mr. G. Wright of the Physics Workshop for their suggestions for the design and the construction of the target mounting system. Many thanks to Mr. A. Hopkins, Mr. F. Khan, Mr. T. Kennedy, Mr. J. Phull and Mr. K. Mahmood for their assistance and moral support at the Department. I should like to thank Dr. L.G. Earwaker, Mr. R. Bassett, Mr. I.O. Mottram and all the dynamitron operators for providing experimental facilities at the Radiation Centre.

I am grateful to Mr. R. House for his time and effort given to the photographic work. I also thank Mrs. P.D. Edmonds and Mrs. J. Weedon, who typed this thesis.

Financial support was provided partially by M.E.T. (Muslim Educational Trust, London) and the fee was awarded by the British Council during this work. Finally, I would like to thank my father, Mohammed Ramzan Khan, my mother, Bashiran Begum, for their long patience, sacrifices and moral support during the whole period of my studyship.

TABLE OF CONTENTS

LIST OF FIGURES

LIST OF FIGURES (continued)

LIST OF FIGURES (continued)

* Photographic plates

LIST OF TABLES

CHAPTER ONE

INTRODUCTION

The identification of unknown constituents of matter and the determination of their quantities are widely utilized in natural sciences. Therefore they are studied by the application of a variety of techniques. Neutron activation analysis (Curl 68), x-ray fluorescence analysis (CooJ 73,GouF 73, LubM 72), flame emission spectrometry (Daw B 71), atomic absorption analysis (MarG 71, KeiM 76) and chargedparticle induced x-ray analysis (FolF 74, DecG 75) have been used for many years. Proton induced x-ray emission (PIXE) analysis is one of several methods utilizing x-ray emission by charged particles and photons to determine the unidentified elements and trace impurities which are generally known as x-ray fluorescence methods. An increasing number of experimentalists are using this technique since early 1970's with the development of solid state detectors, i.e. Si (Li) and Ge (Li) and the signal processing system (MusR 73, LanD 72, MugA 72 and CamJ 72).

In the case of chargedparticle bombardment on a sample material or target, the predominant interaction is the collision of chargedparticle (WolR 73) with the orbital electronsof the atom of the target sample. If an electron from an inner shell is removed (MerZ 57) and a vacancy is created, an electron from a higher energy shell may fill the vacancy, resulting in the emission of x-ray with the energy associated with the change in binding energy of the transition electron. For example, in the case of K_{α} x-rays, a vacancy is created in the K-shell which is filled by an electron from the L-shell. The emitted x-rays are

called characteristic x-rays. Each element emits its own characteristic x-rays under irradiation. These x-rays allow for the identification of each element in a target, because atoms of each element have unique energy levels. The detector, either silicon or germanium crystal which is lithium drifted, measures the intensity of x-rays by sending the number of its disturbances (signal) to the amplifier where each signal is measured as a current pulse such that the magnitude of the pulse depends upon the energy of x-rays. Each pulse is amplified further and finally processed and presented as a voltage pulse to an analyser.

In this way, the identification of the energies of x-rays forms the basis of the qualitative analysis and measurement of the number of the detected x-rays (intensity) is the basis of quantitative analysis. The identification of the energy of the characteristic x-rays depends on the detector's ability to resolve two signals due to the x-rays of very small energy difference.

PIXE analysis can be used to detect all elements (multielemental) except those of low atomic number. The exact limit for the light elements detection depends on the apparatus and the experimental arrangements. X-ray energies of low atomic number elements are mainly absorbed by the detector's window and the intervening air path between the detector and target chamber.

Concentrations of element, down to sub part per million, may be determined for the elements between the atomic number 15 to 50 (CooJ 73) using PIXE analysis. The detection limits can be improved with a suitable combination of proton energy and the target matrix.

J.L. Duggan et al (DugJ 72) have tabulated the limits of the detectable amounts by several analytical methods as shown in Figure 1.1, and have given the lowest sensitivity for PIXE analysis as being two orders of magnitude better than neutron activation analysis. T.B. Johansson et al (JohT 70), J.A. Cooper (CooJ 73), H. Rudolph et al (RudH 72), B.K. Barnes et al (BarB 74) and R.L. Watson et al (WatR 71) have also compared the capabilities of x-ray fluorescence methods using target metallic foils, biological and clinical samples. The excitation source in most cases was protons.

Many other factors affect the detection limits of a particular source. R.M. Wheeler (WheR 73), F. Folkmann (FolF 75A,B) and F. Folkmann et al (FolF 74A,B) have studied several aspects of detection system, theory and implication of analysis and the effects of related photon emission by the secondary electrons and the source particle (production of background radiation or bremsstrahlung) to the main phenomena of x-ray emission respectively. A recent comparison of detection limits and suitability between photons and protons as excitation sources by F.S. Goulding et al (GouF 77) using 5 mg/cm^2 thick biological specimens shows preference to the proton beam as an exciting source in x-ray fluorescence. Similarly, R.D. Vis et al (VisR 77) preferred proton beam for serum analysis by comparing the sensitivities of the analysis using proton, deuteron and α-particles. F. Folkmann et al (FolF 74B) calculated the x-ray emission cross section induced by proton, alpha and oxygen ion and compared the

Fig. 1.1.

Trace Element Analysis and its limit for various methods

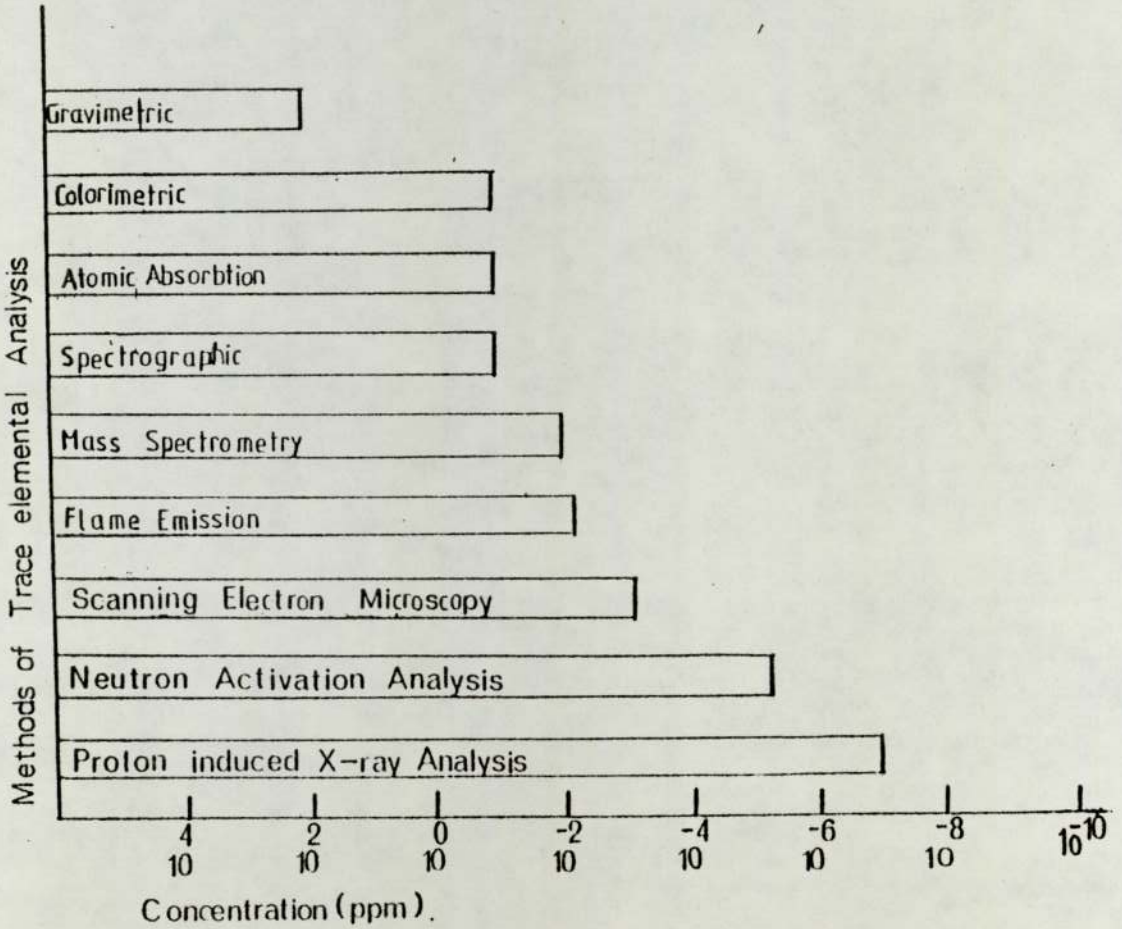

concentrations detected for trace elements of atomic number $Z > 25 < 100$ using a carbon matrix as shown in figure 2.4. He concluded that there is no advantage in using heavier ions other than protons as an excitation source. D.M. Pool et al (PooD 68) studied the peak to background ratios of x-rays on aluminium and copper with 2, 2.5 MeV proton and 20keV electron beams and observed ten times higher values of the ratios on both the targets for protons. Furthermore, detailed information is available for production and ionisation cross sections for various elements in case of protons as an excitation source. This information, coupled with easily available proton source in many laboratories, enables one to use PIXE as a rapid and efficient tool for elemental analysis.

Several applications of PIXE have appeared in the literature (VolV 73, DecG 75, CahT 72) where the results of many workers have been reported in different areas. Its application in Biology and Environmental Studies (WalR 74, BauR76, BowH 74, DemG 74, SchP 72, HasI 77, BarB 74, WatR 74, WalR 77, ManN 77, BonM 75, NieK 76), Chemistry (ThoJ 56) and Medicine (OngP 73, WatR 74, RinH 77, FolF 74B) have justified the use of this technique. The use of thin target in which a very small fraction of proton energy is absorbed is common in PIXE nowadays (DecG 75). The advantage of thin target analysis is uniform generation of x-ray yield throughout the target because the x-ray production cross section remains nearly constant, a high peak to background ratio and negligible absorption of characteristic x-rays (FolF 74A).

Thick targets in which the protons of a given energy

lose their energy completely, have been criticized due to inhomogeneities within the target and the yield correction factors (WilR 77) which must be employed for quantitative analysis. F. Folkmann (FolF 75) compared the concentration sensitivities of thick and thin targets of aluminium and carbon. He found an identical peak to background ratio for the thin targets for the trace elements of high atomic numbers ($Z > 35$) and slightly lower for $Z < 35$. Since the standard thick and thin targets are not available particularly of biological nature, the standard materials (NBS and IBS) are used to make such targets for system calibration (WilR 77, CamJ 77).

Many techniques for biological target preparation, particularly thin target preparation, have been published and reported in x-ray fluorescence and atomic absorption analysis (UmbC 73, BeaR 74, HidK 74, JolR 71, ValV 73, RudH 72, SanH 71, MurL, UndT 71, HerA 73, WatR 71, FloR 72, GorB 72, KliJ 72, HasI 77, ValV 74, WilR 77, CamJ 77) and their merits and shortcomings compared with several other techniques including PIXE analysis.

Several methods to prepare thin biological targets are reported in electron microscopy (StrA 69), atomic absorption spectrometry (MurL, WebJ 73, ChuF 74) and x-ray fluorescence analysis (WalR 74, HidK 74, JolR 71, LivH, ValV 73). R.K. Jolly (JolR 71) summarised a number of methods for preparing a uniform thin target from biological and environmental materials. He measured grain size (10 to 20 microns) of homogenised fish sprayed on a glass slide with a nebulizer. N.F. Mangelson et al (ManN 77) and I. Hasselmann et al (HasI 77) have described sample preparation procedure for biological

materials (female pima indian autopsy sample and rat liver respectively) and then compared the sensitivities using PIXE analysis. I. Hasselmann et al (HasI 77) homogenised the target material (rat liver) many times using centrifugal separator for large grains to rehomogenise them. He achieved the target samples of 40 μg to 170 μg by weight.

Since thin targets of biological nature are fragile and non self supportive, backing materials of low atomic number and of high mechanical strength are usually suitable for thin deposits. A.W. Herman et al (HerA 73) studied different backing materials using chargedparticles to select the most suitable target backing for biological materials. He found formvar a very low background carrier material but it does not withstand the destructive effect of the beam. Many commercial organic backing materials, viz Kapton, Mylar, Formvar and Nuclepore filters although have some disadvantages of fragility, weakness and instability, but they are preferred due to their low contribution to the background radiation.

R. Walter et al (WalR 74), V. Valkovic et al (ValV 74), H. Kaji et al (KajH 77) have also studied the background radiation with protons and preferred the use of organic backing materials. N.F. Mangelson (ManN 77) has summarised and tabulated the characteristics of various inorganic backing foils such as carbon, aluminium and organic carrier materials mentioned above, using PIXE analysis.

Several experiments were carried out for thin target deposits on various foils in the present work. A nuclepore

filter of 8 μm porosity was found suitable for deposits of biological materials. Target specimens were first homogenised and then digested using deionised water and a digestive solution of tetra n-butyl ammonium hydroxide $(CH_3(CH_2)_3)_4.N.OH$ in tolune/methanol of 0.1 N (normality) from BDH. The use of a similar basic agent for wet ashing, i.e. tetra methyl ammonium hydroxide (TMAH) has been reported by N.F. Mangelson (ManN 77) and L. Murthy (MurL). Spectroscopic pure aluminium foils were also used to carry thin biological films in this work. Prepared targets were doped internally with a standard solution to justify the sample preparation method investigated in this study. The thickness of the prepared biological target deposits was calculated gravimetrically and the deposits of 1 mg/cm^2 to 3 mg/cm^2 thickness were achieved.

Since the facility for thin target analysis was not available at the target chamber provided at the end of the proton beam line to the Dynamitron installed at Radiation Centre, Birmingham, a study (HerA 73, FelE 72, HasI 77, ValV 74, RydG 75, SteH 67, KhaJ 64) of thin target chambers was done. A thin target rotating assembly was designed, which extended the mechanism of the existing target chamber and provides the remote control of either thick or thin targets. It is constructed of stainless steel and can be changed over to the thick target holding system easily. In case of thin target measurements, the protons are collected on a specially designed Faraday cup behind the target. An aluminium cam, its base, target frames, target rotary system and a vertical support to the system were made at Physics Workshop of the University of Aston in Birmingham.

The reproducibility and the reliability of the target rotary system was examined by irradiating metallic foils with protons in the energy range of 2.4 - 2.8 MeV. The reproducibility checks on the metallic foils proved the reliability of the designed target system.

Target preparation technique was very time consuming, but the quantitative analysis of such targets was simple and easy. The capabilities of PIXE analysis were demonstrated using the prepared doped and undoped thin and semi-thick targets of biological materials, such as sheep's liver and kidney, milk and human whole blood. A standard biological material, bovine liver (NBS - SRM 1577) and a bioenvironmental sample known as Salajeet from Northern Pakistan was also analysed. A few identified trace elements are discussed briefly indicating their dietary and clinical significances.

Quantitative analysis of the standard biological material justifies the measurements made on the dopant at different concentration in various targets mentioned. The relative measurements of $K\alpha$ x-ray for Fe and several other major trace elements in the standard material show reproduceable results within 14%. Experimental values found for most of the major trace elements agree with the NBS values.

The present work has demonstrated the capability of PIXE technique in the analysis of materials available in small quantities and therefore can be used for biological specimens taken at biopsy.

CHAPTER TWO

PHENOMENA OF CHARGED PARTICLE INDUCED X-RAY ANALYSIS

2.1. INTRODUCTION

A heavy charged particle loses its energy in passing through matter by means of collision and radiation processes. It emits electromagnetic radiation (photons) in the form of continuous "white" radiation called bremsstrahlung (braking radiation) generated mainly by deceleration of incident particles due to the coulomb interactions with the atomic nuclei of the target material. In addition, there are other processes which contribute to the continuous spectrum originating from the knocked-on-electrons.

A "characteristic" spectrum of discrete lines or peaks in the spectrum may also be generated due to the inner shell ionisation and subsequent electronic transition between the energy levels which are governed by the selection rules.

The inner shell vacancy which is created due to the removal of an electron is quickly filled (in $< 10^{-15}$ sec) by an electron from a less tightly bound shell with the simultaneous emission of a photon (characteristic x-ray) of energy equal to the difference between the initial and final states of the transit electron. Thus a vacancy is created in higher shell and the process is repeated again for this shell. This leads to a cascade of electronic transitions with the emission of characteristic x-rays and the creation of vacancies in the higher shell, until finally a free electron is captured by the ionised atom into the outermost orbit.

A vacancy may also be filled through a non-radiative

transition and the excess energy dissipates through the ejection of an electron from a higher shell of the same atom with a kinetic energy equal to the energy difference between the energy of photon and the binding energy of the electron. This process is called Auger effect and may take place due to the subsequent loss of emitted x-ray photon from K-shell, producing an Auger electron and so creating a vacancy in L-shell. The Auger electron may create vacancies in higher energy shells, if sufficiently energetic, otherwise it escapes.

Since the energy of an emitted characteristic x-ray depends on the binding energies of shells, the x-rays emitted are characteristic of the bombarded atom, and the identification of x-ray energies forms the basis of elemental analysis. A particular x-ray line or a peak in a PIXE spectrum indicates the presence of its associated element in the target material and the intensity or the number of x-rays measures the amount or the quantity of that element. The lower level of trace elemental detection for an unknown specimen or material depends on the experimental approach and many other factors such as the intensity of x-rays, their production cross section and the generation of background radiations.

2.2. PHENOMENA OF X-RAY EMISSION

2.2.1. Structure of an atom

An atom is composed of a central positive nucleus surrounded by moving electrons in well defined shells. These orbital electrons are bound in their respective orbits due to an interactive force with the positive charge at the nucleus. The motion of an electron in hydrogen and hydrogen-like atoms can be described quantum mechanically by the Schrodinger equation:

$$\nabla^2\psi + \frac{2m}{\hbar^2}(E-V)\psi = 0 \qquad (2.1.)$$

where m is the mass, E is the total energy and V is the potential energy of the electron $\hbar = h/2\pi$, when h is the Plank's constant and ψ is the electronic wave function. The state of each electron in the atom is determined by the quantum numbers represented by the letters n, l, m (WhiA 34) based on respectively the total, angular and magnetic discrete values which can be written as follows:

$n = 1, 2, 3$ ----------	total or principal quantum number
$l = 0, 1, 2,$ ----------	n - 1 angular quantum number
$m_l = 0, \pm 1, \pm 2$ ----------	$\pm$ (n - 1) magnetic quantum number
$m_s = 1/2, -1/2$	spin quantum number

Each atomic energy level is quantized and has discrete energy according to the well-known expression (WhiA)

$$E_x = -\frac{(me^4z^2)}{8n^2h^2\varepsilon_o^2} \quad \text{Joules} \qquad (2.2)$$

where z is the atomic number, e is the charge of an electron and ε_o is the permitivity of free space.

Therefore the electrons occupy the defined shells or the quantum states confocal to the nucleus. Increasingly these quantum states are labelled with a letter notation (K, L, M, N, O ... etc.) and further divided into (2n - 1) sub-levels according to the values of n, l and m_s as shown in the table 2.1. J is the spin orbital quantum number, such that $J = l + m_s$.

TABLE 2.1.

Quantum Number	Shell		Angular momentum	Spin orbital quantum Number	Number of electrons
n = 1	K		l = 0	J = 1/2	2
n = 2	L	L_1	l = 0	J = 1/2	2
		L_{11}	l = 1	J = 1/2	
		L_{111}	l = 1	J = 3/2	6
n = 3	M	M_1	l = 0	J = 1/2	2
		M_{11}	l = 1	J = 1/2	
		M_{111}	l = 1	J = 3/2	6
		M_{1V}	l = 2	J = 3/2	
		M_V	l = 2	J = 5/2	10
n = 4	N	N_1	l = 0	J = 1/2	2
		N_{11}	l = 1	J = 1/2	2

..... and so on.

The electrons in any sub-shell have the same angular quantum number "l". Electrons for which l = 0, 1, 2, 3 ..... are called s, p, d, f electrons which stand for sharp, principal, diffuse and fundamental energy levels respectively. The number of electrons in a shell or a sub-shell is determined by the Pauli exclusion principle, which is stated as "no two electrons in the same atom can have all of their quantum numbers the same".

Applying the Pauli exclusion principle, the number of electrons in a subshell and shell will be respectively $2(2l + 1)$ and $\sum_{l=0}^{n-1} 2(2l + 1) = 2n^2$. The number of electrons in the subshells are also tabulated in the table 2.1.

2.2.2. Electronic transitions and the emission of x-rays

A. X-Ray Fluorescence

The condition for excitation of an atom and x-ray emission consists in the removal of an electron from one of the inner shells or subshells. The removal may be accomplished by the impact of a charged particle or by the absorption of a photon (WolR 73). The created vacancy may be filled by the transition of an electron from one of the neighbouring outer shells with the simultaneous emission of an x-ray of energy $(Ex) = h\nu$ such that

$$h\nu = E_{final} - E_{initial} \qquad (2.3)$$

Using the expression (2.2) in the above equation for n^{th} shell, the energy "Ex" of the x-ray emitted will be:

$$Ex = \frac{m Z^2 e^4}{8 \varepsilon_0^2 h^2} \left(\frac{1}{n^2} - \frac{1}{m^2} \right) \text{ where} \qquad (2.3.A)$$

$m = (n + 1)$ and $n = 1, 2, 3 -$

The following x-ray lines may be detected:-

Considering transitions to n = 1 (K shell) from n = 2 and 3 respectively, two principal x-rays of higher energy will be:-

K_α corresponding to L shell to K shell transitions

K_{β_1} corresponding to M shell to K shell transition.

A weaker contribution may also be seen in higher elements $Z \geqslant 31$

K_{β_2} corresponding to N shell to K shell transitions.

Transitions to the L shell will give rise to a lower energy x-rays and forms the x-ray lines to the L series as shown in the figure 2.1. All these lines have a fine structure because of the small difference in the energy of the sub-shells, i.e. $K\alpha_1$ and $K\alpha_2$ respectively to the transitions from L_{III} and L_{II} sub-shell to n = 1 (K shell). These electronic transitions are governed by the selection rules (CarE 75), which are :-

Δn is arbitrary

$\Delta l = \pm 1$

$\Delta ml = +1, 0, -1$

The transition finally ceases, when the ion captures an electron. Figure 2.1 (DysN73) also shows most of characteristic emission transitions, following the energy levels with the conventional notations such as α, β, γ --- etc. Figure 3.20 A shows a pure element x-ray spectrum indicating MnK_α and K_β x-ray peaks and Figure 3.20 illustrates different elemental peaks in an x-ray spectrum of a target of biological nature. There are two other ways by which the created vacancy may be filled - Auger effect and Coster-Kronig transitions, both of which are non-radiative.

B. Auger Effect

In the characteristic x-ray emission process, if the emitted x-ray possesses sufficient energy to remove an electron of a higher shell of the same atom, then the photon may disappear and electron of energy E_A is emitted, such that $E_A = h\nu - E_B$ where E_B is the binding energy of the electron and $h\nu$ is the energy of the photon. Such an electron is called an Auger electron and is emitted from the L shell or higher shells. It can

Fig. 2.1

Electronic Transitions

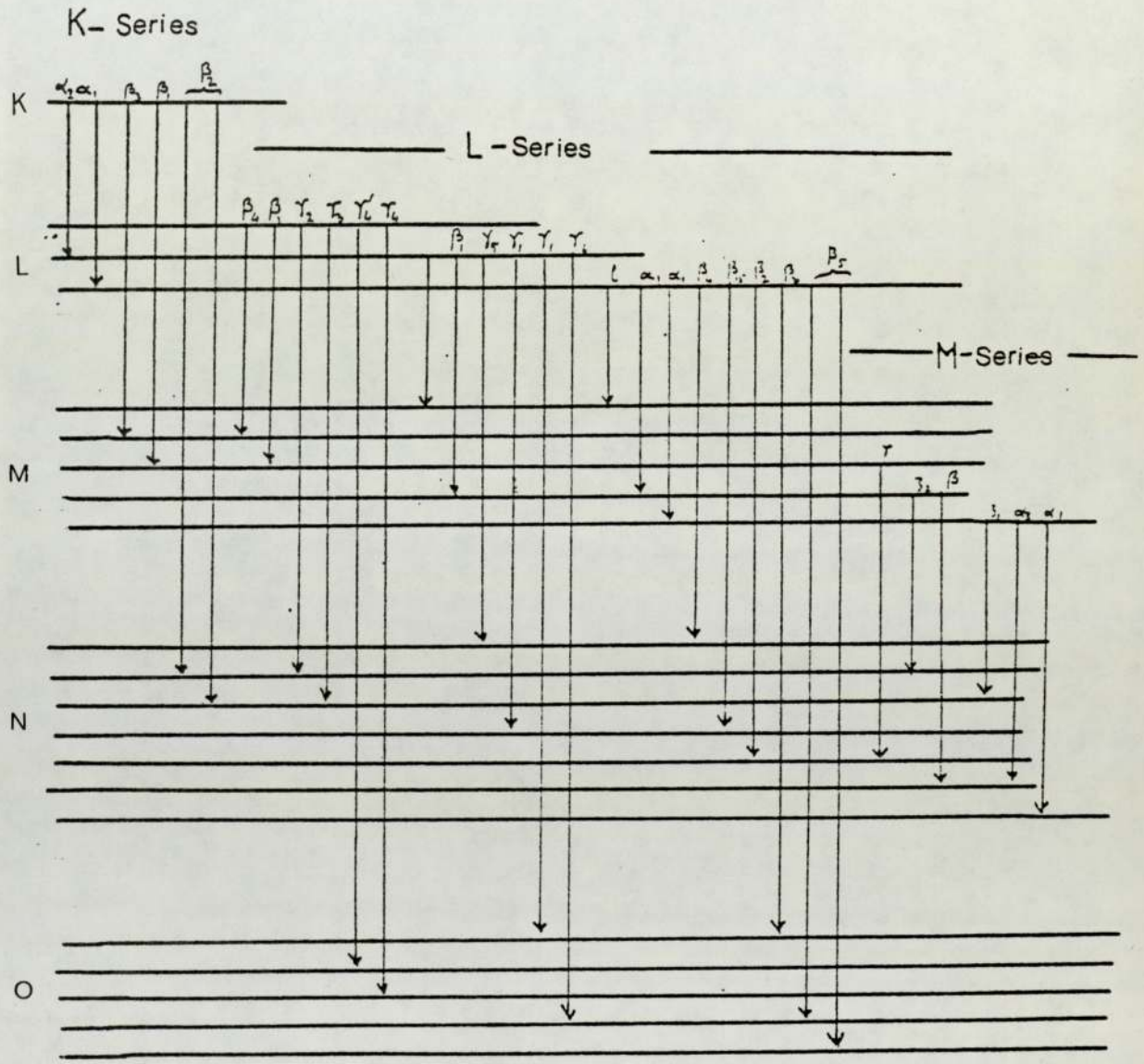

also create further vacancy in the higher levels of the atom provided it has the required energy (WolR 1973) otherwise it dissipates its energy in the atomic lattice.

C. Coster-Kronig transitions

The transitions between the subshells of a shell, which take place due to the difference in their angular momentum quantum number are called Coster-Kronig transitions (BeaR). A vacancy location may shift to a higher subshell before being filled by intershell transition due to such inter subshell transitions.

Due to these effects, the x-ray fluorescence yield is not the same as the vacancy production or ionisation process. The three of the processes compete in filling a vacancy in a given level and are characterized by a term "level width" for an excited state such that " Γ ", the total width, is the sum of the three partial widths (CavE 1975).

$$\Gamma = \Gamma_R + \Gamma_R + \Gamma_C \qquad (2.4)$$

where Γ_R = Radiative width

Γ_A = Auger electron production width

Γ_C = Coster-Kronig production width.

2.2.3. Production of characteristic x-rays and ionisation probability.

The x-ray production probability " σ_{xi} " for i^{th} shell is related to the ionisation probability " σ_i " by the expression:

$$\sigma_{xi} = \sigma_i \times w_i \qquad (2.5)$$

Where w_i is the fluorescence yield for i^{th} shell and σ_i is defined as the probability of a vacancy to be filled in the i^{th} shell through a radiative transition.

It may also be inferred from equation(2.5) that only a part of the created vacancies are filled through the emission of characteristic x-rays and the rest exist as the primary vacancies in the i^{th} shell. Therefore the fluorescence yield for K^{th} shell can be written:

$$\omega_K = I_K / nk \qquad (2.6)$$

where I_K is the total number of characteristic K x-rays emitted from the sample and nk is the total number of primary K shell vacancies.

If the initial ionisation in the L_I, L_{II} and L_{III} subshells are n_{L_1}, $n_{L_{11}}$ and $n_{L_{111}}$ respectively, then the x-ray fluorescence yield from the subshells will be given by:

$$\omega_1 = (I_1 / nL_I)$$

$$\omega_2 = (I_{11} / (nL_{11} + f_{12} nL_1)) \qquad (2.6\ A)$$

$$\omega_3 = (I_{111} / (nL_{111} + f_{23} nL_{11} + (f_{13} + f_{12} f_{23}) nL_1))$$

where fij is the probability of a Coster-Kronig transition between two subshells (i and j) and I_1, I_{II} and I_{III} are the total x-ray yields from those subshells.

Data values, both theoretical and experimental for fluorescence yield and Coster-Kronig yields, have been given by Bambyneck (BamW 72).

2.3. ORIGIN OF BACKGROUND RADIATION (BREMSSTRAHLUNG)

2.3.1. Indirect process of background radiation

A charged particle of mass M and energy E transforms a part of its energy to the atomic electrons of mass m during its collision with the target atom. The electrons are removed from the loosely bound outer shells of the atom and cause bremsstrahlung spectrum. Thus the charged particle loses its energy into the target material. The bremsstrahlung spectrum is generated due to the coulomb interactions of the electrone with the atomic nuclei. The maximum energy "E_s" that can be transferred to a free electron by the incident particle is

$$E_s = (4\ m\ M/\ (M + m)^2).Ep \qquad (2.7)$$

In case of protons of 2.5 MeV energy,

$$E_s \backsim \frac{4Mm}{M^2} \cdot Ep = \frac{4}{1836} \times 2.5 \times 10^3 = 5.4 \text{ keV}.$$

The secondary electrons travel a very small distance compared to the distance covered by the incident particle generating bremsstrahlung before they lose their energy completely. This process is known as indirect process of bremsstrahlung production and has its end point of energy around $E_s = \frac{4\ m}{M}\ Ep$.

Therefore the production of background radiation (bremsstrahlung) is much higher in the energy region $E_x < E_s$ of the characteristic x-rays than in the energy region where $E_x > E_s$.

The proton may collide occasionally with more tightly bound inner shell electrons, giving rise to an additional secondary component of bremsstrahlung above the end point energy. But this

factor is very small, therefore bremsstrahlung spectrum is very much more intense at low energies $< E_s$ as shown in the figure 2.2 (FolF 1974). The effective cross-section for the production of bremsstrahlung of energy interval between E_e and $E_e + dE_e$ is given by Folkman et al.

$$\frac{d\sigma_b}{dE}(E_\gamma) = \int_{E_\gamma}^{\infty} g(Ee, E_\gamma)\,\sigma_e(E_e)\,dE_e \qquad (2.8)$$

where $\sigma_e(E_e)$ is the cross section for the production of secondary electrons at E_e energy, such that:

$$\sigma_e(E_e) = \int_{Ee}^{\infty} d\sigma_e/dE_e(E_\delta)\,dE_\delta \qquad (2.8\ A)$$

and

$$g(E_e, E_\gamma) = (1/Sm(E_e)AM)\,\frac{d\sigma_\gamma}{dE_\gamma}(E_e, E_\gamma) \qquad (2.8\ B)$$

The factor $dE\,(1/Sm(E_e)\,AM$ is the number of atoms/unit area, corresponding to the energy loss dE.

Sm = the stopping power (energy.(mass/unit area)$^{-1}$)

A = the mass number of target atom

M = the mass number of incident particle

$\frac{d\sigma_\gamma}{dE_\gamma}(E_e, E_\gamma)$ is the bremsstrahlung cross section for an electron of energy E_e.

The integrated cross section of photon production $\sigma_b(E_\gamma)$ from integral equation (2.8) was calculated using the binary encounter approximation by F. Folkman et al (FolF 1974) in two steps. First, they calculated the probability of the production of secondary electrons of energy E_δ in the range of E_e and $E_e + dE_e$ and then the photon production cross section in the energy interval between E_γ and $E_\gamma + dE_\gamma$ due to the secondary electron of

Fig. 2.2

Background radiation

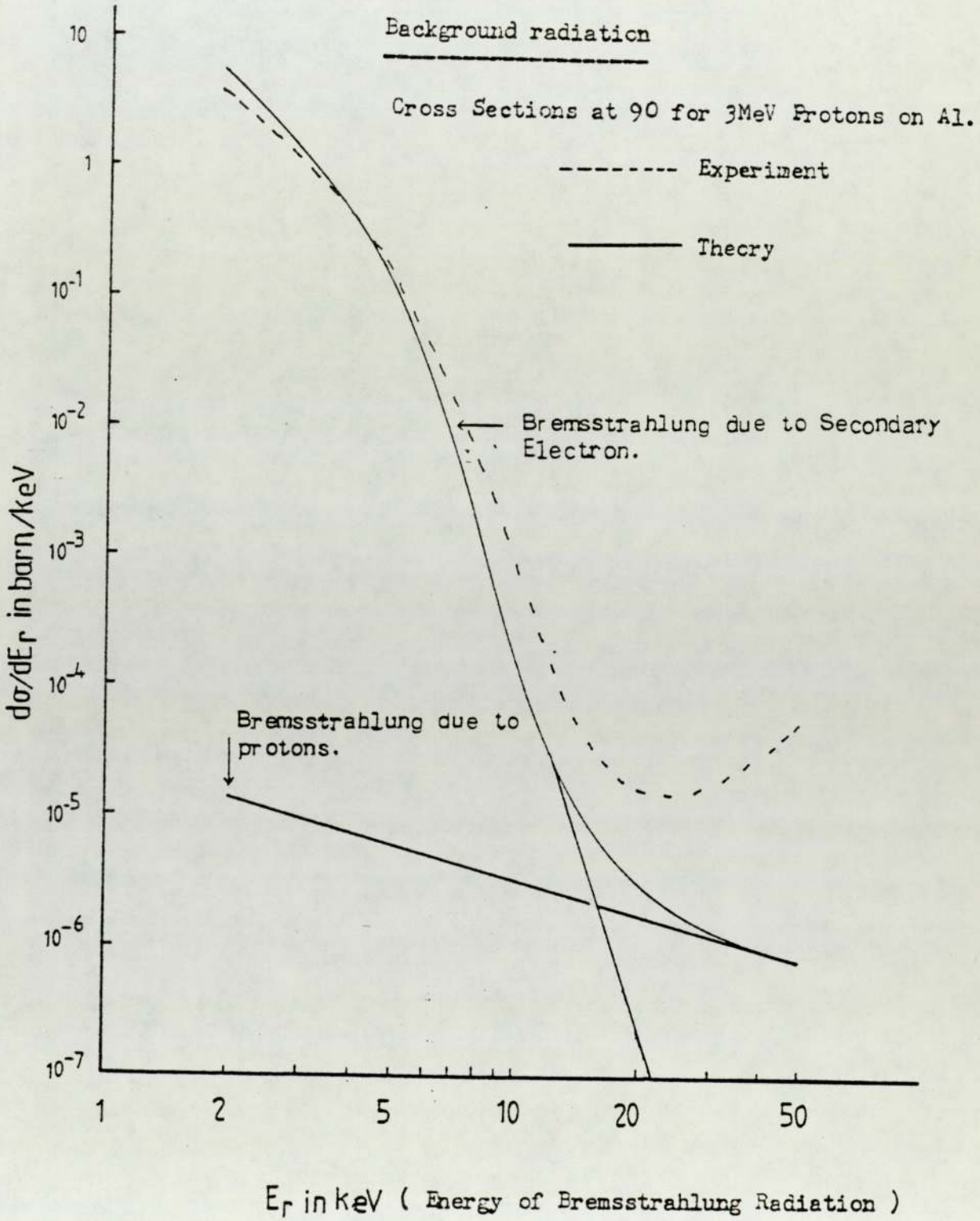

energy E_δ . They found that σ_b is proportional to E_p^4 and decreases as E_γ^{-8} (KhaM 76 B) where E_p is the energy of the incident charged particle.

The continuous spectrum also includes the contribution due to the direct bremsstrahlung generated through the interaction of incident particle with the bombarded nuclei.

2.3.2. Bremsstrahlung due to the incident particle (direct production of background radiation)

Production of the second type of background radiation is due to the projectile directly and its intensity is almost flat at the lower end of the energy spectrum. It is generated through the direct close collision of the projectiles (Zp, Ap, Ep) and the target nucleus (Z, A). The production cross section for such background radiation is given by Alder et al (AldK 56).

$$(d\sigma_\gamma^B/dE_\gamma) = C\frac{ApZpZ^2}{EpE_\gamma}\,(Zp/Ap - Z/A) \qquad (2.9)$$

where (Zp, Ap, Ep) are the atomic number, mass number and energy of the projectile respectively. (Z, A) are the atomic number and the atomic mass of the collided atom respectively. E_γ is the energy of the electromagnetic radiation produced and C is a constant.

The cross section in equation (2.9) is a slowly varying function of Ep and E_γ and depends upon the target projectile combination. The term (Zp/Ap - Z/A) in equation (2.9) is an important factor, because of Zp/Ap which is $\lesssim 1$ for protons. Therefore bremsstrahlung production depends on the term Z/A. In case of non-self supportive thin targets, a selection of carrier foils of $Z/A \lesssim 1$ is useful to diminish the background generated

by protons. And an optimum peak-to-background ratio can be achieved.

The comparison of cross section for direct bremsstrahlung production with the probability of indirect process versus their energies is shown in figure 2.2. It shows that the contribution for the production of high energy photons is negligible in case of indirect production of bremsstrahlung. The contribution to background radiation at high energies is due mainly to the direct process of proton bremsstrahlung.

Folkman et al (FolF 1974) found experimentally that the distribution of the background radiations is isotropic. Contrarily H. Kaji et al (KajH 1977) observed the angular dependence of the production of bremsstrahlung. He found a low ($\sim$ 89 %) production of bremsstrahlung at 135^{o} for the x-rays of 5.5 to 6 keV energy. The incident proton beam was 3.5 MeV and Mylar and aluminium foils were used as backing materials.

2.4. Charged Particle interaction with matter and energy loss

A charged particle loses its energy in passing through matter mainly by interacting with the atomic electrons, experiencing the coulomb force. The particle collides with many atoms through its passage until it is slowed down from its initial energy to zero. This process is regarded as elastic, because a very small amount of work is required to excite or remove the electron by the projectile. In general, the projectile loses its energy by collision and radiation process.

Energy loss by collision includes inelastic collisions with both electron and nuclei and nuclear reactions. Energy loss through radiation includes the process of projectile and nucleus coulomb interacting force and Cherenkov radiative energy losses. Cherenkov radiation loss becomes possible when the velocity of the incident particles exceeds the phase velocity of light in the medium of their passage (BerC).

Energy loss through collision is the principal channel of the loss of energy at the energies of interest. Production of the secondary electrons is the main process during collision, whereas the production of direct or primary bremsstrahlung is the main process in radiative loss.

The basic formula for the energy loss per unit distance "dE/dx" is the Bethe Block formula based on quantum mechanics (83).

$$-dE/dx = (Zp^2 e^4 / 4\pi m v^2 \varepsilon_o^2) \cdot N\bar{Z} \log \frac{2mv^2}{I} \quad (\text{joules/m}) \qquad (2.10)$$

where v and Zp are respectively the velocity and atomic number of the incident particle. Z, N and I respectively are the atomic number, number of atoms/m^3 and ionisation potential

of the target material. m and e are respectively the mass and charge of electron and ε_o is the permitivity of free space. The ionisation potential "I" is related to the atome number through the relation:

$$I = k Z \qquad (2.11)$$

where $k = 11.5$ eV.

"I" is deduced usually from experimental results. For relativitic incident particles, expression (10) is extended as follows:

$$-dT/dx = (Zp^2 e^4 / 4\pi m v^2 \varepsilon_o^2).NZ \left(\log \frac{2mv^2}{I} - \log(I-\beta^2) - \beta^2\right) \quad \text{(joules/m)} \qquad (2.12)$$

where $\beta = v/c$ and c being the velocity of light.

The term $\log \left(\frac{2m v^2}{I}\right)$ is negative, in case when $\frac{2m v^2}{I} < 1$ or $\frac{4m}{MI} Ep < 1$ where Ep and M respectively are the energy and mass of the incident particle.

Therefore formula (2.10) cannot be used for $Ep < 450$ I. Also $(\log \frac{4m}{MI} Ep)$ is a slow varying function of "Ep". Therefore, a non-relativistic energy loss for a known media can be written to a good approximation, using formula (2.10), as:

$$-dE/dx \propto Z^2/v^2$$

The factors of the recombination effect on the average charge of the incident particle and the adiabatic effect on the electron are not taken into account in the derivation of Bethe and Block formula (LivM 1937) when the velocity of incident particle is less than the velocity of bound electrons. Thus it cannot be

used successfully at low energies below 0.2 MeV. The corrections for these two effects have been applied by Northcliffe (NorL 60) in the Bethe Block formula and the values were improved over a wide range of energy.

Williamson et al (WilC 67) used a semi-emperical formula for an average charge of the incident particle (Ze) such that

$$Z(E) = Z\tanh(\beta/\alpha Z\sqrt{\pi/2})$$

where α is the fine structure constant

$$= \frac{1}{137.039} \quad \text{and} \quad \beta = v/c$$

They have also corrected Bethe Block formula for the adiabatic effect. Their modified Bethe Block formula makes a reasonable estimate of low energy stopping power and ranges and gives positive values. The departure of calculated values of stopping power and range by Janni et al (JanF 65) from the values calculated by Williamson et al (WilC 67) was studied by M.R. Khan et al (KhaM 77). The difference between the two data sets ranged from $\backsim \pm$ 4% at 1 MeV to $\pm$ 1% at 3 MeV in case of proton as incident particles.

2.5. INNER SHELL IONISATION

2.5.1. Ionisation of atom by charged particle

The excitation of atom by charged particles and heavier ions may be used to ionise the inner shell electrons resulting in the emission of characteristics x-rays. Merzbacker and Lewis (MerZ 57) have employed the expression for maximum energy transfer "E_s" to the unbound electron by the incident particle (Equation 2.7) as a model (approximation) for a classical collision. For protons

$$E_s = \frac{4m}{M} E_p \backsim E_p/450 \qquad (2.13)$$

using expression (2.13) for 2.5 MeV protons, $E_s \simeq$ 5.4 keV and if the proton inner shell collision is considered to be a free collision, then characteristic x-ray production below $E_p = 450\ E_I$ should not occur, E_I being the ionisation energy of the associated shell (or subshell). Taking an example of Iron (Fe)$K\alpha$ x-ray, which are expected to be emitted by the protons of energy above 2.7 MeV, but in practice, they can be excited from very low energy (as low as 140 keV) protons (DugJ 1972), (HanJ 1957). Therefore this model is not valid, even as a first approximation for ionisation process (GerT 33).

The inner shell ionisation process is considered to be as the inelastic collision in which the atom acts as a whole with the incident particle such that its momentum is transferred to the inner shell electrons through the energy levels. The collision is therefore required to be treated in terms of quantum mechanics, with the consideration of two common experimental facts.

1. Intensities for $K\alpha_1$ and $L\alpha_1$ transitions are very high relative to other transitions of the same series (BamW 1972).

2. The interaction probabilities are very large for low atomic numbers and increase rapidly with increasing particle energy (DecG 1975).

Investigations on x-ray production and comparison of the experimental results with the theoretical predictions for ionisation cross section is an important area of interest (KhaM 76, DecG 75, KhaM, LinJ 72) .

Many workers (MerZ 1957), (GarJ 1970), (MesS 1958),

(HanJ 1973) and (BasG 1973) have attempted to formulate an expression to describe inner shell ionisation on the basis of inelastic collision and three basic theoretical methods (CheJ 75) have been developed.

1. P.W.B.A. (Plane Wave Born Approximation)

A quantum mechanical description of the phenomena, in which the projectile is assumed to be a plane wave in its initial and final states.

2. B.E.A. (Binary Encounter Approximation)

This is a classical approach to describe the process including the electronic binding energy consideration. This theoretical picture has been introduced by Garcia (GarJ 70)(GarJ 73).

3. Modified Versions of P.W.B.A. and B.E.A. and emperical formulae

P.W.B.A. and B.E.A. are modified taking account of their discrepancies and empirical formulae are estimated for a wide range of energy of the projectile.

2.5.2. P.W.B.A. Theory

Merzbacher and Lewis(1957) presented a detailed discussion of inelastic atomic collisions in the plane wave Born Approximation. Theoretical values for the ionisation cross section as a function of projectile energy have also been calculated. The inner shell ionisation cross section for K shell is given by the expression

$$\sigma_K \simeq (2^{10}\pi(Ze^2)^2) \cdot E_s^4/45.E_k^6 \qquad (2.14)$$

where E_k is the K shell ionisation energy and Z is target atomic number. For L and M shell, the calculations for ionisation cross section are more complicated due to more electrons

and their angular momenta. Merzbacher and Lewis (MerE 1957) also derived an expression for the ionisation cross section " σ_i " for any shell i, such that

$$\sigma_i = \frac{8\pi Z_p^2 a_o^2}{(Z_{zi})^4 \eta_i} \; f_i\,(\eta_i/\theta_i^2) \qquad (2.15)$$

where Z_p = charge of the incident particle

Z_{zi} = effective charge of the atomic i^{th} shell

θ_i = ($I_i^2/Z_i R_\infty$) called as screening parameter

I_i = ideal ionisation energy in the absence of outer screening for i^{th} shell

i = refers to the radiation emitted

R_∞ = 13.6

η_i = $\frac{mEi}{M Z_i^2 R}$ such that η_i is dimensionless and mainly dependent on the projectile energy for the ionisation of i^{th} shell

E_i = the minimum energy for ionisation of i^{th} shell

f = a factor dependent of the electronic wave function

a_o = Bohr radius of hydrogen

Formula (2.15) may also be used for individual subshells and total ionisation cross section for any shell can be achieved. This formula gives a reasonable agreement of ionisation cross section with the experimental values except at very low energies of incident charge particles for which $E_s \ll E_I$. The reason for this low energy discrepancy is the second order effects, of which the first and the most important is the deflection of the projectile by the nuclear coulomb field.

The second effect is the perturbation of the atomic shell by the projectile (binding effect). These two effects were not taken into account in P.W.B.A. The inaccuracy of non-relativistic method of P.W.B.A. for low energy charged particles was explained, first, by Hansteen et al (HanJ 1957) , who suggested that the inaccuracy in low energy values could be improved by taking consideration of the coulomb deflection between the bombarding particle and the target nucleus.

Several other workers (LeaR 1973), (OgiW 1964), (LinJ 1972) have also mentioned that their values differ from the theoretical predictions of P.W.B.A. Investigations of x-ray production using protons of energy (1 - 3 MeV) for a few elements have been carried out by Khan et al (KhaM 1977) and the results have been compared with P.W.B.A. theory and its correction for binding energy and coulomb deflection (P.W.B.A. B.C. theory). They have used the reduced cross section $\sigma_k / (\sigma_{ok} / \Theta_k)$ against universal variable (η_k / Θ_k^2) for such comparisons, such that σ_k is experimentally derived K-shell ionisation cross section, $\sigma_{ok} = ((Z_1/Z_{2k})^2 8\pi a_o/Z_{2k})$ is the cross section scaling unit, η_k is the ratio of the squares of the incident particle velocity and the mean K-shell electron velocity of the target, and $\Theta_k = 13.6 Z_{2k}^2$ (K-shell binding energy in eV).

2.5.3. B.E.A. Theory

Recently Garcia (GarJ 73) has used a classical two body encounter approximation including a modification to take into account the nuclear repulsion of the projectile. This theory is referred to as the binary encounter approximation (B.E.A.). It gives a reasonable estimate of cross sections in a direct and simple way for many target projectile collisions.

This theory gives the most exact description of the two bodies close collision. The ionisation cross section for any shell or subshell can be derived on the basis of hydrogenic velocity distribution of electrons using the expression (GarJ 1973):

$$\sigma_i = Zp^2/E_i^2 f\cdot(E/Mp \cdot E_i, Mp) \qquad (2.16)$$

where Z_p and M_p are the charge and mass of projectile, E_i is the binding energy of the i^{th} shell or subshell. The product of the cross section and the square of binding energy $(E_i)^2$ is a universal function and a plot of $E_i^2\sigma_i/Zp^2$ versus $E_p/M_p E_i$ yields the same results for all target atoms, like the factors of η and Θ defined in Born approximation (Section 2.5.2.).

R.Lear et al (73) pointed out that B.E.A. values are less than P.W.B.A. values by a factor of approximately ≤ 2 . However, this new model is seen to compare more favourably with the measurement of both high and low energetic protons (LinJ 1972) .

2.5.4. Modifications

In general, slight differences are found between B.E.A. and P.W.B.A. with the binding energy corrections. The modifications of electronic binding energy and nuclear deflection at low energies in P.W.B.A. theory were made by Basbas et al (BasB 1974). They have shown an improvement in P.W.B.A. ionisation cross section values at low energies comparing with the values of scaled experimental cross sections.

Hansen (HanJ 1973) suggested the modifications to B.E.A. to account for the discrepancies which arise by its application for heavy and complex atoms.

Such predicted values of the cross section are lower than the values of B.E.A. theory as shown in the figure 2.3. In general, both of the theories (B.E.A. and P.W.B.A.) fit the experimental data within 10% for proton energies greater than 0.8 MeV (GraT 1973). It is noted that the difference between the two theories is typically 5 - 10% to choose either of the two for the energies above 0.8 MeV.

Messelt (MesS 1958) has compared his results using the experimental quantity $\phi = (Z^4\Theta/3.51)\sigma_k \cdot 10^{16}$ together with the values of other workers with the corresponding values of " ϕ_o " obtained by using the theoretical predictions of Henneberg (HenW 33), who employed non-relativistic Born approximation to calculate the ionisation cross section

$$"\sigma_{th}" = \frac{3.51}{Z^4\Theta} \cdot \phi_o(\eta') \cdot 10^{-16} \text{ cm}^2 \qquad (2.17)$$

where Θ = K shell screening parameter and a ratio of the observed K-shell ionisation energy E_k to the ideal ionisation energy E_k in the absence of outer screening.

$\eta' = \frac{4mEp}{M \cdot I_k}$ a dimensionless, proton energy dependent parameter similar to η in Born approximation,

and $$\phi_o(\eta') = 2/5_e(-4\eta'/1+\eta').(4\eta'/1+\eta')^4\left\{\frac{1}{4} + \frac{1}{12}\left(\frac{4\eta'}{1+\eta'}\right) + \ldots\right\} \qquad (2.17\ A)$$

The comparisons show large discrepancy between the experimental values of the function ϕ and the corresponding values of ϕ_o for heavy elements. Messelt derived an empirical formula and compared the same experimental values in Z dependent

Fig. 2.3

Ionisation Cross Sections

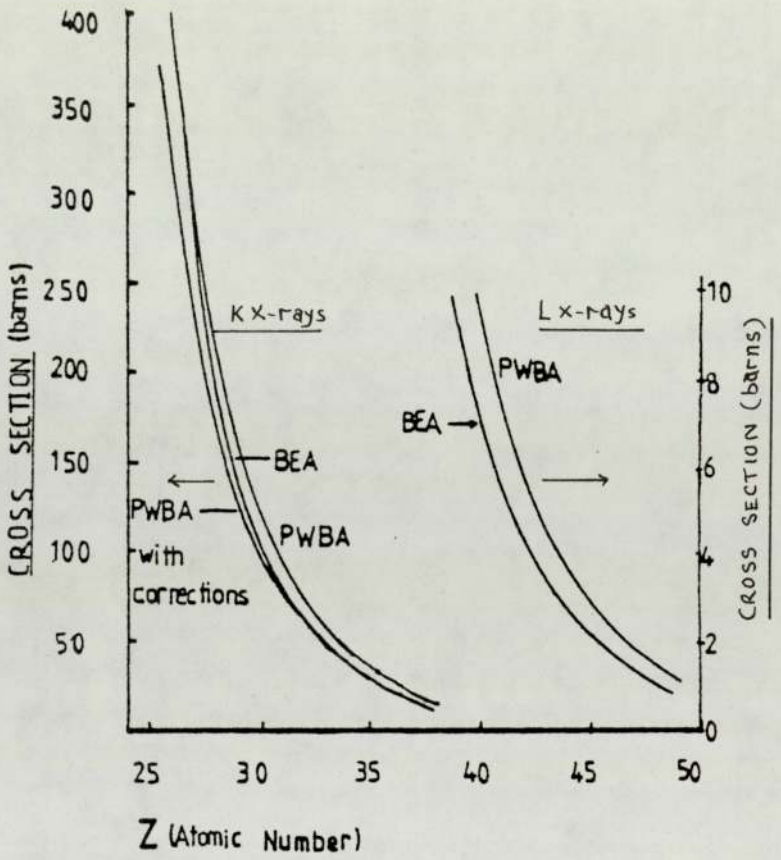

ionisation cross section " $\sigma_k Z^{3/2}$ " with the corresponding values using his own formula:

$$\sigma_K \simeq (\Phi_1(\eta'). 6.1.10^{-21} cm^2)/Z^{3/2} \qquad (2.18)$$

$$\text{where } \Phi_1(\eta') = e^{-Z\eta'/(1+\eta')}.\left(\frac{4\eta'}{1+\eta'}\right)^4.e^{\frac{-0.067}{\eta'}} \qquad (2.18\ A)$$

The comparison shows that all the experimental values are reproduceable for non-relativistic cases. This indicates Z dependence of the formulae, which is less in Messelt's emperical formula.

An emperical expression based on atomic number "Z" and energy of proton has also been derived by M.R. Khan et al (KhaM 77) using their values of excitation functions for several elements at the proton energies between 1 - 3 MeV. This is represented in the following form:

$$\sigma_I(E) = \text{Exp}(b_o(E) + b_1(E) \log Z + b_2(E)(\log Z)^2) \qquad (2.19)$$

where Z is the atomic number and E is the energy of proton. b_o, b_1 and b_2 are the energy dependent coefficients obtained by regression analysis.

This empirical formula is valid within the ranges $1.3 < E < 3$ MeV and $23 < Z < 50$ and the accuracy expected for the formula is reported within 10%.

CHAPTER THREE

INSTRUMENTATION AND PHYSICAL SYSTEM

The PIXE analysis system covers a wide range of equipment. The basic arrangement is shown schematically in figure 3.1 and it will be discussed as follows:

1. The Dynamitron, the generation of proton beam and its characteristics;
2. Target chamber;
3. Proton current measuring system and voltage to frequency converter;
4. X-ray detection system and its characteristics;
5. Data acquisition system;
6. General set-up of the experiment and precautions.

3.1. The Dynamitron

The proton beam, used in this work, was generated by a commercial R.D.I. Dynamitron at the Joint Birmingham Radiation Centre. The Dynamitron is a variable energy high current accelerator which can be operated at voltages up to three million volts. Either continuous or pulsed ion or electron beam can be provided. The pulsed duration and repetition rate of the pulsed beam can be selected over a wide energy range (1 to 3 MeV). The electrons and positive ions (usually protons) can also be used to produce secondary particles (WeaD 74).

Technical details of the Dynamitron

A radio frequency oscillator operating at about 130 kHz is used to feed the power to the two large semi-cylindrical plates inside the pressure vessel. The plates (the dees) are capacitively coupled to the semicircular rings (the corona rings)

Fig. 3.1

Experimental arrangement

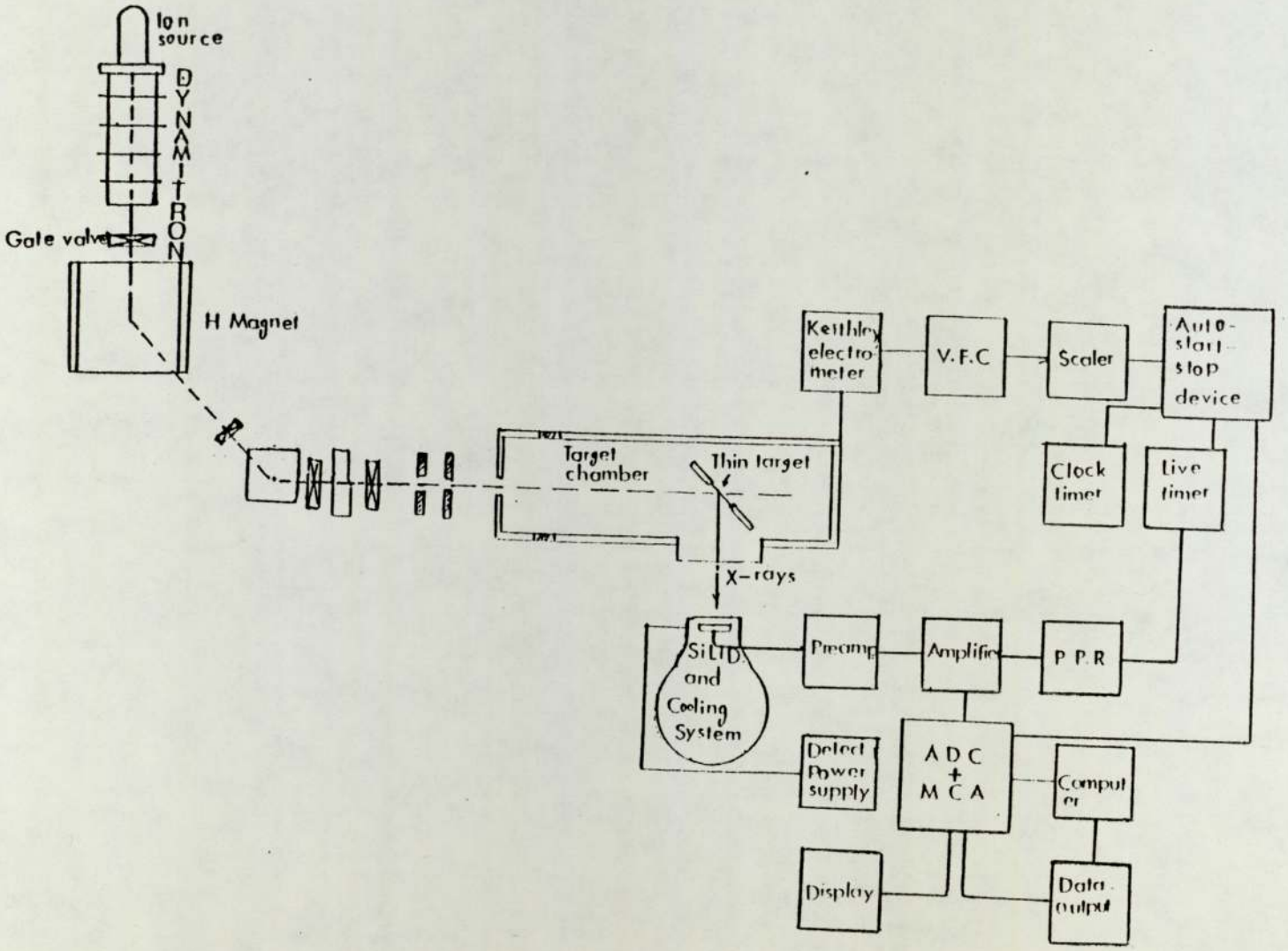

Fig. 3.2. about the acceleration column which are separated by rectifiers forming a chain from the bottom to the top. A D.C. potential is built up at the high voltage terminal by 64 stages of rectification along the vertical column. The rectifiers are required to be placed in reverse in order to change the polarity of the beam.

Ions are produced in a duoplasmatron ion source using hydrogen or deuterium. They are separated with respect to their masses by placing the ion source at an angle to the acceleration column under the influence of a permanent magnet. The selection of the potential to extract the ions (the extraction voltage) determines the mass of ions to be inserted to the acceleration column.

Beam current from a few nano ampere to about 2 mA can be obtained with a beam diameter of about 10 mm at the exit of the machine. The vertical downward accelerated beam could either be used further down in the electron gamma room or could be bent at 45^{o} either into "Aston beam" room or into 'low scatter lower' room by subjecting it to the field of an H-magnet in the magnet room as shown in Figure 3.3. The entire Dynamitron system, including the target chamber, was operated under moderately hard vacuum, usually about (5×10^{-5} to 5×10^{-6} torr).

Characteristics of Dynamitron Beam

A series of resistors of the total value of 10^{10} ohms is used to draw current down to the base from the terminal to stabilize the Dynamitron. The current is monitored by a digital voltmeter across a 500 ohms resistor at the control desk and the beam energy is read indirectly. A maximum ripple of 3 keV FWHM

Fig. 3.2

The Dynamitron

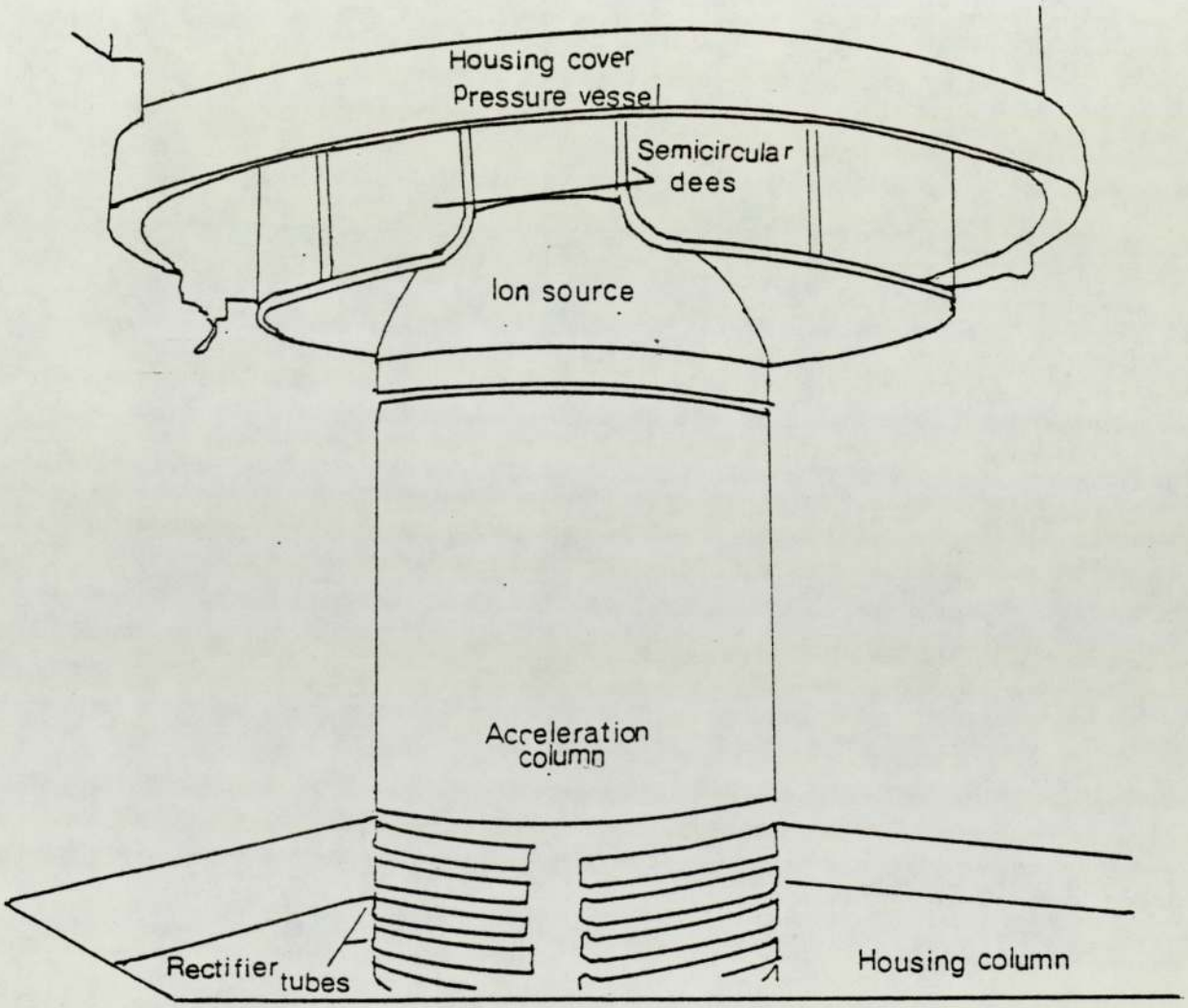

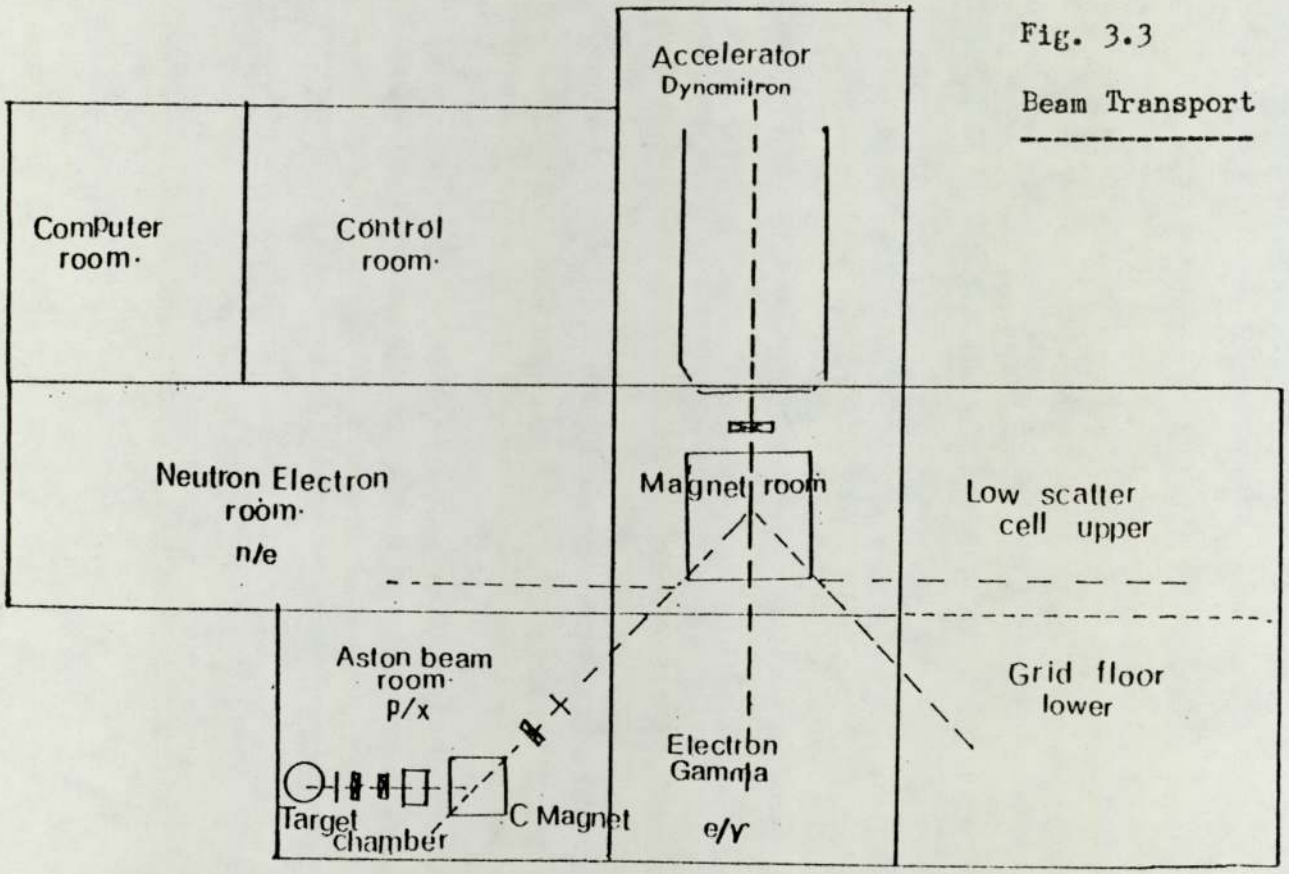

Fig. 3.3

Beam Transport

was reported for proton beam (WeaD 1974) and the drift in energy was claimed to be less than 100 eV for an hour period.

3.2. Target Chamber

The rectangular housing block (14 x 16 x 28) cm^3 target chamber was made up of 10 mm stainless steel plates (Drg. 74). It had a glass plate of half an inch thickness at one end and on one side. The other side plate had a circular window of 50 μm of thickness of melinex material to allow x-rays to reach the detector from the target. The window of the organic material separates the vacuum system from the atmospheric pressure. The chamber was connected with sealed couplings to a four inch diameter beam pipe which had two collimating apertures. The chamber was made electrically isolated from the beam pipe by an insulation ring during later studies. The target chamber housed a rotatable target holder, which could only be used to mount thick targets.

3.2.1. Modifications to the Target Chamber

A thin and semi-thick target rotary assembly consisting of hinged mounting fingers for eight targets, a hanging column (vertical support) with a base to support the cam, which locates the target to the beam, and a Faraday cup, were designed as shown in the figure 3.4. This system was designed to accomplish thin and semi-thick target measurements and will be discussed later.

The target rotary system was mounted on an aluminium motor shaft, which was rotated by an electric motor placed on the top of the chamber. The motor could be operated either by an on/off switch at the head of the chamber or from the experimenter's desk using a target changing and positioning module. Eight

Fig. 3.4

Target Rotary System mounted (Drawing)

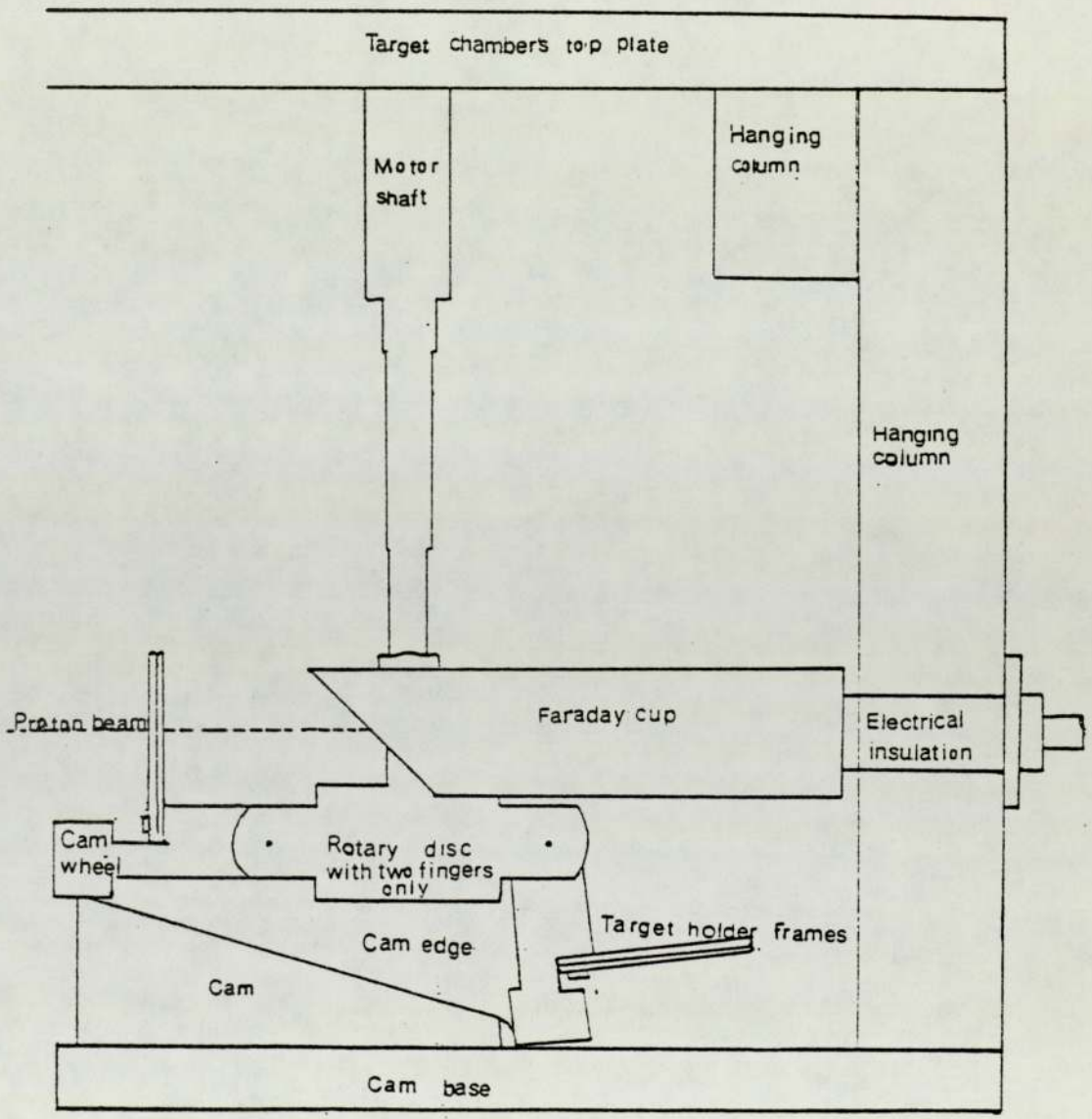

FIGURE 3.5

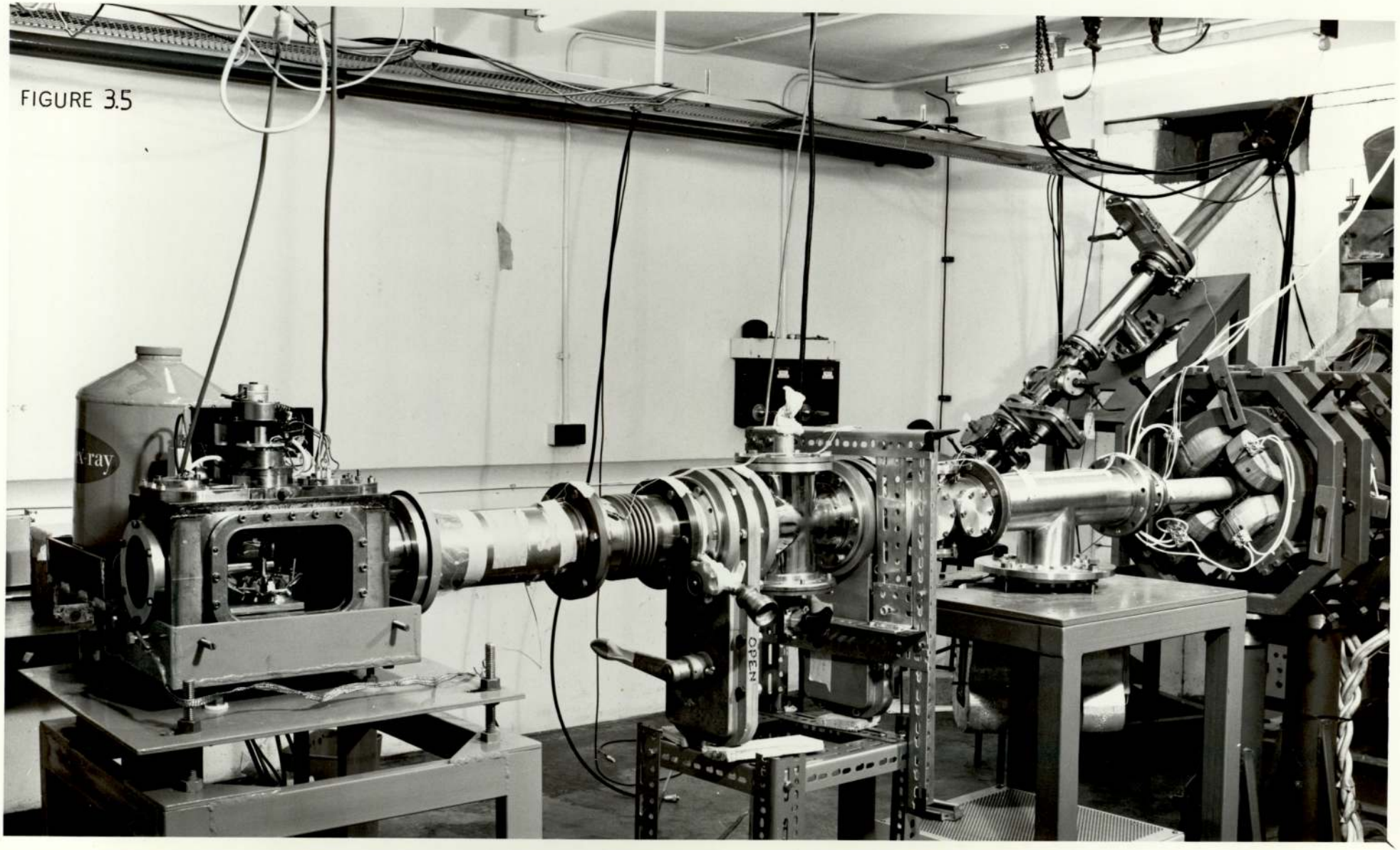

targets, mountable on this system, could be analysed without breaking the vacuum of the chamber.

The target chamber also housed an electron filter and a Faraday cup. A gate valve was used to isolate the target chamber vacuum system from the beam line vacuum, which further could be isolated from the main Dynamitron vacuum using similar gate valve. The target chamber is shown at the end of the beam line at Aston Beam room as shown in Figure 3.5.

3.2.2. The Collimating Apertures

The collimating apertures were two tantalum circular sheets with the circular opening of 1.5 mm and 2 mm diameter respectively.

Fig. 3.6.

The Collimating apertures for proton beam

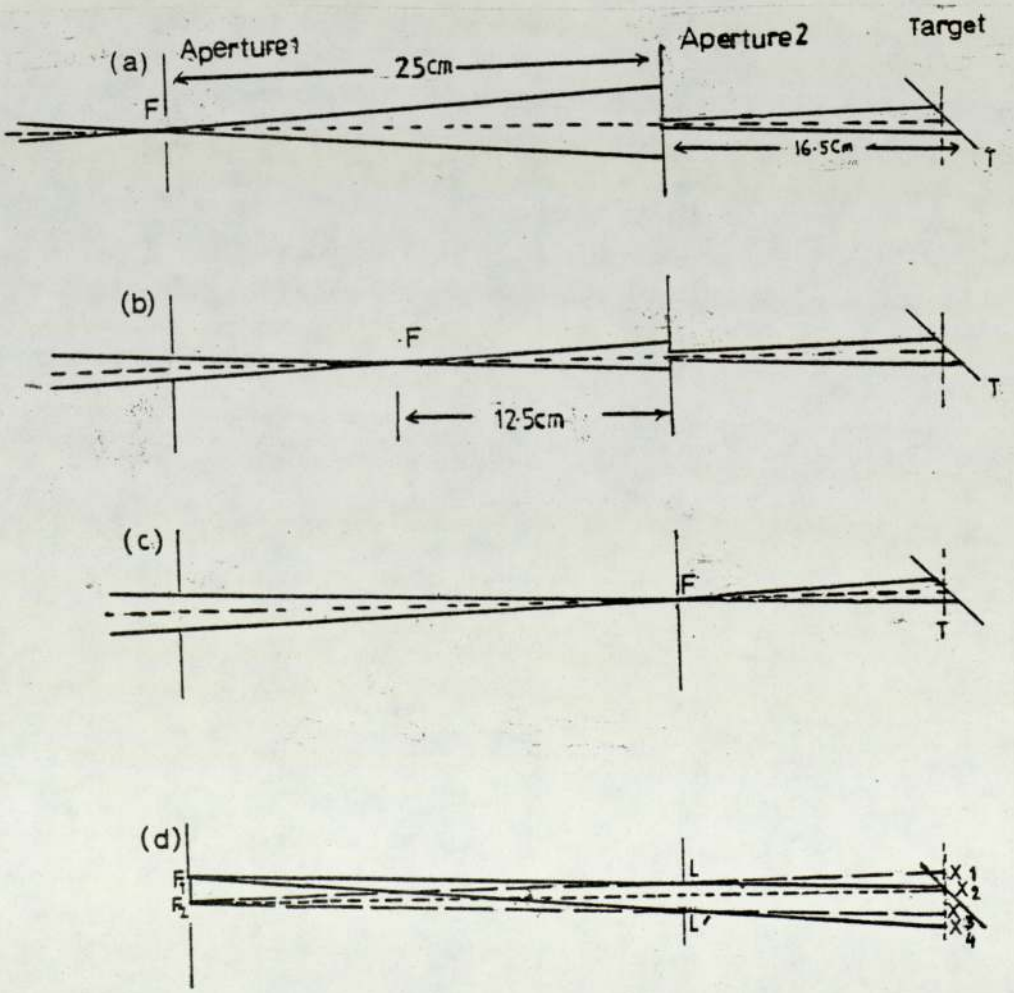

They were placed 25 cms apart in the horizontal beam pipe with the 4 inch diameter support discs having holes provided for the vacuum port. They were designed to ensure the proton beam struck the target in any case of the beam defocusing along its axis. Since the target was positioned to be irradiated at 45^{o}, the beam of the diameter x had an elliptical spot on the target. The scheme for the beam projection is illustrated in the figure 3.6, assuming that the beam is symmetrical along the axis of the beam pipe.

The diameter of the aperture toward the target chamber = 0.15 cm.

The diameter of the aperture toward the beam pipe = 0.2 cm.

Distance between the two apertures = 25 cm.

Distance between the second aperture and the target = 16.5 cm.

From the geometry of the figure 3.6, it is evident:

a) in the case of the beam focussing at the first aperture, the diameter of the beam "x" is $x/41.5 = 0.15/25$ or $x \simeq 0.25$ cm.

b) in the case of the beam focussing at the centre of the two apertures, the diameter of the beam is $x/29 = 0.15/12.5$ or $x \simeq 0.35$ cm.

c) in the case of the beam focussing at the second aperture, the diameter of the beam is $x/16.5 = 0.2/25$ or $x \simeq 0.13$ cm.

d) the beam was also projected on the target in case of any defocussing anywhere along the diameter of the first aperture. Two cases are shown in the figure 3.6.d, where the beam is focussed at two points F_1 and F_2 along the aperture, projecting the beam spot of x_1x_3 and x_2x_4 cm in diameter at the target position.

The diagrams are shown in broken and in complete lines with a shift "y", such that in the two similar triangles F_1F_2L' and $x_3x_4\ L'$:

$$\frac{x_3x_4}{F_1F_2} = \frac{L'x_3}{F_2L'} \quad \text{or } y = \frac{0.1 \times 16.500076}{25.000112}$$

$$= 0.066 \text{ cm}$$

Therefore the beam shift was not more than ±0·66 mm in case of two extreme cases of the beam focusing, i.e. by the opposite edges of the aperture.

The above conditions show that the beam diameters of the apertures and their location provide the proton beam on the target in case of any defocusing of the beam along and vertical to the axis of the apertures, as shown in figure 3.6.a, b, c, d.

3.2.3. Faraday cup

The Faraday cup employed consisted of a cylindrical aluminium tube such that its base was mounted on a horizontal ceramic cylinder, which was connected to the hanging column as shown in the figure 3.4. The tube may be connected electrically to the target chamber. A copper wire covered with ceramic beads was used to connect with the beam current measuring device.

3.3. KEITHLEY ELECTROMETER AND VOLTAGE TO FREQUENCY CONVERTER

3.3.1. Keithley electrometer

The proton current was measured by a Keithley electrometer in the control panel. The Keithley is a high impedance ($10^6\ \Omega$ to $10^{13}\ \Omega$) electrometer and reads a full scale deflection current through a potential difference of 1 volt across its impedance, such that whenever the switch (to select a scale of current) was changed, the input impedance changes and the output voltage corresponds to

the full scale deflection (1 volt) remains constant, i.e. 10^{-6} ampere range has 10^{6} Ω impedance and 10^{-8} ampere has 10^{8} Ω of impedance. The electrometer can measure the current from 0.3 amps to 10^{-13} amps with a claimed accuracy of ± 2% to ± 5% (Keith).

Two modes of feedback can be employed depending upon the conditions of the target cooling system or any leakage of current at target chamber.

3.3.2. Voltage to frequency converter (V.F.C.).

The voltage signal from the Keithley electrometer was fed to a voltage to frequency converter (V.F.C.), which produces a pulse chain of 10^{5} Hz for a 1 volt input. Therefore a proportional frequency to the input voltage could be read in a digital signal in multiples of ten on a five or six decade scaler.

3.3.3. Auto Start/Stop Device

The N.I.M. scaling unit at the experimenter's desk had a special provision for the experimenters to use the scaler timer at the required start/stop or reset positions. All the units were controlled by the scaler timer when inserted in the special slots of the unit.

3.4. X-RAY DETECTION SYSTEM AND ITS CHARACTERISTICS

3.4.1. X-Ray Detectors

The basic requirements of a detector for the present work are high resolution, high sensitivity and compatibility with the processing system.

There are three types of detectors available for x-ray detection - Scintillation detector NaI (Tl), Gas proportional detector (Xe gas) and semiconductor detector, viz germanium and silicon lithium drifted. Since semiconductor detectors have high resolution and particularly Si (Li) detector suits to the energy range $\backsim$ 3 keV to 30 keV of the characteristic x-rays, it was used for the analysis reported herein.

A silicon lithium drifted detector was used in the present work and could be set up at $\backsim$ 7.6 cm from the target, as the nearest distance. The emitted x-rays passed through the melinex window travelling a distance of 6.5 cm in vacuum and few mm in air and struck the Beryllium window of 12.5 μm thick before they reached the detector. The Beryllium window protects the vacuum of the detection system and also helps absorbing the low energy x-rays below 2 keV from the target. The intensity of the low energy x-rays could further be eliminated out of the energy spectrum using an absorber or filter. Calculating for 10% of Fe K_{α} x-ray intensity loss, we used a 12.5 μm thick aluminium absorber before the detector's window. Such a detection system analyses the characteristic x-rays of different energies simultaneously above 3 keV. The details of the system are discussed according to the following points:-

1. Detector and its associated cryogenic sub-system;
2. Preamplifier;
3. The amplifier and the pulse pile-up rejector;
4. Live time measuring system;
5. The performance characteristics of the system.

3.4.2. Detector and its associated cryogenic sub-system

The most important part of any detection system is the detector itself. The basic requirements for a suitable detector are:

1. High resolution;
2. High sensitivity;
3. Simple and easy maintenance;
4. Linear relationship of input and output signals at a given count rate.

A.H.F. Muggleton (MugA 1972) has compared the high performance capabilities of the semiconductor detector with the other type of detectors on the basis of resolution and detection efficiency and found suitable performance characteristics for solid state detector Si (Li). Several other experimenters (LauD 1972), (MugA 1972), (CamJ 1972), (HanJ 1973), (PalJ 1968), (WooR 1971) have also compared the resolutions and efficiencies of silicon and germanium solid state detectors and observed Si (Li) solid state detectors, competitive and advantageous for the detection of x-rays of 4 keV to 30 keV energy. Hansen et al (HanJ 1973) found the resolution of Si (Li) solid state detector as high as twice that of Ge (Li) at 14.4 keV x-ray energy. Although the ionisation potential of germanium is less than that of silicon, the smaller energy

band gap increases the detector noise and consequently decrease the resolution capability, therefore each of the two detectors requires an individual determination of performance characteristics, depending upon its size and shape.

The cryogenic sub-system is the core of the x-ray fluorescence detection system. A Kevex 3201 cryogenic sub-system was used in the present work. It consists of a 3 mm thick lithium drifted silicon detector mounted in contact with the cooled horizontal dipstick with the liquid nitrogen refilling collar (cryostat), a pulse optical feedback preamplifier and the liquid nitrogen dewar. The cryogenic system and the detector head assembly were kept under vacuum surrounded by an outer housing. A thin 12.5 μm beryllium window was used in front of the detector for vacuum seal, and protected by an adjustable Plexiglass cover. Such a detector cryostat assembly is shown in the figure 3.7. A typical high performance detector has an area of 25 mm^2 and a thickness of 3 mm (MugA 1972) . Present measurements were made on a P-type detector crystal of 30.3 square mm^2 area and of a thickness of 3 mm having gold layers of 200 A^o thick on both the sides, acting as the electrical contacts for the applied voltage $\approx$ 2000 V/cm.

A semiconductor detector can be described as an ionisation chamber in which the solid state crystal absorbs the entering x-rays producing free charge carriers (the minimum ionisation potential for silicon atoms is 1.1 eV), i.e. electron-hole pair. The number of electron-hole pairs are proportional to the energy of the x-rays and move under the influence of the high electric field, the collected current determines the amplitude of the signal which is further amplified and shaped to a pulse whose height is

Fig. 3.7

Detector Cryostat Assemly

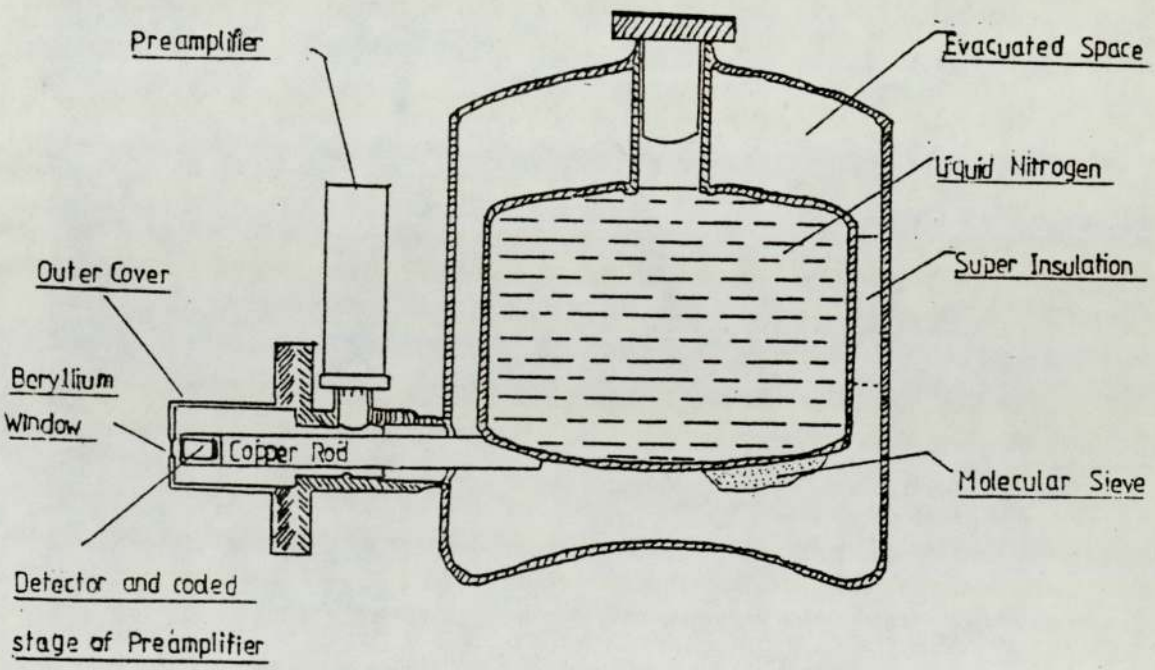

proportional to the energy lost by x-ray. Lithium is drifted, under controlled conditionsthrough the crystal to remove the effects of the impurities present in few parts per billion (MugA 72). An ideal n - i - p diode structure is formed through this compensation of electrically active impurities in the crystal, but the lithium compensation is unstable at the room temperature due to the higher mobility of lithium atoms. Therefore it is necessary to maintain the detector at low temperature. Further, the detector must be cooled at liquid nitrogen temperature to minimise the electrical noise produced by the thermal excited carriers in the crystal material.

The vacuum is maintained in the cryostat using a molecular sieve in contact with the walls of the liquid nitrogen refilling dewar. When the sieve is cooled to liquid nitrogen temperature, it has characteristics to absorb the gas many times its own volume.

Care must be taken in handling and using the detector due to fragility of the beryllium window. A lead aperture of 2 mm diameter was used to define the area of the detector and to eliminate the edge effect near the lateral surface of the sensitive crystal volume. Due to this effect, the charge carriers created near the lateral surface may be carried off through the surface.

3.4.3. Preamplifier

A preamplifier is an integral part of the detector's assembly. The first stage of the preamplifier is a field effect transistor (F.E.T.). It is located by the detector and connected to a heat sink cooled to liquid nitrogen temperature in the evacuated space, as shown in the figure 3.8. The charge signal

from the detector is integrated through the preamplifier which includes a feed back circuit to keep the operating conditions unaffected - figure 3.9. Normally a resistor is connected in parallel with F.E.T. to provide a by-pass, Figure 3.9.a., but it exhibits noise and lengthens the shaping time, resulting in poor resolution and consequently affecting the count rate capabilities. A series of advances has been made over the past years (LanD 1972) to modify the feed back circuits and briefly illustrated in the two circuits, i.e. figures 3.9.b. and 3.9.c. The resistor is replaced by the light coupling from a light emitting diode (L.E.D.) to the photosensitive drain gate F.E.T. junction (figure 3.9.b.). This simple system has a drawback of pulsing at high count rate, which occurs due to the non-linearity of L.E.D. current - light relationship and degrades the detector's performance at higher count rates. A pulsed optical feedback scheme (Fig. 3.9.c.) (LanD 71) is employed to reject all such pulses by feeding a reject wave form from a level sensor to the main amplifier until the system resumes the normal operation. A pulse optical system is a high performance system in terms of low noise and high resolution characteristics, but degrades in count rate performance.

A similar pulsed optical feed back system (Kevex 2002) was used in the present work. The specification of resolution for such an assembly was $\lesssim$ 161 eV for x-rays of 5.9 keV energy. The output was with the negative reset pulses from the Kevex 2002 preamplifier. Its output impedence was 50 Ω , where the input charge conversion was approximately 4.5 mV/10 keV. The collection voltage was applied to the p^+ side of the diode, and the n^+ side was being coupled to the first stage of the preamplifier (Kevex).

Fig. 3.8

X-ray detector Mount

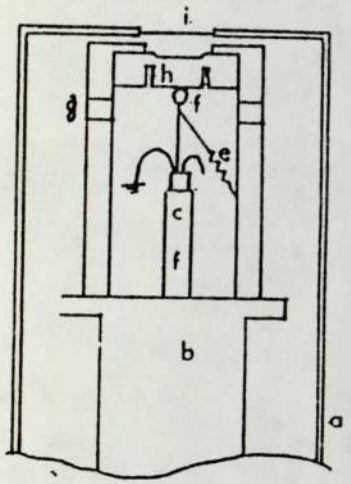

a) Detector housing

b) Copper cold finger

c) Pulse generator

d) F E T

e) Feed back resistor

f) P T F E

g) Aluminium oxide

h) Detector

1) Beryllium window

Fig. 3.9

Pulsed light feedback preamplifier

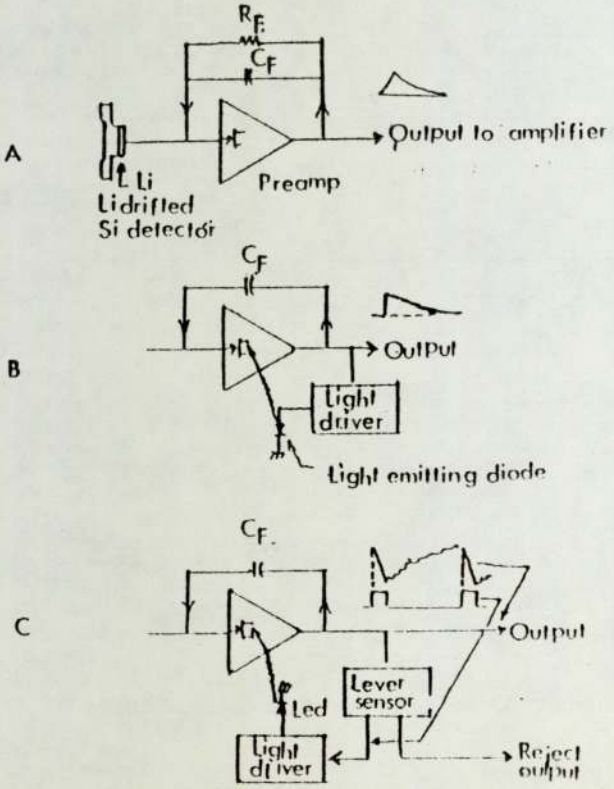

3.4.4. Bias Supply

A Kevex 4600 detector bias supply was used to provide power to the detector and to the amplifier. This NIM sub-system is designed to provide highly stable ripple free high voltage from 0 - 2000 volts in 100 volts increments. A protection circuit is incorporated to disconnect the high voltage supply to the detector in case of low vacuum. A vacuum monitor is incorporated on the front panel to show the pressure such that 1 micron represents 100% full scale deflection and 90% of F.S.D. is $\backsim$ 25 microns and the bias supply cuts off exceeding 20 micron pressure. The manufacturer's specification for temperature stability is $<$ 0.02% per centigrade and line stability is $<$ 0.02%. It has an impedance of 65 mega-ohms and has a ripple and noise level below 100 V r.m.s.

3.4.5. The Amplifier

The analytical performace characteristics, i.e. the high resolution, high sensitivity and accuracy of a detection system are based on the various parameters of its sub-units. Parameters such as pulse shaping, base line stability, noise suppression, pulse pile up rejection, linearity and D.C. restoration are connected with overall amplification of the signal, and the excellent compromise of all the parameters results in the high performance characteristics of the detector.

The output of the preamplifier was coupled to an amplifier system where the pulses are differentiated, shaped and amplified before they are allowed to proceed to the multichannel pulse height analyser (P.H.A.) for recording and manipulation.

A simplified diagram of the amplifier system used in the pulsed optical feed back unit is shown in the figure 3.10. Amplified pulses from the integrators are fed to the base line restorer, which restores the base line of the signal at zero volt. This action is inhibited during the reset action of the pulse in the preamplifier. A fast discriminator (Channel) is provided to check the cases where overlapping of the pulse pile up occurs in the amplifier. In case of no pile up, the pulse is examined for its voltage level (VA) in the pulse shaping channel or slow channel with a selected bias (0 - 10 V) and if its level is exceeded, the signal peak is shaped for longer time. The shaped pulse is then sampled by a linear gate, and a flat topped output signal of 2 μs duration is produced such that its amplitude is proportional to the difference between the selected bias level (VB) and the signal level (VA) (LanD 1972).

Pulse Pile up Rejector

A pulse pile up rejector discards the passage of distorted pulses, i.e. the pulses which lose their original amplitude and shape. Pulse pile up process may occur due to any three of the following reasons (WolR 1973), as illustrated in the figure 3.11.

1. Leading edge pile up

A second pulse might arrive and overlap on to the first pulse which is in half of its processing time (time to attain its maximum amplitude). Such a pile up is called leading edge pulse pile up. In this case, both the pulses are discarded.

Fig. 3.10

Amplifier Unit (Block diagram)

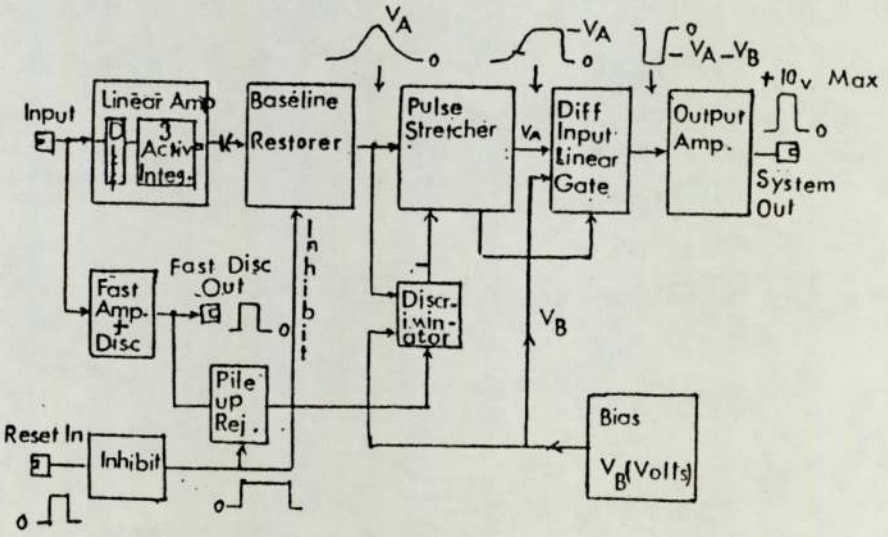

A, 1st pulse

B, 2nd pulse

C, Sum

Fig. 3.11.

Pulse Pile up

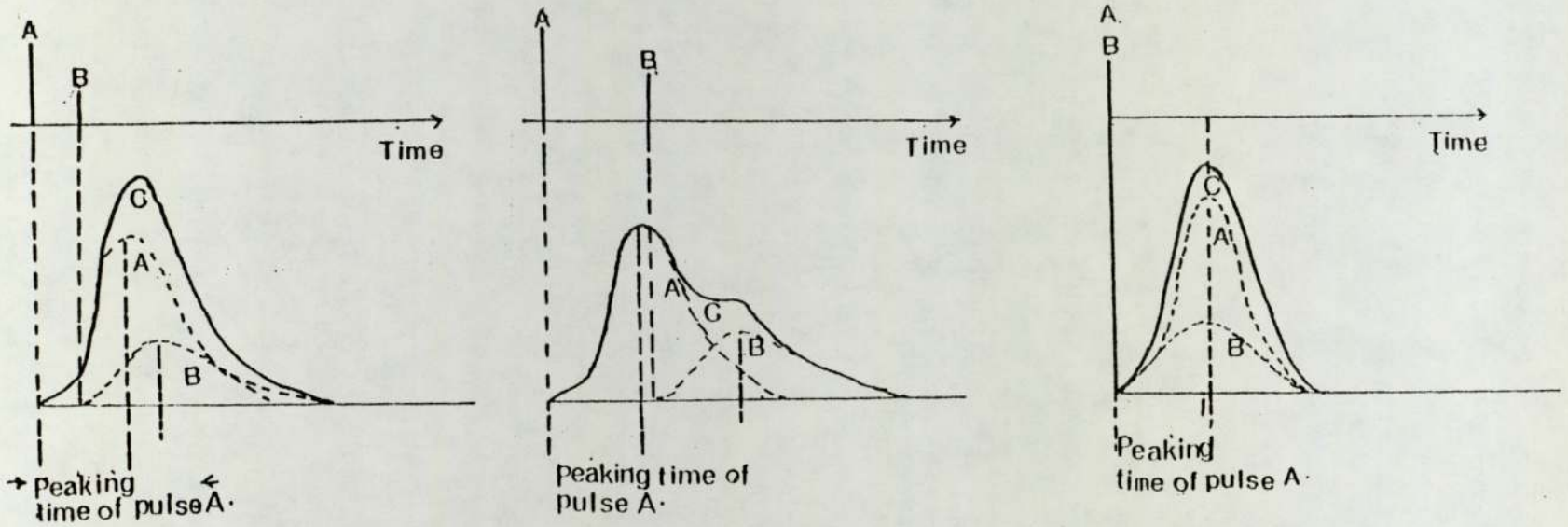

1) Leading edge pileup

2) Trailing edge pileup.

3) Sum pileup

2. Trailing Edge pile up

A second pulse might arrive and overlap on to the first pulse which has already attained its maximum height. Such a pile up is called a trailing edge pulse pile up. The first pulse is retained as it acquired its maximum amplitude before the second pulse, although it loses the shape of the peak.

3. Sum pile up

Two pulses arrive and overlap at the same time and lose their height and shape. They appear somewhere at the energy channel, which locates the sum of the energies of the two pulses in the energy spectrum. Since both of the pulses appear to be one through the pulse pile up rejector, they appear at the high energy end of the spectrum, as shown in the figure 3.12.

Present work was carried out using a Kevex 4500 Px-ray amplifier with a 4590 Kevex pulse pile up rejector. Kevex P x-ray amplifier is a pulse optical feed back type and provides a coarse gain from 1 to 16 in multiples of 2 using a rotary switch. Fine gain is a ten turn control from 1 to 2.2. Post gain facility provides an amplification above base line setting in 1, 2 and 4 units. Gain and base line stabilities are $\pm$ 0.01% per degree centigrade and $\pm$ 200 μV per degree centigrade. The output is direct coupled of maximum + 10 V. Switches for input and output are provided and various time constants are available by changing the circuit card from the amplifier unit. Ten times of the time constant gives the pulse shaping time (pulse width). The pulse optical dead time is adjustable from 50 μs to 500 μ second. It can count 20,000 counts per second of 5.9 keV of

Fig. 3.12
High count rate and pulse pile up

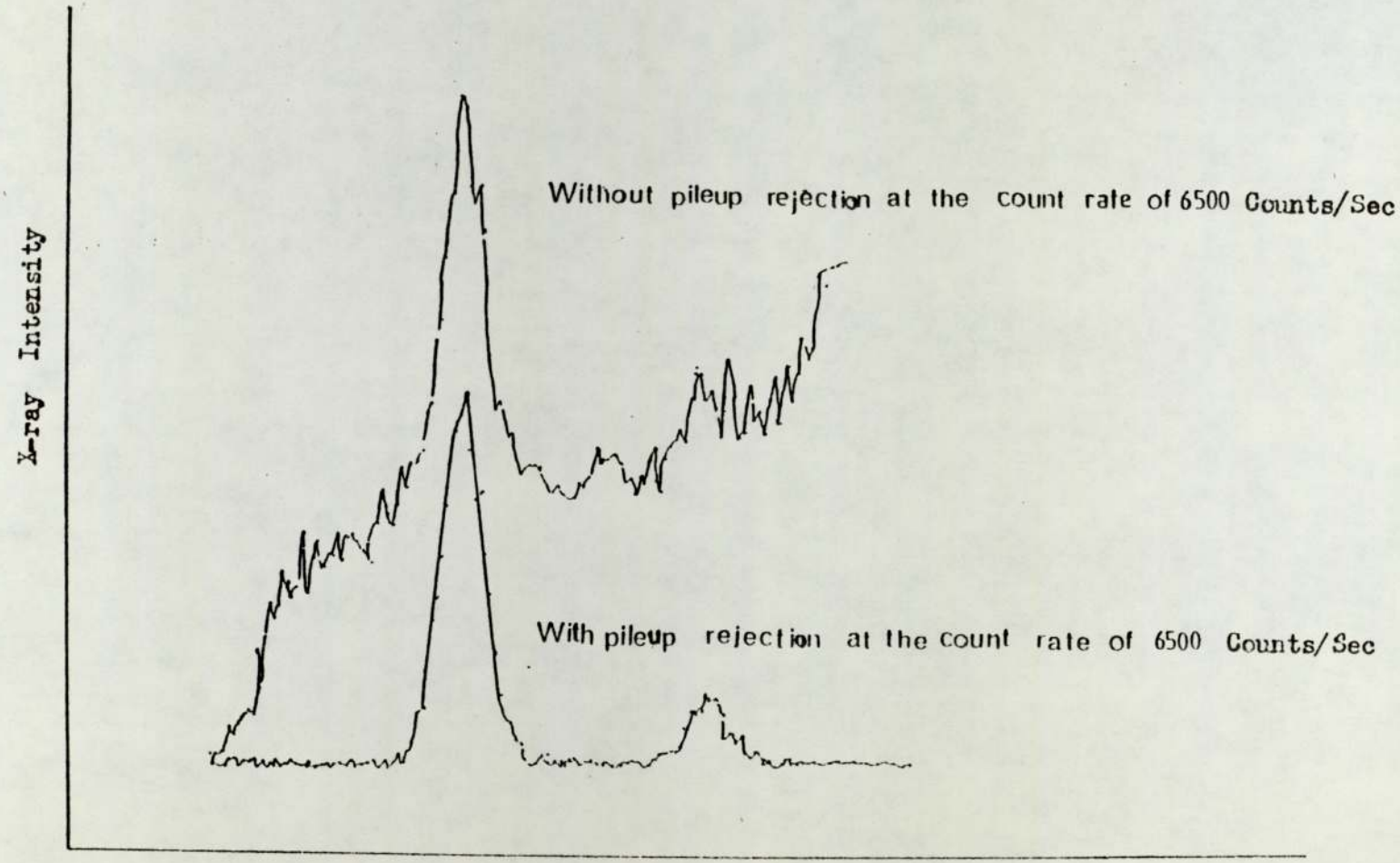

energy. It also provides a busy output for pulse optical reset and pulse shaping time to correct the number of output pulses which are flat topped of 2 μ second duration.

The 4590 Kevex pulse pile up rejector was incorporated in the processing unit, which provides a fast amplifier of 1 μ second pulse pair resolution. The shaping time which is ten times that of shaped pulse can be adjusted through a time constant switch at the front of pulse pile up rejector. An input and output facility in true or complementary logic compatible to transistor transistor logic (T.T.L.) of 0 to 5 volts is also provided. An output of the fast amplifier discriminator channel is located in rear side. Due to the pulse pile up rejection, pulse optical reset time and pulse height analyser (P.H.A.) dead time, the output pulses are less than the input pulses (WolR 1973) and it seems that the system is inoperative for few pulses. The duration of this period is called the dead time and has to be corrected for in quantitative analysis.

3.4.6. The live timer

In order to measure the dead time, a busy signal from the pulse pile up rejection was used to gate a 1 MHz crystal oscillator employed as a clock. The busy signal is + 5 V when the amplifier is inoperative, due to the pulsed optical reset time and the extendable dead time per pulse of the pulse pile up rejection system. The circuit allowed the output of the oscillator signal when the busy signal is 0 volt and it inhibited the output of the oscillator when the busy signal is 5 volt to correct for the dead time. The method of correcting dead time is illustrated in the figure 3.13. (LanD 1972).

Fig. 3.13

Dead time Correction

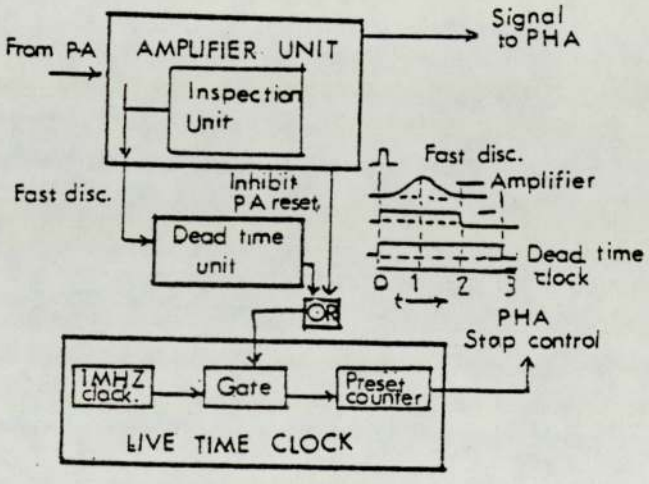

3.5. CHARACTERISTICS OF THE X-RAY DETECTION SYSTEM

3.5.1. Energy Calibration of the Detector

A standard x-ray variable source of 10 m Ci ^{241}Am ceramic sealed primary source of γ-radiation of 60 keV energy with the six turnable targets and a Mn x-ray source (330 μC Fe^{55}) were used to calibrate the detector. The energies of $K\alpha_1$ and $K\beta_1$ x-ray lines (ICRP 59) are tabulated in Table 3.1 with the source and its atomic numbers. These lines were used in calibration, because of their higher intensity than $K\alpha_2$ and $K\beta_2$. A linear relationship between x-ray energies and their respective channels in the multichannel analyser is a characteristic of a detection system at a fixed count rate and gain settings. The least square method was used to calculate the slope (m) and the intercept (c) of the line.

TABLE 3.1.

	Source	Atomic No.	Energy of x-rays in keV	Energy of x-rays in keV
1.	Mn	25	5.898	6.490
2.	Cu	29	8.047	8.904
3.	Rb	37	13.394	14.960
4.	Mo	42	17.473	19.607
5.	Ag	47	22.162	24.943

The detector was calibrated prior to each of the measurements and a typical value of energy at a particular channel from the calibration curve was used to identify an unknown x-ray line in the

energy spectrum. A typical energy calibration of the detector is shown in the figure 3.14.

3.5.2. Detector's efficiency

The efficiency of the detector depends on its own thickness and the thickness of beryllium window. The efficiency for an x-ray of energy Ex was calculated using the following relation.

$$E = 1 - e^{-\mu s(Ex) \cdot d \cdot \rho} \qquad (3.1)$$

where $\mu s(Ex)$ is the mass absorption coefficient in Cm^2/g.

d = the thickness of the detector in cm.

ρ = is the density of the detector = 2.329 g/cm^3.

The above relation was also used to calculate the efficiency of the beryllium window for x-rays of energies 1 to 60 keV. The values for the mass absorption coefficient were taken from Storm and Israel (StoI 1970).

The efficiency of the detector at different x-ray energies was calculated and plotted (figure 3.15). The composite counting efficiency versus x-ray energy from the supplier of the detector is also shown in the figure 3.16.

The decrease in the efficiency of the detector at higher energy above 30 keV was observed due to the passage of a proportional number of x-rays without being absorbed through the detector.

The decrease in the efficiency at low energy below 3 keV was due to x-ray absorption through the beryllium window.

Collimation of the detector is also important since the incomplete charge collection due to the edge effect near the lateral surface of the sensitive volume deteriorates the voltage signal to

Fig. 3.14

Calibration of the Detector

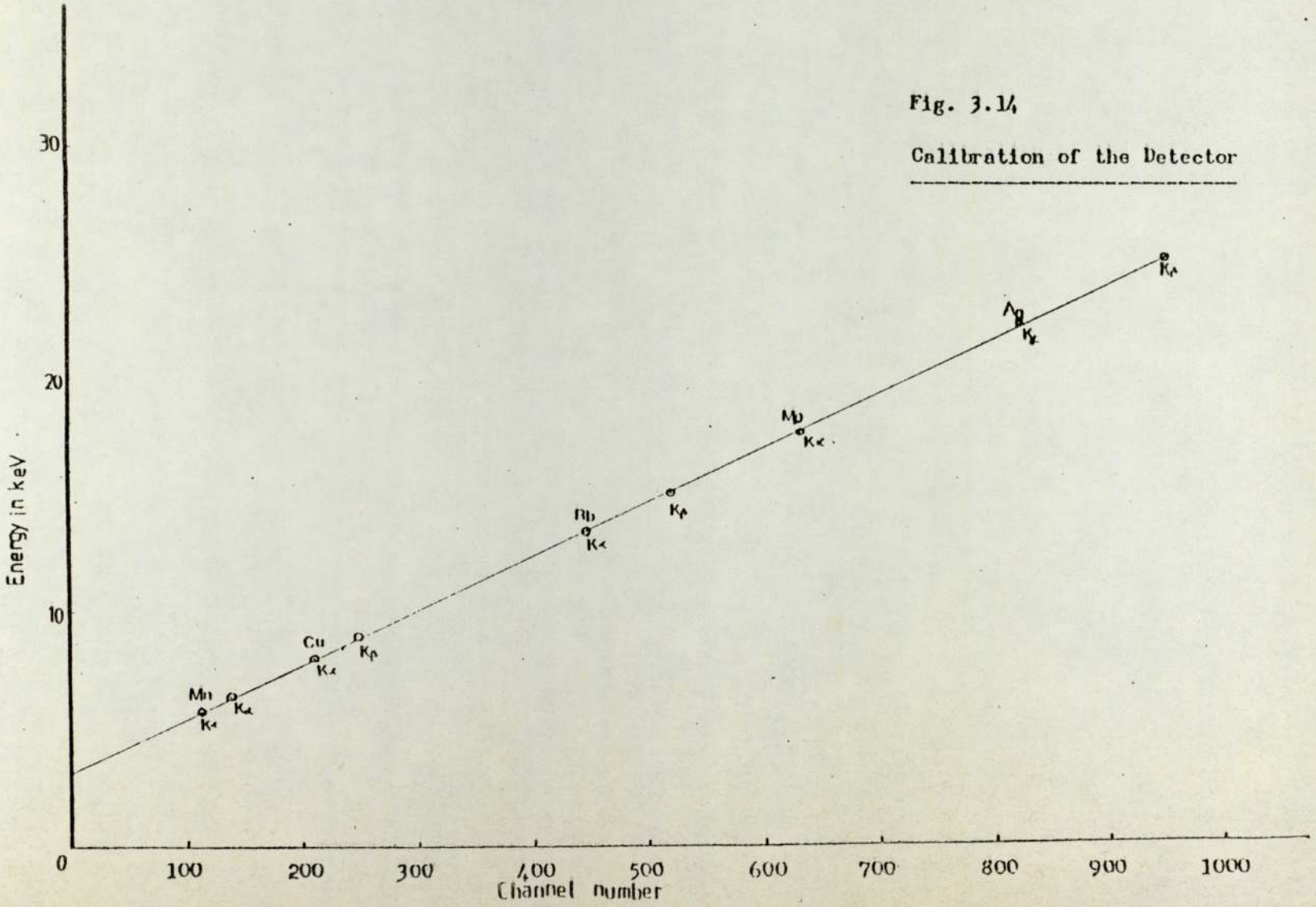

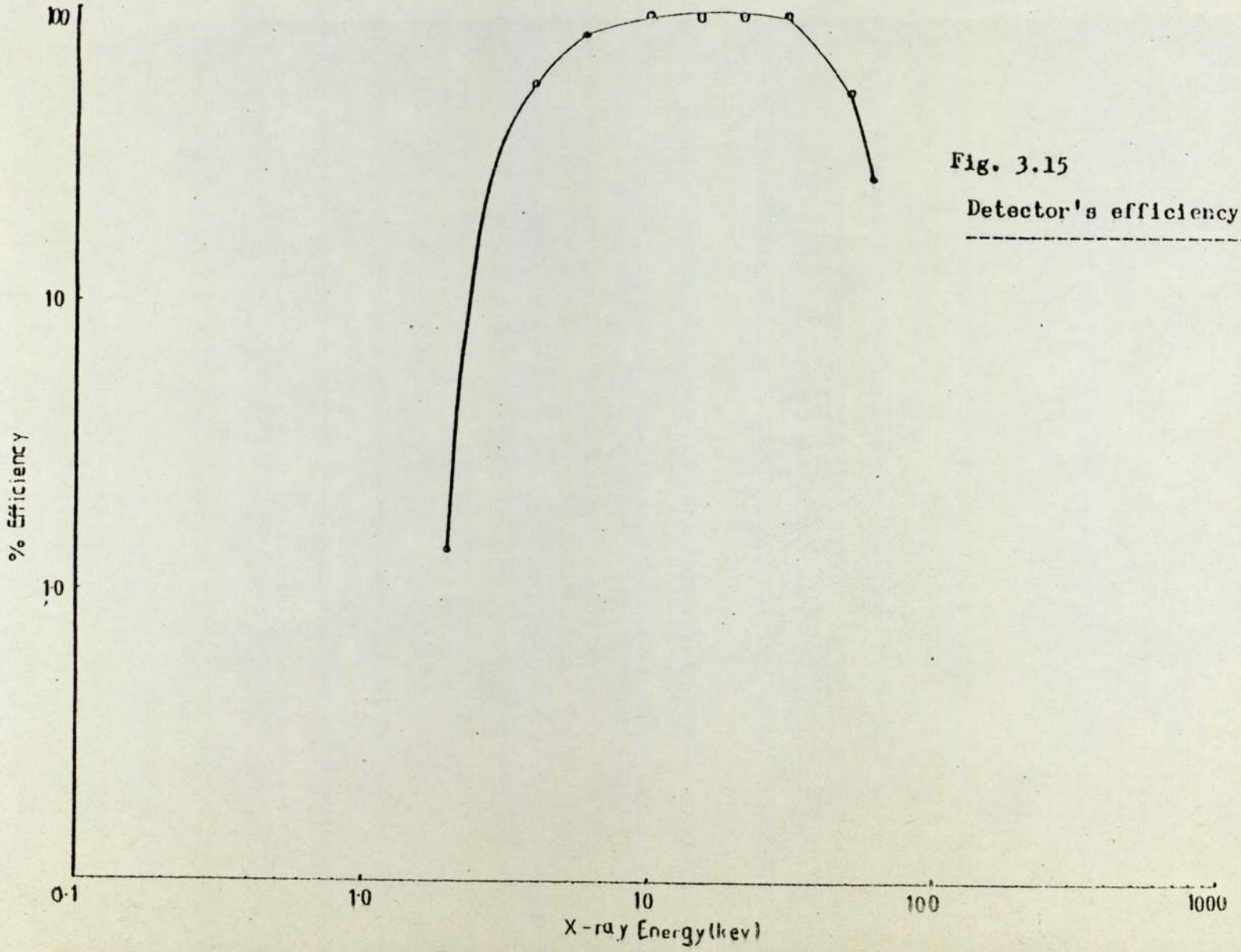

Fig. 3.15

Detector's efficiency (*Experimental*)

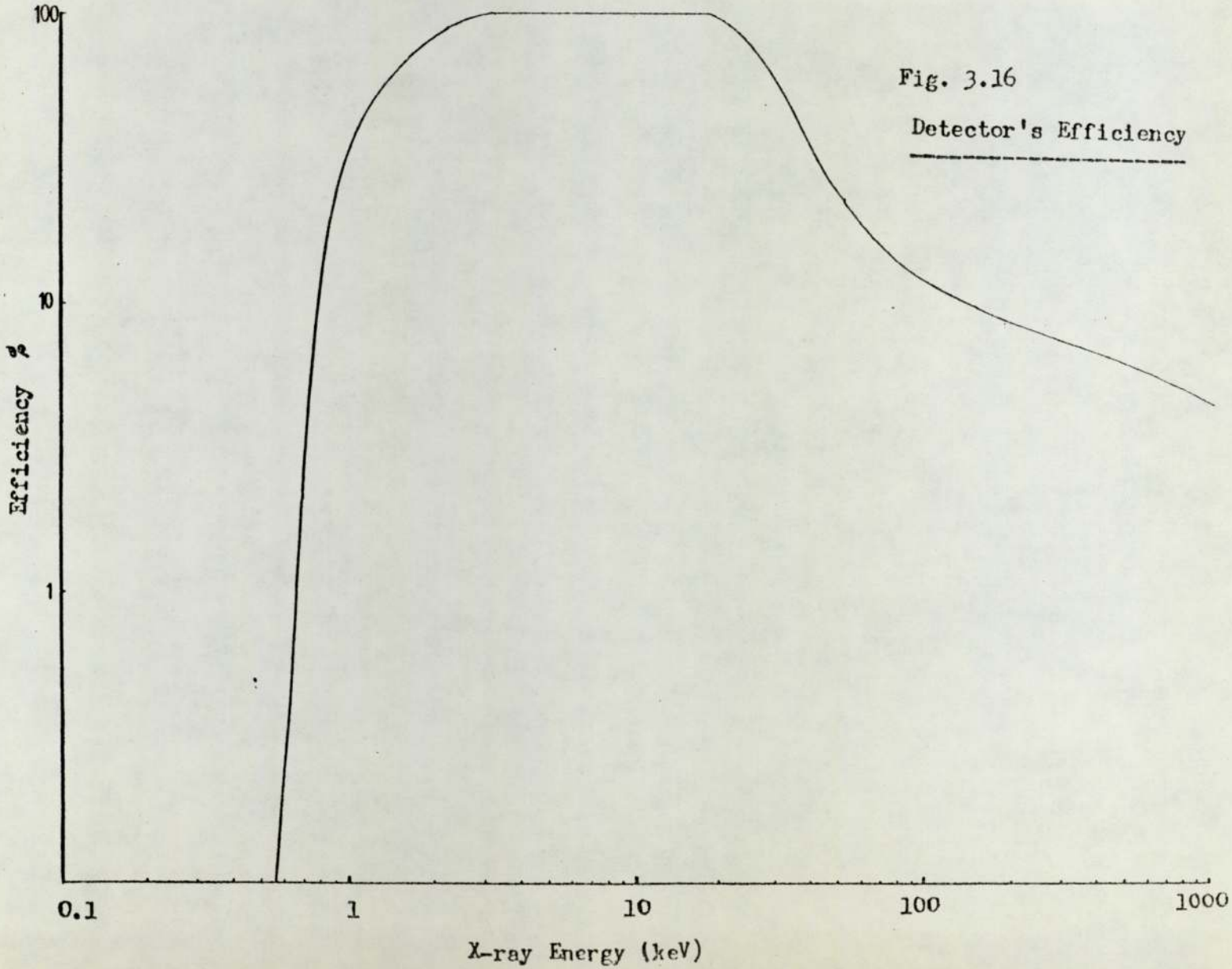

Fig. 3.16

Detector's Efficiency

the preamplifier. A complete charge may be collected on the sensitive volume by collimating the lateral area of the sensitive crystal. The collected charge will be proportional to the area of the collimation because it forms a sharp solid cone to the x-rays path on the target surface.

3.5.3. Live Time Correction and Pulse Pile up rejection Characteristics of the System

To observe the count rate capabilities and real time throughput characteristics of the detection system, an Fe^{55} source was used at various distances from the collimation of the detector to obtain a different x-ray count rate. The graphs in Figure 3.17 show the dead time corrected count rate versus the observed count rate and the real time throughput curve. Related data values and the calculated values are shown in the table 3.2. A.D.C. dead time was not accounted in the calculation since it was much smaller than the total dead time of the system. The counts were corrected using a simple relation:

$$\text{Corrected counts} = \text{observed counts} \times \frac{\text{clock time}}{\text{live time}}$$

The curve is shown in the figure 3.18 and it is evident from the curve that there is no decrement in the corresponding output count rate up to 10,000 C.P.S. rate. The curve also shows that our dead time correction system is correct within 3% for the highest count rate of 10,000 C.P.S.

3.5.4. Resolution of the detector

The resolution of the detector is defined as the full width half maximum (F.W.H.M.) of Mn K_α (5.89 keV) x-ray lines at a count rate of 1000 C.P.S. (WolR 1973) and the F.W.H.M. due

Table 3.2.

A = input/second	B = output/second	live time seconds	log A	log B	log corrected counts
12807	2723	22.11	4.10	3.43	4.08
12357	2776	23.89	4.09	3.44	4.06
10464	2895	28.53	4.01	3.46	4.00
8914	2997	34.63	3.94	3.47	3.93
8026	3040	38.93	3.90	3.48	3.89
7638	2942	39.51	3.88	3.46	3.87
7142	2918	43.21	3.25	3.46	3.82
5722	2844	55.49	3.75	3.45	3.70
4949	2691	55.49	3.69	3.42	3.68
4155	2456	60.12	3.61	3.38	3.61
3380	2222	66.62	3.52	3.34	3.52
2865	1990	70.34	3.45	3.29	3.45
1931	1483	77.64	3.28	3.17	3.28
1364	1140	84.10	3.13	3.05	3.13
1194	1002	84.86	3.07	3.00	3.07
902	799	89.16	2.95	2.90	2.95
693	627	90.86	2.84	2.79	2.83
570	519	92.02	2.75	2.71	2.75
452	419	93.38	2.65	2.62	2.65
377	352	93.77	2.57	2.54	2.57
315	295	94.53	2.49	2.46	2.49
229	219	95.80	2.35	2.34	2.35
174	166	96.31	2.24	2.22	2.23
135	129	96.06	2.13	2.11	2.12
87	83	96.30	1.94	1.92	1.93
61	57	94.96	1.78	1.76	1.78
43	39	92.85	1.63	1.59	1.63

* Analysis time = 100 seconds.

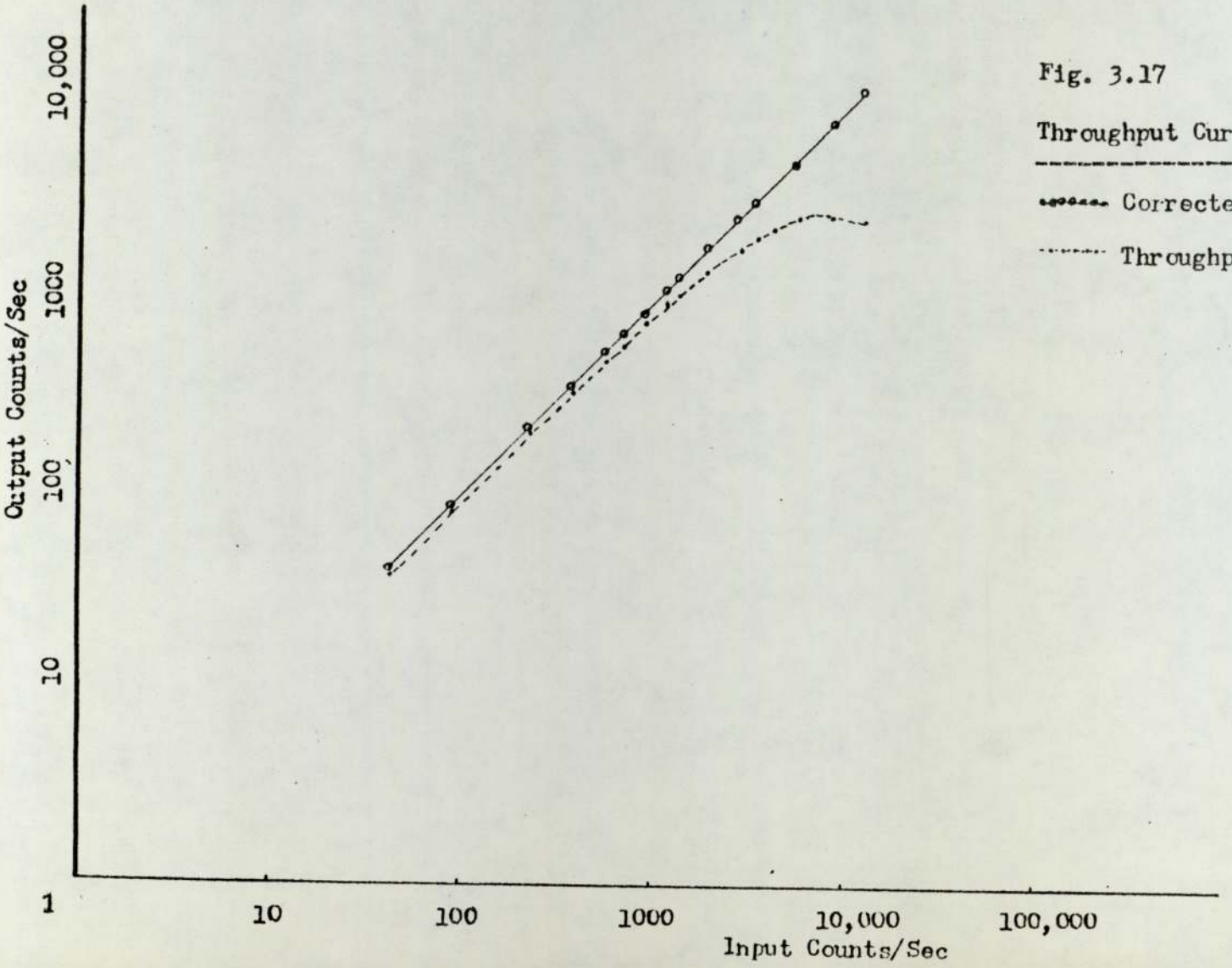

Fig. 3.17

Throughput Curve I

Corrected

Throughput

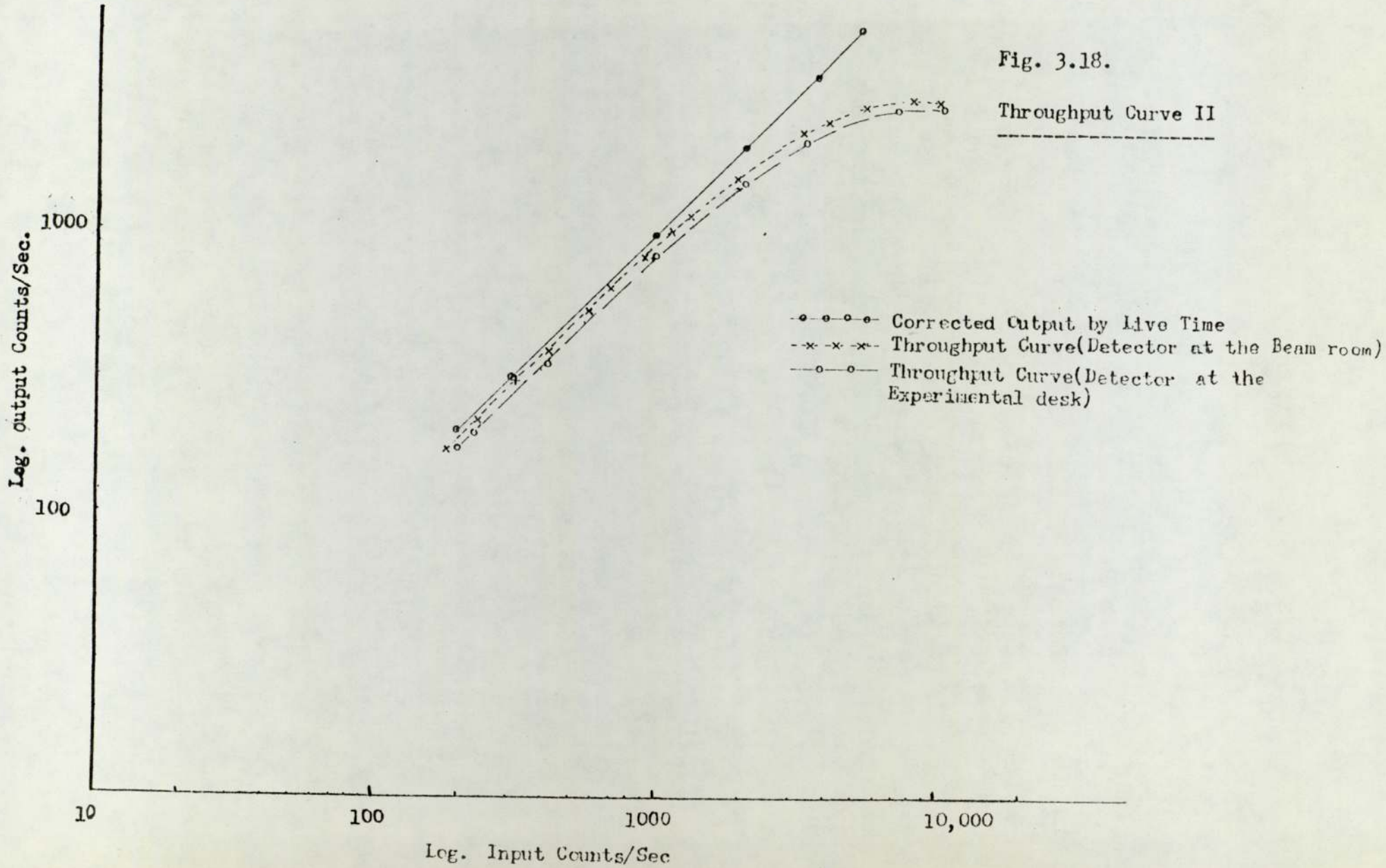

Fig. 3.18.

Throughput Curve II

to the statistical spread, which is:

$$(\triangle E) = 2.35 \sqrt{F \mathcal{E} E} \quad \text{ev} \qquad (3.2)$$

where F = Fano Factor (a dimensionless factor
= 0.087 $\pm$ 0.03)

$\mathcal{E}$ = eV/electron hole pair of the detector's
crystal = 2.6 eV

E = Energy of the x-ray in eV.

The total resolution of the detector is the quadratic sum of the two factors, as shown in the following expression:

$$\text{F.W.H.M.} = \sqrt{(\triangle E)^2 \text{ detector} + (\triangle E)^2 \text{ noise}} \qquad (3.3)$$

The main contribution to degrade the resolution of the detector is the electronic noise due to the charge carriers in the crystal and the pulse shaping process. Electronic noise can be suppressed by the following precautions, which are usually employed:

1. Lowering the temperature of the detector and preamplifier;
2. Proper tightening of the wires and cable connections;
3. Proper insulation of the internal connections and the elimination of earth loop.

Other factors such as improper collimation and physical noise (microphones) degrade the resolution as well. The working resolution of the Kevex detector was found to be $\backsim$ 178 eV at Mn Kα (5.89 keV) as shown in the figure 3.19.

3.5.5. Microphonics

The low energy x-ray detection system was very sensitive to microphonics. This affected the resolution capability of the detector. Therefore, care must be required in filling the liquid

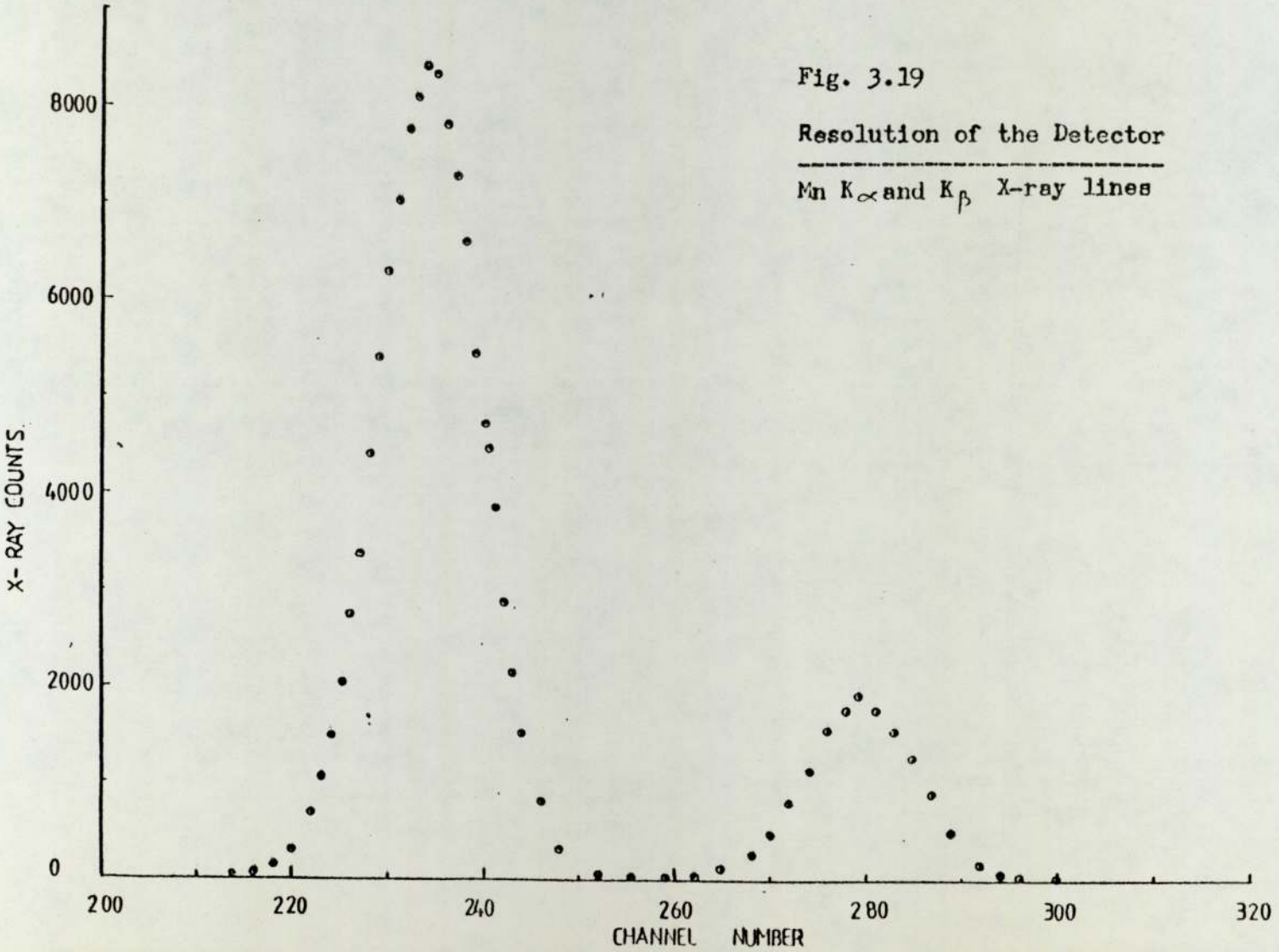

Fig. 3.19

Resolution of the Detector

Mn K_{α} and K_{β} X-ray lines

nitrogen dewar. Its isolation with other equipment is also an important factor to minimise the environmental noise. Very low frequency vibrations are filtered out by the limited amplifier band pass. Usually such problems are serious at long shaping time constants. The applications of appropriate precautions may help reduce the effects of microphonics.

3.6. DATA ACQUISITION SYSTEM

The signal processing system was coupled to the 5406 B H.P. nuclear data acquisition system through the direct input. The system consisted of a multiparameter multichannel analyser and an analogue to digital converter (A.D.C.). The multichannel analyser processed the pulses and stored them in its electronic memory as a function of energy with the help of a 5416 B 200 MHz A.D.C. A number of three A.D.C's are available at any given time but only one A.D.C. was required to process the data for the present work.

The A.D.C. input accepts a D.C. signal between 0 volt to 10 volts. An analogue offset control adjustment between -1 volt to + 1 volt and an upper and lower level discriminators were available to select an input window for the signal. Either fixed or variable analysis time on clock time or live time mode could be selected on the A.D.C. and it could be operated either on normal coincidence or anticoincidence mode.

Any channel out of 2^n could be chosen for the data output such that $n \geqslant 4$ and $\leqslant 13$. A digital offset was also available. A multidimensional display with x - y markers to choose a channel or a group of channels was used with the various

selection of counts per division. Coarse and a fine range of switches were available.

An x - y plotter unit was also available to obtain a hard copy of the spectrum or a group of few channels in required type of graph, using system commands. A copy of such plotted spectrum is shown in the figure 3.20.

The signal is stored in integrated memory from A.D.C. in the multichannel analyser. A common principle of pulse amplitude to time conversion is adopted with the use of a capacitor. The charging time interval of the capacitor was used to gate a constant frequency oscillator. Therefore an initial pulse amplitude represented by a number of pulses known as "address" and identified as the "event" was stored in a memory cell or channel. It is added each time the energy of A.D.C. signal increased according to energy/channel relationship.

The time taken by a signal from A.D.C. to be converted to the number of pulses at the memory or channel is called an A.D.C. analysis time and during this conversion the system may exhibit a dead time in which it could not process further signals. This time is very small comparing the dead time of the processing system. In the multichannel analyser the stored amplitude of the input signals are converted in the binary codes and are sent to the computers. The accumulated data can be studied at the display unit and can be manipulated and analysed using the system commands and it further can be used by stacking them on the magnetic tape or paper tape. The data can be stacked temporarily on the files where further analysis can be done by writing and using R.T.E. (Real Time Executive) programmes. The data acquisition system used in the work is shown in figure 3.21.

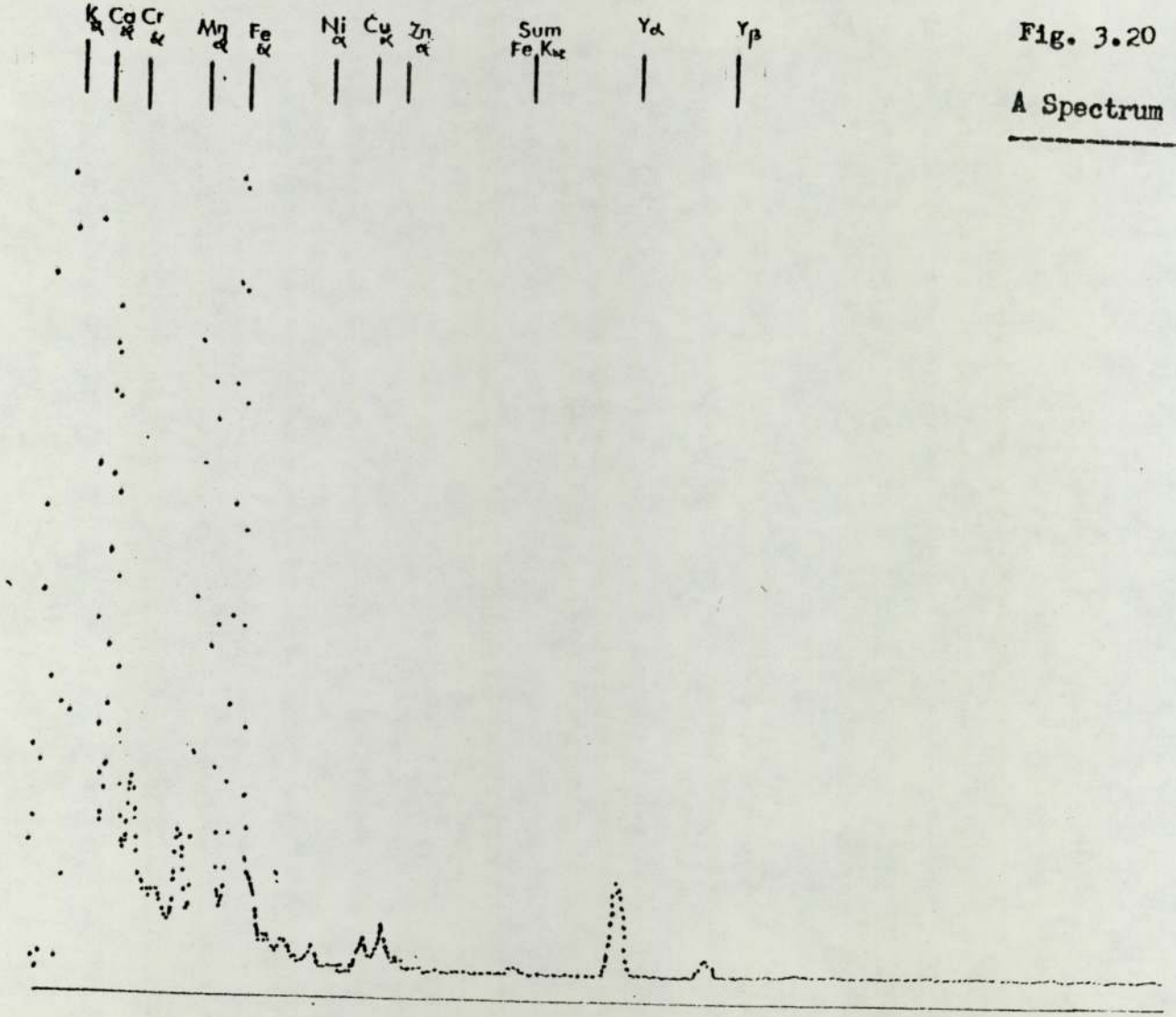

Fig. 3.20

A Spectrum output

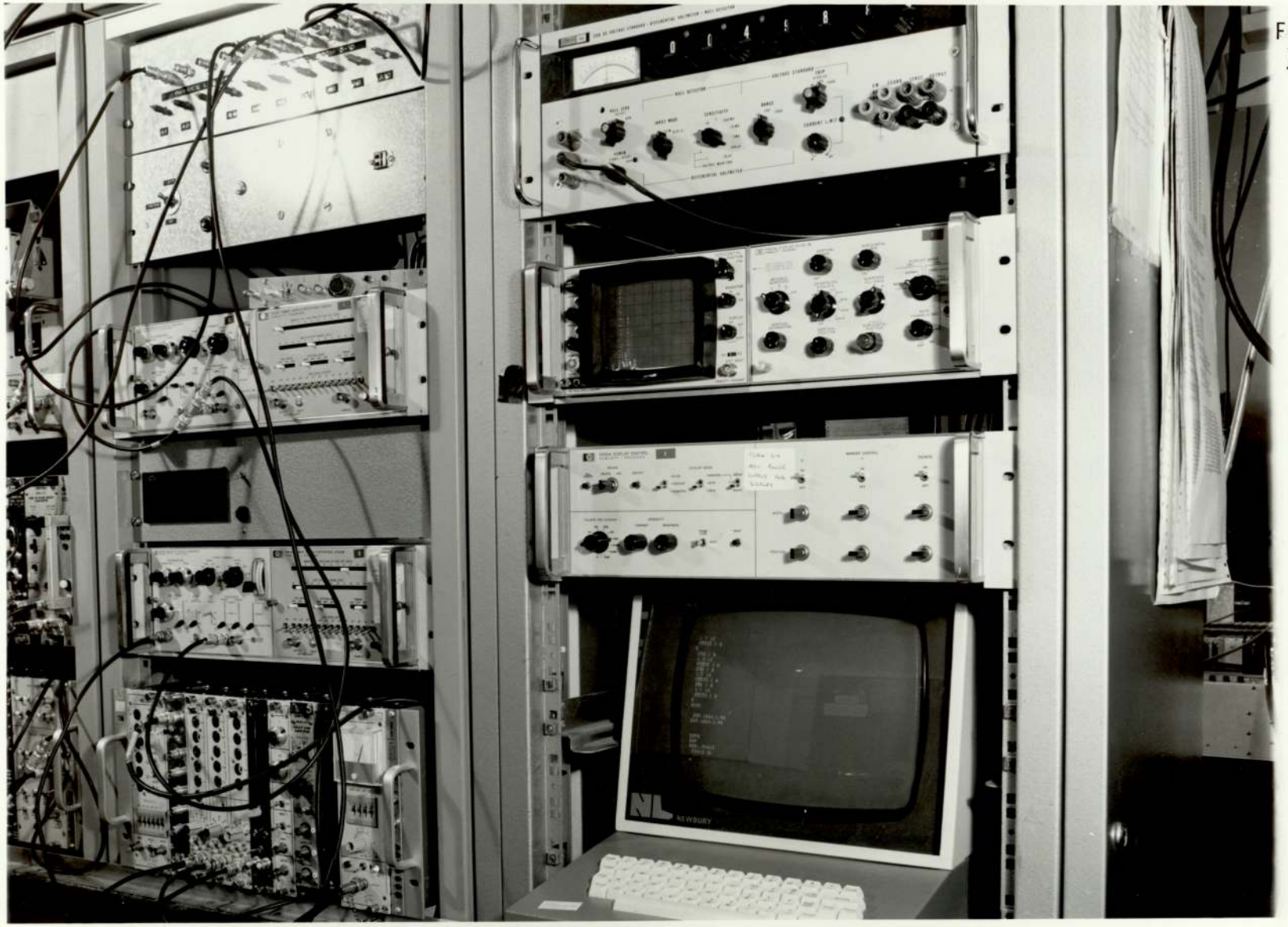

FIGURE
3.21

CHAPTER FOUR

EXPERIMENTAL TECHNIQUES AND ROTARY TARGET ASSEMBLY

4.1. EXPERIMENTAL TECHNIQUES

The sensitivity for charged particle induced x-ray emission analysis depends upon many factors, which include:

1. Projectile type;
2. The thickness and uniformity of the targets;
3. Energy and current of the incident beam;
4. Heating and charging effects of non-conducting targets;
5. The performance characteristics of the detection system.

4.1.1. Projectile type

A variety of charged particles can be used to induce characteristic x-rays of materials. A study of the advantages and disadvantages of a projectile is necessary to assess the usefulness of a particular type.

i) Electrons

Electrons accelerated in appropriate machines (StrA 1969) or beta particles from radio isotopic sources can be used to induce x-ray fluorescence. Several disadvantages, however, are associated with their use. Mainly the background photons (bremsstrahlung) resulting from the acceleration of the electrons in the nuclear coulomb field of the target atom is very large. This reduces the sensitivity of the system, particularly for elements of low atomic number ($Z \leq 25$). D.M. Pool et al (PooD 1968) compared the total performance capabilities of protons of widely varying energies with the corresponding electron excitation of copper and aluminium K x-rays. They found a 10-fold improvement over electron excitation for protons. Similar comparison for aluminium and

silicon K x-rays shows even more improvement for protons than electrons.

ii) Protons

The principal advantage of employing protons is the low level of background radiations, because of their heavy mass compared with the electron mass. An optimum signal-to-background ratio can be achieved using a thin target, in which protons interact with only a few of the target atoms and dissipate only a small fraction of their total energy. Proton beams of any desired energy may be obtained with an accelerator, depending upon its range of operation. Protons are better to employ for the detection of the elements close to sodium than the other particles as observed by Watson et al (WatR 1974).

iii) Alpha particles

These charged particles are available during the nuclear decay processes from a wide variety of heavy elements $Z > 83$. Such alpha particle sources or isotopic elements are portable and require no electric power supply. Most alpha emitter isotopes are not pure alpha emitters, as beta particles and photons as well as positrons in some cases are emitted during the decay process. Alpha particles can also be accelerated in a high energy machine. Cahill (CahT 1972) and Watson et al (WatR 1974) used alpha particles from cyclotrons for characteristic x-rays study. Watson et al found maximum sensitivity for elements from sulphur through zinc for α particles in his comparative study for various projectiles.

iv) Other heavy charged particles

Heavy projectiles of mass greater than four can also be used for x-ray fluorescence analysis. Since such projectiles

have their own electronic system to interact with the target atom, inner shell ionisation process becomes multiple, due to the interference of interaction between the target atom and heavy projectiles. The resulting characteristic x-ray spectrum is more complex than protons. Watson et al (WatR 1974) plotted K x-ray peak-to-background ratios as a function of projectile atomic number for a variety of elements and found a relatively higher ratio for Na, S, Cr and Zinc for protons than for deuterons. The peak-to-background for the same elements, however, was not as high in the case of heavy ions. J.A. Cooper (CooJ 1973) compared the sensitivities of charged particles using various environmental samples. He observed that high energy (30 MeV) alpha particles are not as efficient as those of low energy (2 MeV) protons.

Although ionisation cross sections for equal energy of high Z projectiles are higher, the production of background radiations from secondary electrons will follow this same projectile Z dependance, resulting in no net gain in the sensitivities due to the secondary electron bremsstrahlung. The primary bremsstrahlung will be significantly less due to the mass dependance. F. Folkman et al (FolF 1974A) compared the trace elemental sensitivities using p , α and ^{16}O and giving a peak-to-background ratio of 1 for 3 MeV/a.m.u. projectiles on carbon. They found a higher sensitivity for protons as shown in figure 4.1., using their experimental results and theoretical calculations.

4.1.2. Target thickness and its uniformity

i) Thick targets

Targets in which protons of given energy are absorbed completely are called thick targets. Increasing the proton energy

Fig. 4.1

Sensitivity of P, α and heavy ion

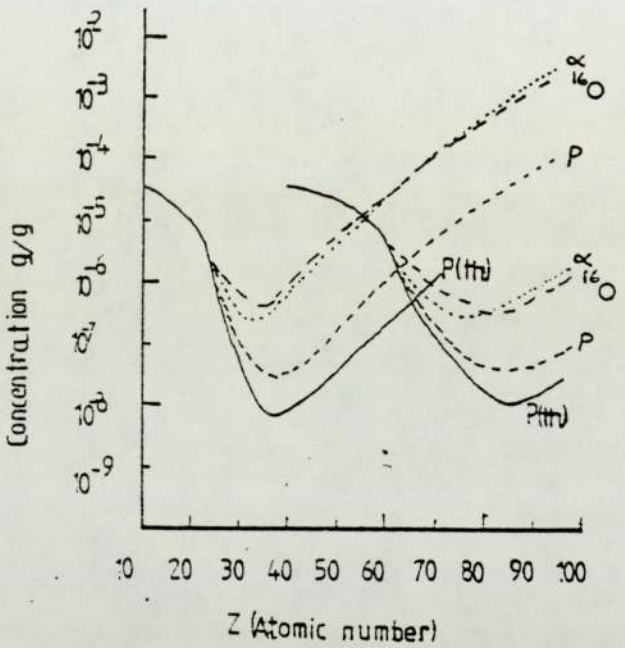

Fig. 4.2

Sensitivity of thick and thin targets

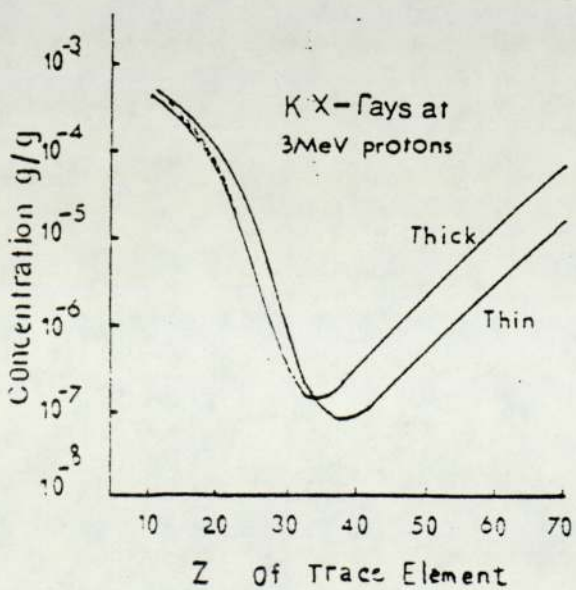

will deposit more energy in such targets with the resulting increase in x-ray yield depending upon the x-ray production cross section. A thick target for 1 MeV protons may act as a semi-thick or thin target for the protons with higher energy, due to their long range in the same material. Since the matrix and the higher elemental concentrations $>$ 500 p.p.m. in targets particularly thick, may affect the characteristic x-ray yields through absorption during their emergence to the target surface, x-ray absorption correction factors must be used in the calculation for x-ray yields. Furthermore, since ionisation cross sections fall with the relative decrease in the proton energy in the target matrix, energy loss per unit distance for the protons should also be employed in the yield calculation. The expression for the thick target yield for K_{α} x-rays, therefore, can be written as:

$$Y_k = n_p N . E_k \frac{\Omega}{4\pi} . e^{-\Sigma \mu_{sk} ds} \int_{E_p}^{E} \sigma_k(E) . e^{-\mu_{mk} . t} . \left(\frac{dE}{dt}\right)^{-1} . dE \qquad (4.1)$$

where Y_k = the characteristic x-ray yield for K-shell

E_k = the efficiency of the detector for K radiations

Ω = the solid angle subtended at the detector by x-rays

N = number of the target atoms /c.c.

σ_k = x-ray production cross section for K-shell

n_p = the number of protons impinging on the target

$e^{-\mu_{mk} . t}$ = the absorption factor for x-rays in the target matrix of thickness t, such that μ_{mk} is the K x-ray absorption coefficient of the matrix

$e^{-\sum \mu_{sK}.ds}$ = the absorption correction factor for K x-rays during the passage through the materials "s" between the target and the detector surface, such that μ_{sK} are their absorption co-efficients and ds are the intermediate thicknesses of the materials "s" between the target and the detector

$(dE/dx)^{-1}$ = the stopping power of the target matrix

$t = x \sec\theta$ where x is the thickness of the target material and θ is the incident angle to the beam.

F. Folkman (FolF 1975A) described most of the factors of equation 4.1 in detail for the studies of sensitivity achieveable using thick sample in PIXE analysis. He defined an exponent "Y" depending strongly on the radiated energy E_γ in units of "E_s" the maximum energy transferable to the electron from the bombarding proton such that the bremsstrahlung production cross section at proton energy "E" is:

$$\sigma_{SEB}(E) = \left(\frac{E}{E_p}\right)^{Y} . \sigma_{SEB}(E_p) \qquad (4.1.A)$$

where σ_{SEB} is the secondary electron bremsstrahlung (S.E.B.) and E_p is the initial energy of protons.

A rapid variation of $Y \sim 8$ for $E_\gamma > 0.8E_s$ was seen for E_p = 2 and 3 MeV on carbon and aluminium matrices, due to the primary strong decrease with E_γ, resulting the shift of the complete S.E.B. spectrum to the smaller energy end of the spectrum. Therefore the effect of S.E.B. spectrum shift enhances the detection of characteristic x-rays at this energy region, as can be seen from the thick target curve (figure 4.2) for elements of $Z \leqslant 28$ where the sensitivity is higher than thin target. The dashed curve shows the absorption low energy x-ray effect, which reduces the

sensitivity of thick target analysis. Total absorption of K x-rays of elements ranging from Z 18 to 48 have been tabulated by Deconninck et al (DecG 75) in their own matrices as well as those of copper, iron, aluminium and carbon. They have given absorption of 2.2%, 1.1% and 0.9% in 20 micron thick carbon matrix for Fe, Cu and Zn x-rays respectively. F. Folkman (FolF 75A) have claimed a better analytical condition of a factor 2 than in the thin target for the low energy region of the spectrum.

ii) Thin Target and its criterion

Targets in which proton energy loss is negligible and in which the characteristic x-rays suffer less attenuation as a consequence are called thin targets. The x-ray production cross-section is least affected, for an incident proton beam of a given energy and current.

In such targets the yield will be much less than that of a thick target and so the bremsstrahlung radiation will also be considerably less. F. Folkman (FolF 75A) claimed five times higher sensitivity of elemental detection in their targets than for thick targets for the elements of $Z \geq 22$.

Since the correction factors for the proton energy loss, absorption of characteristic x-rays and the variation of x-ray - production cross-section due to the decrease in proton energy in the target matrix are negligible, expression (4.1) can therefore be written as:

$$Y_k = n_p . E_k . \frac{\Omega}{4\pi} \cdot e^{-\Sigma \mu_{Sk} dk} \cdot N \cdot t \cdot \sigma_k (Ep) \qquad (4.2)$$

where $t = x \sec \theta$ where x is the actual thickness of the target.

Expression (4.2) is applicable for an ideal situation, where a few

collisions are considered. Therefore a limit of accuracy or a criterion of thin targets is to be employed in case of their use. J.L. Campbell 1977 has employed a thin target specimen criterion (T.S.C.) in which the effective (mean) x-ray production cross section $\bar{\sigma}_k(E_p)$ is based on a value of 95% of the cross section at initial energy of protons. For instance, a proton beam of 2.5 MeV energy loses an energy of 0.12 MeV in 1 mg/cm^2 thick carbon target, while the iron x-ray production cross section decreases by 12% across it (CamJ 1977) . Therefore the effective iron x-ray production cross section is taken as 6% less than the x-ray cross section at the initial energy of protons. Thus, using the values of x-ray production cross section used are 5% less than the initial energy. This target specimen criterion (T.S.C.), stopping power and range for protons of energy E_p in a carbon target are shown in figure 4.3.

J.L. Campbell (CamJ 1977) also employed carbon as a representative of dried biological material. Hence ashed or dried biological target specimens of 1 mg/cm^2 thicknesses may be considered as thin targets to the proton beam of 2.5 MeV. This limit may vary according to the matrix of biological specimen and its preparation methods.

iii) Semi-thick Targets

Thick targets in which the energy of projectile does not absorb completely are called semi-thick targets. Typical values for x-ray absorption at different energies have been reported by J.L. Campbell (CamJ 1977) for 1 mg/cm^2 thick carbon target samples. For instance, 99.6% of Fe K_α x-rays and 98% of Ca K_α x-rays transmit through the target. Thus the x-ray

Fig.4.3

Range, energy loss and thin specimen Criterion

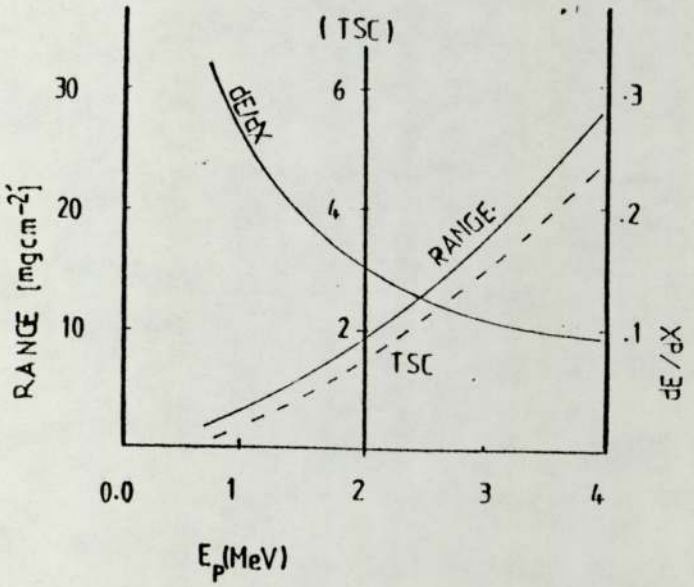

Fig. 4.4.

Relative ionisation cross sections at various proton energies

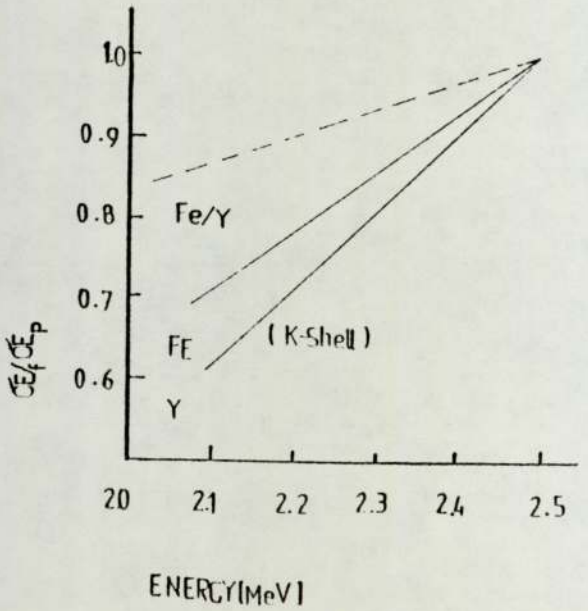

attenuation corrections must be employed as in equastion 4.1, which can be modified to take an average value of x-ray production cross section and stopping power to calculate an accurate elemental abundance for biological targets of thicknesses between 1 mg/cm^2 to 12 mg/cm^2 at the proton energy of 2.5 MeV. Carbon targets are infinitely thick at 12 mg/cm^2 thicknesses. Modified expression for elemental abundance from semi-thick target can be written as:

$$Y_k\left(\frac{Ep + Ef}{2}\right) = \left(n_p \cdot E_k \frac{\Omega}{4\pi} \cdot e^{-\sum \mu_{sk} dk}\right) \cdot N \cdot \sigma_k\left(\frac{Ep+Ef}{2}\right) \int \left(d\left(\frac{Ep+Ef}{2}\right)/dt\right)^{-1} \cdot d\left(\frac{Ep+Ef}{2}\right) \cdot e^{-\mu_{mk} \cdot t} \quad (4.3)$$

where E_p = the initial energy of proton beam

E_f = the final energy of proton beam after emerging out of the target

Since the characteristic x-ray yield is mainly related to the thickness of the target "t" and the energy of protons ($\sigma_k \propto Ep^4$), semi-thick targets at an energy range of 2 to 3 MeV are usually employed in PIXE analysis (CamJ 77). Such targets produce a satisfactory x-ray yield and the expression 4.3 calculates an average yield.

4.1.3. Use of Internal Standards

J.L. Campbell 1977 also pointed out the suitability of internal standardisation for thin targets at higher energies ($E_p > 2.5$ MeV). Using an internal standard, semi-thick targets at a given high energy may be treated as thin targets and the unknown quantities of elements may also be determined using relative analysis technique. A value of 2.5 mg/cm^2 at 2.5 MeV proton energy was estimated by J.L. Campbell for standardised

targets applying (T.S.C.) instead of a value of 1 mg/cm^2 thickness of biological thin targets at the same energy of proton in case of external standard. Because a mean cross section ratio 5% less than the ratio at E_f and E_p implies an energy loss of 0.3 MeV and a corresponding thickness of 2.5 mg/cm^2. Therefore a 2.5 times thick target may be tolerated, if internal standards are employed, provided internal standard is uniformly distributed in the target matrix. Figure 4.4 shows the values of $\sigma_k(E_f)/\sigma_k(E_p)$ for iron and yittrium at different energies of proton. The $K\alpha$ x-ray production cross ratios for Fe and Y against their energies are also plotted.

We have carried out several experiments to set up a standard target preparation method capable of producing targets of biological nature of $\lesssim$ 2.5 mg/cm^2 thickness. Internal standards have been used for these targets for relative analysis and are treated as thin targets in the calculation for elemental concentration. The method is described and its achievement will be discussed in the next chapter.

4.1.4. Beam energy and current dependent effects

Since the production of bremsstrahlung depends mainly on the energy of protons and the target matrix, it is to be expected that the sensitivity of the PIXE analysis will vary with proton energy.

Therefore, the bombarding energy must be adjusted to give an optimum condition for the trace element considered, and the optimum region corresponds to elements of $K\alpha$ x-rays, between 1.4 E_s and 4 E_s (where E_s is the maximum energy transferable to the electron by the bombarding proton).

F. Folkman et al (FolF 1974) studied the projectile energy dependent effect on the sensitivity of PIXE method using a thin carbon matrix. He observed a shift in sensitivity to high elements for each increment of proton energy as shown in the figure 4.5. It can be concluded from the figure that the energy region of 2 - 4 MeV provides a lower limit of detection ($<1\ \mu g/g$) for the trace elements of atomic number between 24 to 62. Experimental work of J.L. Campbell (CamJ 1977) and R.D. Willis et al (WilR 1977) shows that a proton energy "E_p" of 2.5 MeV provides the best compromise to collect a good statistics of data from both thick and thin biological targets. We have employed an energy range (2.4 - 2.8 MeV) in this work and achieved sufficient data within a reasonable irradiation time.

For accurate measurements of elemental concentrations, the target current must be collected with all possible care. Escape of secondary electrons from the target surface or from the Faraday cup may lead to the wrong interpretation of the characteristic x-rays in absolute measurements. A very low beam current ≤ 10 n A has few disadvantages besides an advantage of the stability of the biological targets against the beam, and the use of beam current above 50 n A has an immediate undesirable effect of destroying the target specimen of biological matrix due to a high energy deposition rate. Beam current of 10 - 30 n A has been used in the present work.

4.1.5. Heating and charging effects of non-conducting targets

A high rate of energy deposition on the target by the proton beam generates a high temperature locally, in the region of the beam spot resulting in burning of the target. Burning of the

Fig. 4.5

Sensitivity of PIXE analysis at different energies

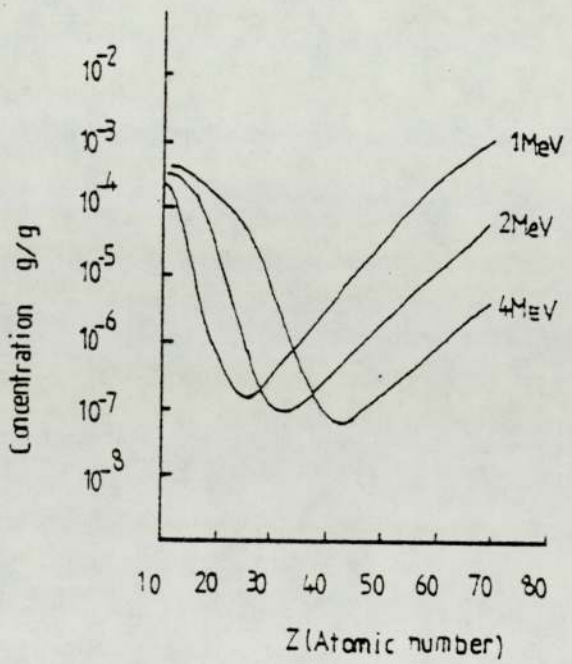

targets may provide unpredictable or incomplete x-ray yield leading to a wrong interpretation of the trace elements.

The present measurements indicated that a beam current of between 10 and 20 n A was the most appropriate at an energy of 2.5 MeV.

Heat dissipation and charge build-up effects which may be observed in the thick biological targets are, however, not a serious problem for thin non-conducting targets, because only a fraction of the proton energy is deposited in the targets. Charging effect which is a major source of background radiation generation in thick targets (AhlM 75) is not present at all in the thin targets as protons leave the target and no discharge occurs inside the target, which acts as insulation between target conducting layer and the surface of the target.

4.2 TARGET MEASUREMENT SYSTEM

4.2.1. Target chamber and the system design for thin target measurement

Experimenters at Birmingham Radiation Centre have a provision to use a target chamber at the end of the beam line in Aston beam room. Several targets can be mounted on a multiple target holder, which is rotated in the target chamber by an electric motor. The motor is operated either using an on/off switch on the target head assembly, or using a target changing and positioning electronic module (SamA 77), which can be placed in the experimenter's console. An electronic video unit may further be linked with an electronic camera and can be used to watch the movement and position of the targets. The change for the required position of

the target can be made in steps without breaking the vacuum. This allows several targets and standards to be analysed before changing to another set of targets.

The proton current is collected on the multiple target holder and conducted to the current measuring device through a conducting touch bar. Copper wires covered with ceramic beads are used for conduction of charge in the chamber.

The target chamber was limited to the use of the thick targets only, as the thin and semi-thick targets could not be mounted on the target holder available. Therefore a thick and thin target holder system which could be accommodated in the target chamber was required to accomplish both thick and thin target analysis. Since the construction and mechanism of most of the target chambers reported in the literature in PIXE analysis (WalR 1974, HerA 1973, WatR 1971, and FelE 1972), allow the use of thin targets, they were reviewed to design an appropriate target rotary system, which can be incorporated into the existing thick target holder. The target chamber reported by A.W. Herman et al (HerA 1973) has a target ladder which moved vertically through six exactly reproducable positions such that the vertical extensions remain within the accelerator's vacuum during irradiation. E.J. Feldle et al and R.L. Watson et al have employed respectively an aluminium sleeve lock with thirteen locating slots machined into it and a rectangular target holder with detachable handles capable of holding 20 targets.

Since the construction of our target chamber has no such typical features and allows a rotating type target holder only, a target rotating system mountable on the motor shaft and supported

Fig. 4.6

Parts of Thin Target mounting Assembly mountable in the Target Chamber

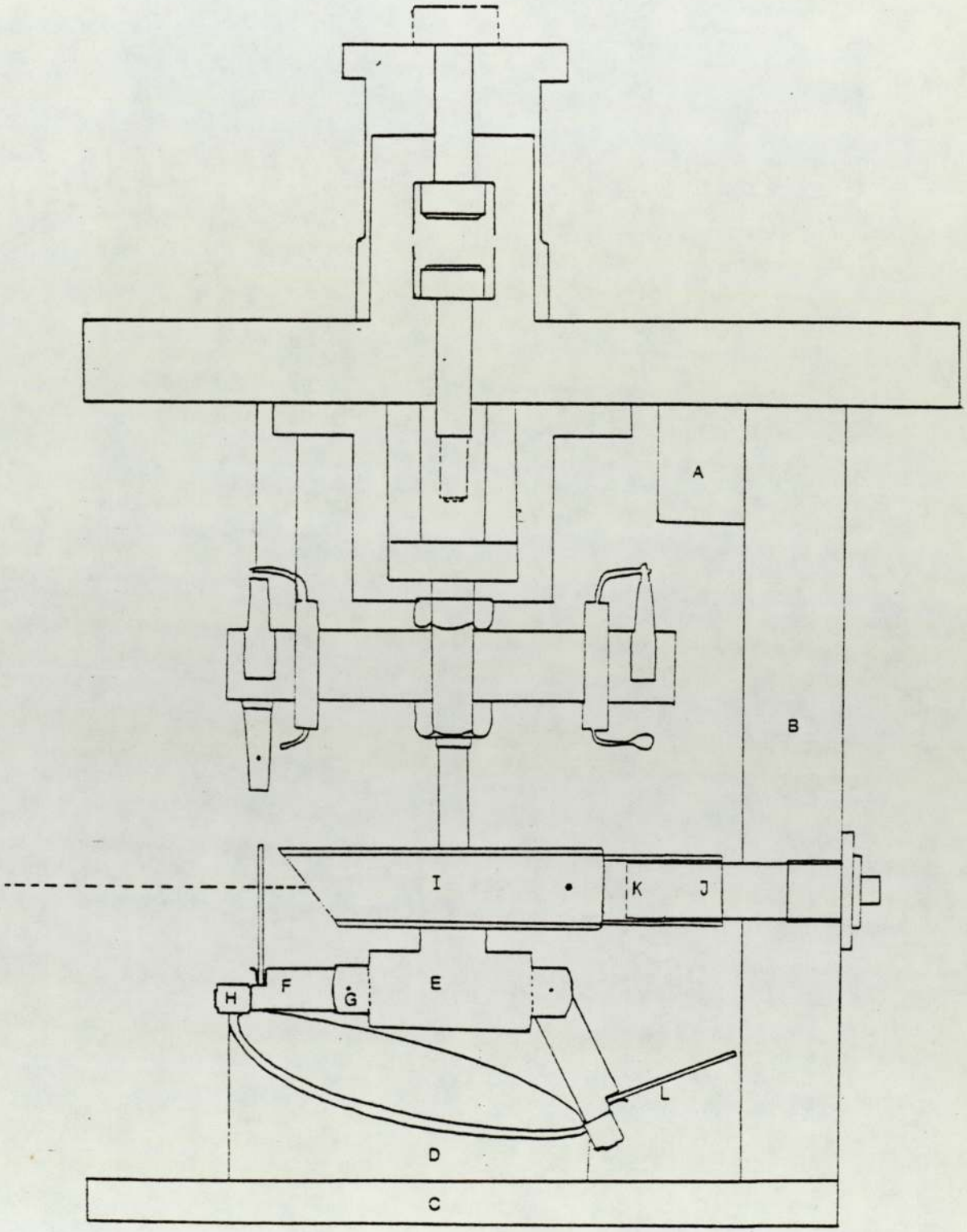

PARTS OF THIN TARGET ASSEMBLY SHOWN IN FIGURE (4.6.)

A = Aluminium block (2 x 2.5 x 5) cm^3 having two screw holes for top plate connections.

B = Al vertical support to the base C for cam D and Faraday cup I. (2 x 2.5 x 12.3) cm^3 with two horizontal holes for the block A.

C = Al base for cam D (0.5 x 7.5 x 12.5) cm^3.

D = Aluminium cam mounted to the base.

E = Stainless steel thin target rotary cylindrical octagonal block, (3.0 dia. x 1.9) cm^3 having eight hinged blocks.

F = Stainless steel hinged finger for thin target frame hinged with the block.

G = Block hinges (stainless steel).

H = Stainless steel wheel mounted to the finger to slip on the cam.

I = Aluminium Faraday cup (5 x $(0.5)^2 \pi$) cm^3 with a base fixed to a ceramic cylinder.

J = Ceramic cylinder, insulates Faraday cup to the vertical column B and to the whole system.

K = Base to lock and unlock Faraday cup from system.

L = Two aluminium target frames to sandwich the thin or semi-thick targets (2.5 x 2 x.075) cm^3 with a hole of 1.5 cm diameter.

with a hanging column and a cam was designed as shown in the figure 4.6.

i) Target rotary system

A Faraday cup was to be located behind our targets, to monitor the beam current, which could only be located in the space available inside the circular space of the proposed system. The available space was $\backsim$ 3.5 cm in diameter. It was therefore necessary to design a system which allowed the targets to be hinged down to provide sufficient room for the Faraday cup.

An eight finger hinged target rotary system was designed as shown in the drawings in the figure 4.7 such that the space for the Faraday cup was created by lowering down the target samples to the required positions during their rotation. This was achieved by using an oval type cam on which the target holder's wheel slips up and down with respect to the height of the cam. Initial tests were made on a cardboard cam to obtain the correct shape of the cam used. It was erected on a base connected with a vertical column hanging on to the top plate of the chamber. The cam was designed and positioned in such a way that a target could be raised vertically before the beam at an angle of 45^{o} while other target samples lowered down respectively.

ii) Hanging column and the Faraday cup

There were a number of limitations in the design of the target chamber regarding its use for the thin target analysis. Firstly, the aluminium motor shaft was too short to meet the height of a target holder for thin targets. Secondly, the bottom of the target chamber was too low to provide a base for the cam, and thirdly, a connection support for the Faraday cup was not available. A hanging column (vertical support) and its base were designed to

Fig. 4.7

Target Rotary System

Finger Hinged Target Holders with the Target holding Frames

.[Plan View.]

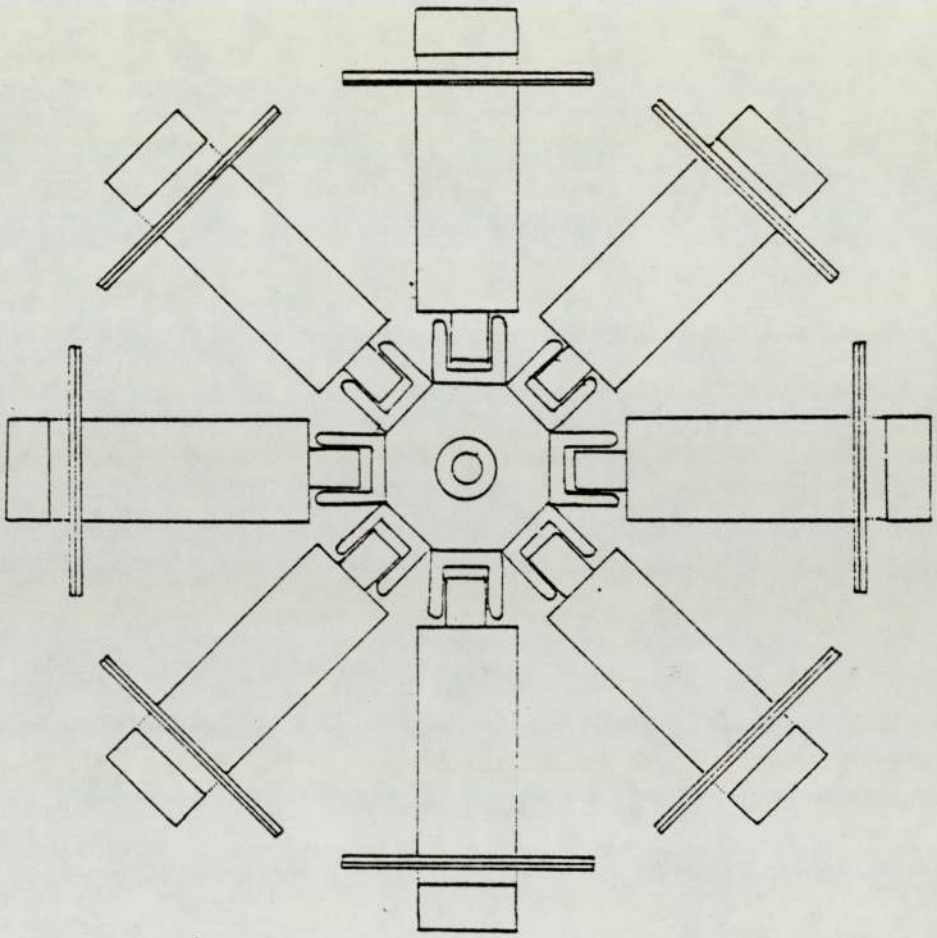

support and to accommodate the target rotary system respectively. The cam was made to mount on the base of the vertical column which hangs from the top plate of the target chamber through a connected block. A ceramic connector cylinder connects through a hollow cylindrical end with the hanging column at an appropriate height to meet the proton beam at the centre of the Faraday cup, which could be pushed over to the ceramic connector. The Faraday cup could also be adjusted to a required distance behind the semi-thick or thin target meeting the beam. A wire connection was made on the Faraday cup to conduct the proton current to the measuring instrument. The hanging column was adjustable before mounting it tightly with the block, which was connected to the top plate of the chamber. The hanging column with the block and the cam was mounted with the target rotary system and is shown in the figure 4.8 along with a target which is sandwiched between the two target holding frames.

iii) Target holding frames

Target holding frames for thick, semi-thick and thin targets were constructed from 0.75 mm thick aluminium sheets which were cut to size in rectangular pieces. Appropriate holes were drilled in the target holding frames to accommodate the target for irradiation.

Each sandwiched target could be mounted on the holder finger with the help of a hook. In such a way, targets could be measured without breaking the vacuum. The whole set-up of the target measuring system mounted and positioned with the top plate of the target chamber is shown in the figure 4.9.

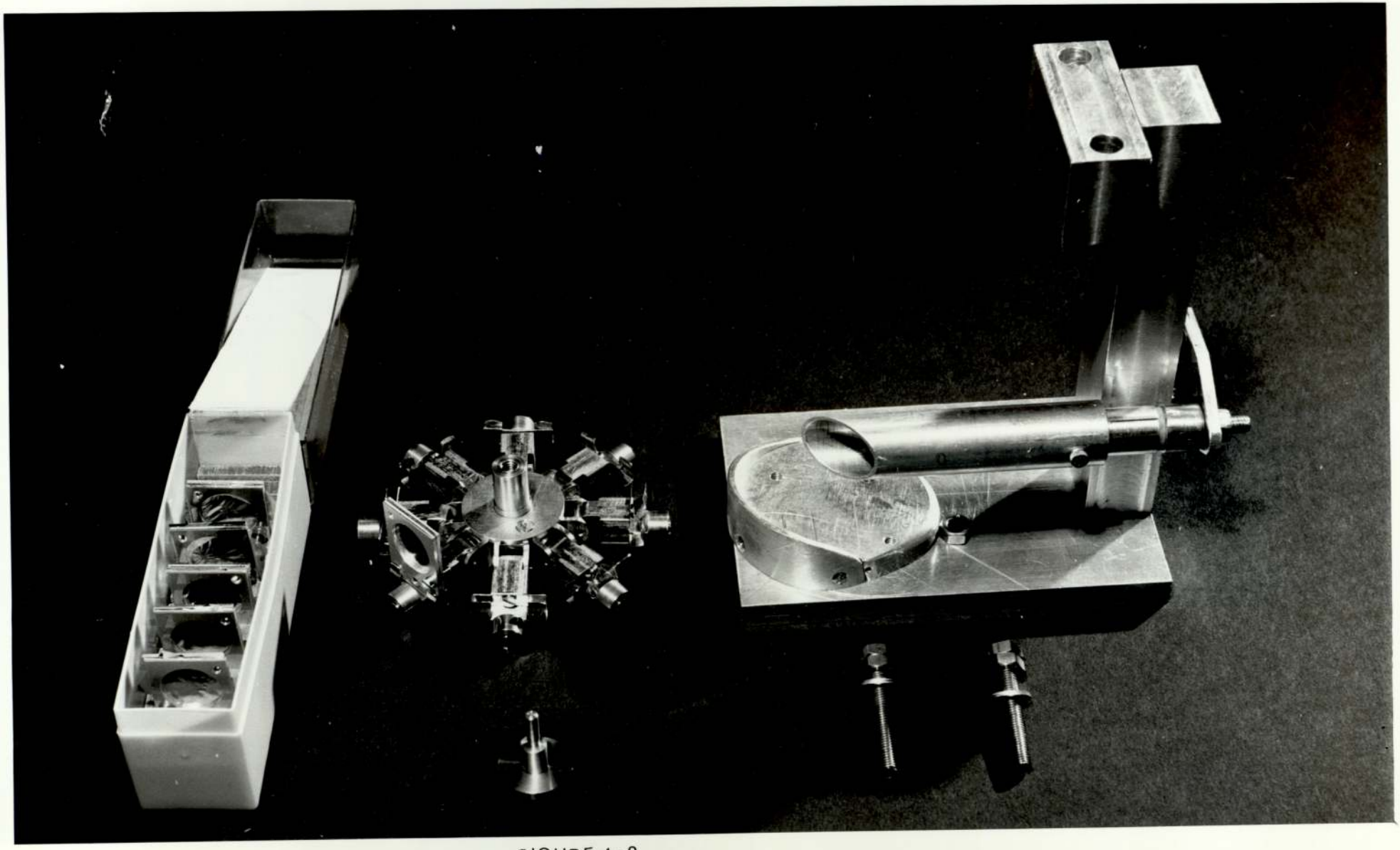

FIGURE 4·8

4.2.2. Dimensions and materials of the target measuring system

The dimensions of the major components are shown, along with the plate, in figure 4.10. The solid angle subtended by the Faraday cup constitutes $\simeq$ 1% of 2π geometry. The dimensions of the target holding frames were based on the appropriate height of the target rotary system, such that it could provide the required space for the Faraday cup and the mounted targets could move up and down freely while rotating. The components of the target rotary system were designed to have appropriate dimensions such that the system as a whole could be able to generate characteristic x-rays from the target at an angle of 45^{o} to the centre of the Melinex window on the chamber while the target is bombarded with the horizontal proton beam at an angle of 45^{o}. The dimensions of the hanging column and the cam were also taken to provide an appropriate connection and position respectively to the Faraday cup and the target rotary system, as seen in figure 4.9.

4.2.3. Mounting methods

The target rotary system was mounted first over the motor shaft after removing the thick target holder and then the hanging column with the cam was mounted carefully such that each target finger rested on the edge of the cam. The position of the target holding frame could be adjusted by untightening the target rotary system in case of its wrong location. A marked line which was drawn at exactly 45 degrees on the base of the cam helps setting the target rotary system to its right location. An on/off switch of the motor which is located at the top of the target chamber (figure 4.9) could be used to set up the rotary system. Slight

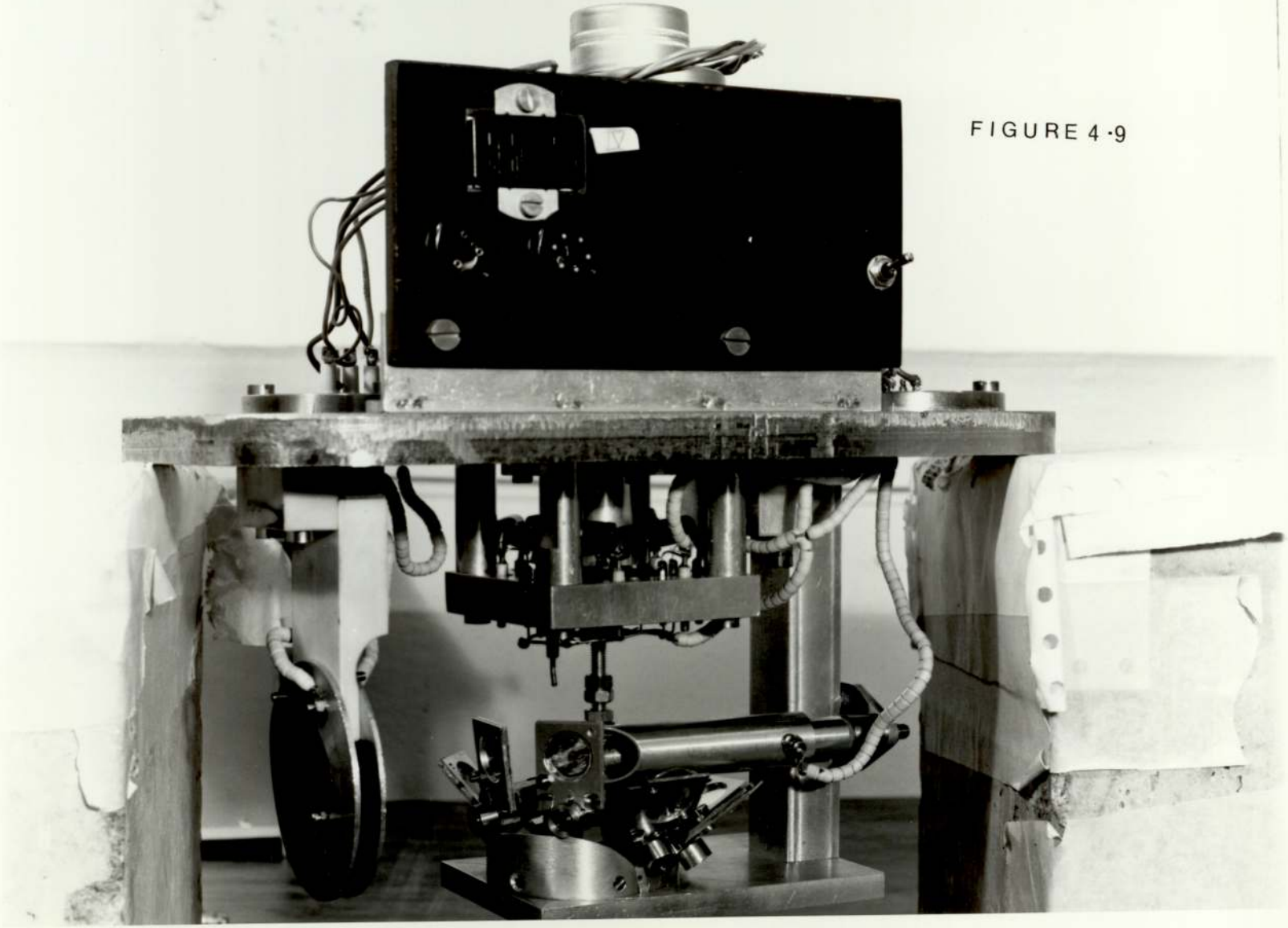

FIGURE 4-9

mislocating of the rotary system could lead to wrong results of the analysis. Similar care is required in setting the hanging column after mounting it. A rectangle was marked on the inner surface of the top plate of the target chamber. Adjustment of the target block with the marked rectangle and careful setting up of the target rotary system ensures that the target measuring system is adequate. Most of the components of the system are shown dismantled in the figure 4.10.

4.3. RESULTS

Semi-thick and thin targets both of metallic and biological nature were analysed using the designed target measuring system and the reliability of the system was established, as explained in Sections 4.3.1. - 4.3.3.

The reproducibility checks on the metallic foils are reported here with respect to the reliability of the designed system. The analysis of biological materials of interest, which is the main part of the present work, will be discussed in a separate chapter.

4.3.1. Reproducibility check

i) Thin copper and gold foil x-ray yields

Spectroscopically pure foils from Goodfellow Metals were used to check the reproducibility of x-ray yields, resulting from their bombardment with accelerated protons, using the target rotary system. Two gold foils of six microns and two copper foils of ten microns thickness were irradiated several times with protons of 2.8 and 2.6 MeV energy. Two similar foils were used to study

the effect of irradiation on similar targets in all cases of the reproducibility checks. The measurement of observed x-ray yield/micro coulomb for $K\alpha$ and $K\beta$ in case of copper and $L\alpha$, $L\beta$, $L\gamma$ and L_l in case of gold are shown in tables 4.1, 4.2 and 4.3. The weighted mean was calculated for each set of measurements on a given target, which was irradiated several times under the same experimental conditions to check the reproducibility. The standard deviation shows the consistency of a set of measurements of a target, being rotated or at a position. The standard deviation on any of the sets of measurements made with 2.8 MeV protons (Table 4.1) is not $>$ 2.2% which shows that the measurements for a given foil are consistent within 2.2% without rotating the targets from their positions. This agrees with the estimated error of 1.5% based on 1% error on the current measurement and on random error of $<$ 1%. The number of measurements made on the copper foil were insufficient for a consistency check, but are included for completeness.

Comparing the yields of the two Au and Cu foils, it was observed that the two similar Au foils differ significantly, i.e. 18%, where the copper foils differ only by $\backsim$ 0.9%. The difference in yield for Au foils indicates that either the target positions were changed due to its rotation or being at a different target finger, causing different angles of incidence to the beam during irradiation, resulting in a significant difference in the x-ray yield. Therefore the same two Au and Cu foils were irradiated again and each target foil was rotated through a complete cycle twice or more and irradiated at each position for

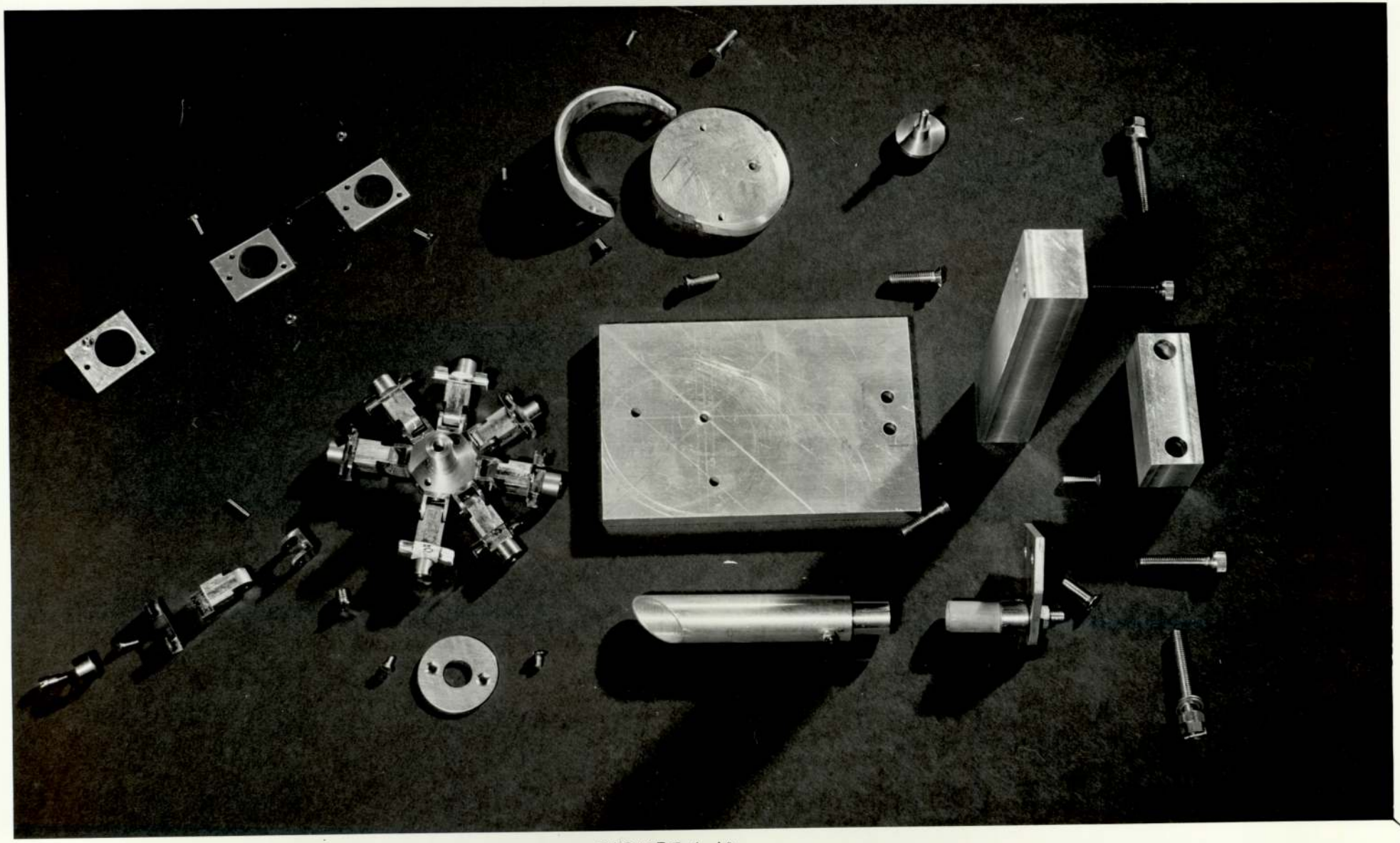

FIGURE 4 -10

TABLE 4.1.

Target to detector distance = 35.8 cm.

TARGET MATERIAL	FOIL 1				FOIL 2				E_p/ Current
	X-ray yield per μC	Weighted mean ± Error	σ	Target Rotation	X-ray yield per μC	Weighted mean ± Error	σ	Target Rotation	
Gold Foil	53521 ± 231 51410 ± 226 53740 ± 232	52885 ± 732 ~ 1.4%	1050 ~ 2%	No	64500 ± 254 62000 ± 249 60990 ± 247 61180 ± 247	62101 ± 472 ~ .76%	1399 ~2.2%	No	E_p = 2.8 MeV Current -8 1 x 10 A
Copper Foil	189211 ± 432 194318 ± 441	191764 ± 2553	2554 ~ 1.3%	No.	189963 ± 438 190209 ± 436	190086 ± 123 ~ .006%	127 ~ 0.06%	No	

several measurements to check the reliability of the target rotary system, which locates the target to its original position. The weighted mean observed x-ray yield was calculated for each set of measurements and tabulated in table 4.2. Each set of measurements is consistent within 2% and the weighted means, each on a set of measurements at a cycle for the same Au foil, differ from each other within $\backsim$ 9.0%. The Cu x-ray yield at the foil's rotation were very consistent, since they differ by $\backsim$ 1%. A difference of $\backsim$ 5% to 20% of yield was observed between the Au foils 1 and 2. The x-ray yields of Cu 1 and 2 were again consistent, but the measurements were insufficient to compare. This shows either the gold foils had kinks or they did not sit at the same position.

Different target positions may affect the observed x-ray yield due to the change in the apparent thickness t and d of the foil, observed by the incident beam and by x-rays during their passage through the foil respectively. The variations in the thickness $t = x \sec\theta$ and $d = x \operatorname{cosec}\theta$ are dependent on the angle of incidence θ of the beam on the target, where x is the actual thickness of the target foil.

We have estimated the variation in the x-ray yield for Au foils due to the changes in both of the apparent thickness t and d corresponding to a change of incident beam angle in setps of 1^{o} from 41^{o} to 49^{o}. The normal target position was 45^{o}. The results are shown graphically in figure 4.11 and show that a variation of $\backsim$ 2.0% and 3.0% in x-ray yield occurs for a change of 1^{o} in the apparent thicknesses t and d respectively. The energy of gold L's x-ray=9.71 keV was used in the calculation. This shows a total increase of $\backsim$ 5.0% in the observed x-ray yield for an increase of 1^{o} in the target position and a corresponding decrease for a decrease of 1^{o} in the target position.

TABLE 4.2.

TARGET MATERIAL	FOIL 1				FOIL 2				E_p/ Current
	X-ray yield per μC	Weighted mean ± Error	$\sigma_{\bar{}}$ %	Target Rotation	X-ray yield per μC	Weighted mean ± Error	$\sigma_{\bar{}}$ %	Target Rotation	
Gold Foil	47955 ± 219 49400 ± 222 48800 ± 221 49200 ± 222 48700 ± 221	48647 ± 249 0.5%	490 1%	1	531800 ± 230 51950 ± 228 51195 ± 226 51320 ± 226	51748 ± 463 0.8%	786 1.5%	1	E_p = 2.6 MeV
					51871 ± 228 51272 ± 226	51571 ± 227 0.4%	299 .5%	2	
	48281 ± 220 47874 ± 219	48077 ± 219 0.5%	203 0.5%	2	55450 ± 235 55130 ± 235 54990 ± 234	55253 ± 160 .3%	192 .4%	3	Current 1×10^{-8} A
	45520 ± 213 45040 ± 212 45000 ± 212 46400 ± 215 45356 ± 213	45365 ± 258 .5%	507 1%	3	50690 ± 225 51020 ± 226 50850 ± 225	50774 ± 160 .3%	184 .3%	4	Target to detector distance = 35.8 cm
Copper Foil	146310 ± 382 149684 ± 387 148047 ± 385 147789 ± 384	147879 ± 384 .3%	1197 .8%	1	142100 ± 377 147690 ± 383 149756 ± 383 148600 ± 385	146647 ± 1690 1.1%	2942 .2%	1	
	150830 ± 388 149565 ± 387 143678 ± 379	147821 ± 384 .3%	3116 2.%	2	148066 ± 385 147754 ± 384	147910 ± 385 .3%	156 .1%	2	

Fig. 4.11

a) Absorption effect.
Increase of x-rays due to the decrease in the thickness d.

b) Production effect.
Increase of x-rays due to increase in the thickness t.

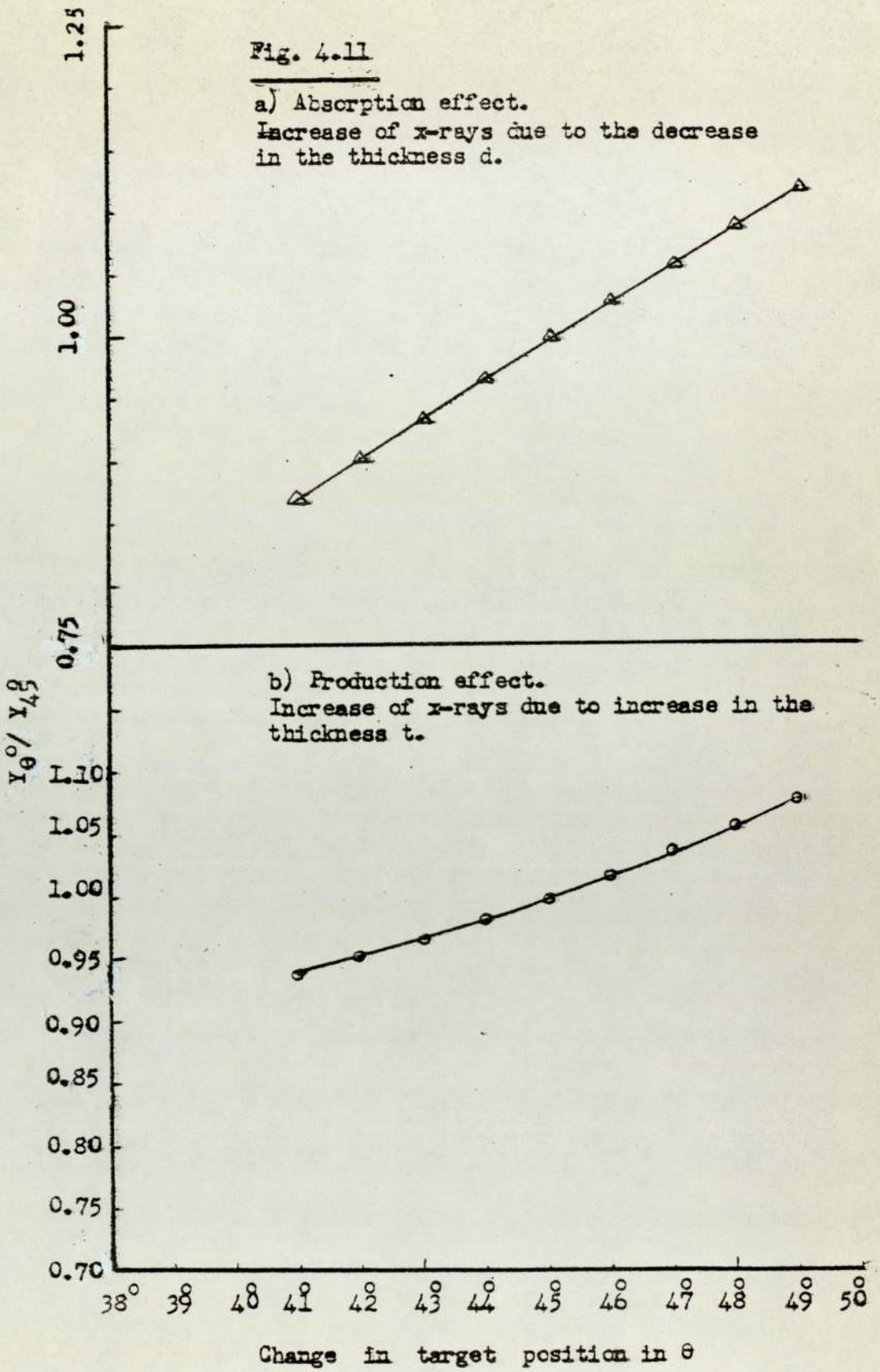

Since the actual thickness of the two Au foils was the same, the variations in the x-ray yields of the two foils would correspond to different target positions. The difference in the x-ray yield between the minimum yield of Au foil 1 and the maximum yield of Au foil 2 was 20% (table 4.2). This variation of the yield corresponds to a shift of $\backsim 4^{o}$ in the target position. Tests showed that a change of this magnitude was not possible with this target assembly.

Since the observed x-ray yield was normalised by the charge collected in the measurements, the reproducibility of the x-ray yield depends on the precision of the charge measurement. This was investigated to assess its contribution to the observed variation in the yield. Two copper foils were irradiated at different beam currents, employing different ranges on the Kiethley electrometer. All sets of measurement are tabulated in the table 4.3 along with their weighted means and standard deviations. A consistency of better than 1% was observed for all sets of measurements, but the yield for each target differed significantly by 20% at different currents.

It was therefore decided to investigate the precision of beam current measurement further.

TABLE 4.3.

Target to detector distance = 35.8 cm.

TARGET MATERIAL	FOIL 1				FOIL 2				E_p/ Current
	X-ray yield per μC	Weighted mean ± Error	σ ~ %	Target Rotation	X-ray yield per μC	Weighted mean ± Error	σ ~ %	Target Rotation	
Copper Foil	101600 ± 319 103005 ± 321 102898 ± 320	102496 ± 451 .4%	638 .6%	No	106336 ± 326 106459 ± 326 105147 ± 324 105402 ± 325 104725 ± 324	105460 ± 368 .3%	676 .6%	No	E_p = 2.4 MeV 1 x 10^{-8} A
	107785 ± 328 107671 ± 328 105625 ± 325 105714 ± 325 105893 ± 325 106334 ± 326 105793 ± 325	106355 ± 352 .3%	864 .9%	No					
	124703 ± 353 124500 ± 353 124763 ± 353 124096 ± 352 124316 ± 352	124432 ± 153 .12%	246 .2%	No	124840 ± 353 123777 ± 352 124553 ± 353 124645 ± 353 123741 ± 351	124445 ± 233 .2%	460 .4%	No	E_p = 2.4 MeV 1 x 10^{-9} A

4.3.2. Keithley electrometer and beam current measurements

In the light of the yield measurements reported in table 4.3., a test was made to check the measurement of current using the Keithley electrometer, which reads a full scale deflection current through 1 volt potential difference across its impedance. It has a range switch and a multiplier switch respectively changeable for (10^{-13} to 10^{-1} A) current and meter scale of 0.01, 0.3, 0.1 and 1 respectively. The current on different scales for a full scale deflection (f.s.d.) was read changing both of the switches at various input impedances, i.e. from $10^8\ \Omega$ to $10^{11}\ \Omega$. Since in this case the reading of current on the Keithley electrometer is dependant on its impedance for $Z > 10^8\ \Omega$, the voltage across the device remains constant at 1 volt, any leakage of current can be detected in the circuit (Figure 4.11A) by comparing the yields/μc at different input impedances as was observed previously at high impedance $\geq 10^9$ ohms. There was no leakage of the current in the circuit on lowering the impedance from $10^9\ \Omega$ of the Keithley electrometer.

In the circuit shown in the figure 4.11.A:

i_L = leakage current

R_L = leakage resistance

i_K = current at the Keithley electrometer (K.E.)

R_K = the effective input resistance of K.E.

As R_L and R_K are parallel, $i = i_L + i_K$ (4.4)

or $$i = \frac{V}{R_L} + \frac{V}{R_K} = V\left(\frac{1}{R_L} + \frac{1}{R_K}\right)$$

Since V is maintained at 1 volt in all cases,

Fig. 4.11A

Beam current measuring System

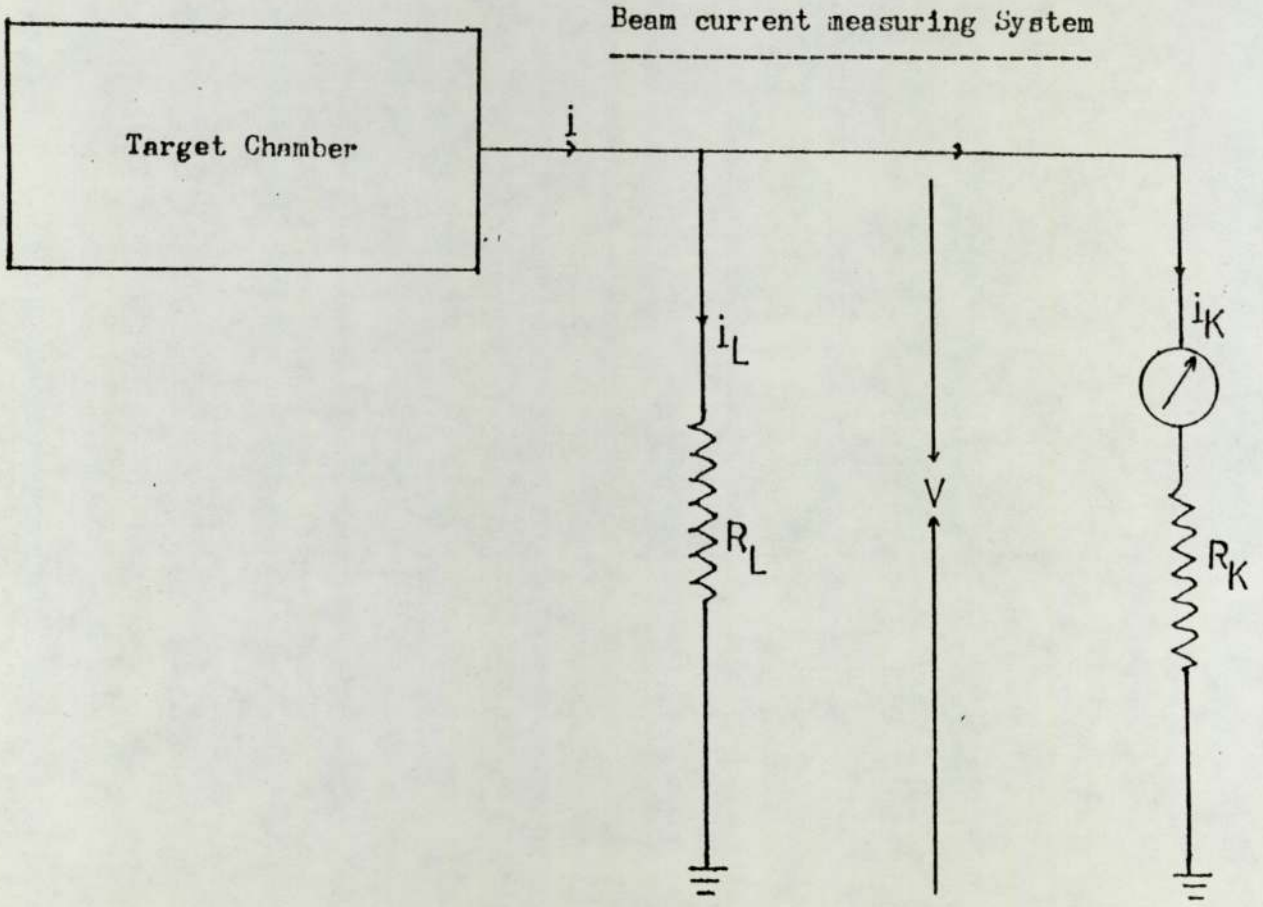

$$i = \frac{R_K + R_L}{R_L R_K} A \qquad (4.5)$$

From figure (4.11A) three possibilities may be observed in current measurement.

1. if $R_K >> R_L$ then there will be significant error in the current measurement;
2. if $R_K = R_L$ then half of the current will be measured;
3. if $R_K << R_L$ then $i_L \simeq 0$;

Last one is a suitable condition to measure an accurate current at the Keithley electrometer. A high impedance or insulation is required between target chamber and ground.

4.3.3. Electrical isolation of the target chamber and reproducibility of the results

Since it was observed that there was a leakage in current from the target chamber at low beam current $\leq 10^{-9}$ A, the target chamber was electrically connected to the Faraday cup and was isolated from the beam pipe and ground to act as a Faraday cup as a whole.

The use of target chamber as a Faraday cup has been a successful method of collecting the net beam current. Duggan et al (DugJ 72) and Johanson et al 1970 have used target chamber to collect the beam and Khan et al (KhaM 76) used a conventional T-piece to collect proton current by isolating it from the beam pipe by employing insulation couplings. To employ this method, an iron stand was provided with the insulation bushes and insulated couplings. They insulate the target chamber from the 4" diameter beam pipe and the floor.

The Faraday cup was also connected electrically to the target chamber to enable this arrangement to neutralize the effect of escaped secondary electrons from the Faraday cup.

Further investigations on the reliability of the designed target rotary system were made after the above modifications for the target current measurement. Two copper foils of 10 microns thickness were again irradiated with protons of 2.4 MeV at different f.s.d. current at Keithley electrometer and at different geometry. They were irradiated several times with the rotation of target and the measurement of the observed x-ray yield/μc for K_α and K_β x-ray lines are tabulated in Table 4.4. Weighted means with their standard errors are also calculated and shown in the table for each f.s.d. of current for the two targets. A good consistency of the x-ray yield was observed for each target and the yields of the two foils at different current agree with 99% confidence, which shows a better agreement than in the previous measurements and indicates the improvements of the measurements after modification of the system.

The reproducibility of the results show the precision and the reliability of the target rotary system. The measurements were made relative to the current measured at the Keithley electrometer and the efficiency parameters and absorption corrections were not taken into account.

The study on the thin target metallic foils using the designed target measuring system for thick and thin target indicated the accuracies of the measurements, achieveable for a

TABLE 4.4.

FOIL 1				FOIL 2				Experimental conditions
No.	Observed x-ray yield for K_α & K_β	Weighted mean ± Error	Target Rotation	No.	Observed x-ray yield for K_α & K_β	Weighted mean ± Error	Target Rotation	
1	241005 ± 490	241771 ± 534 ~ .2% σ = 862 ~ .35%	Target not rotated	1	241544 ± 491	241214 ± 529 ~ .2% σ = 517 ~ .2%	Target not rotated	Ep = 2.4 MeV 3×10^{-9} A
2	242779 ± 492			2	240658 ± 490			
3	240707 ± 490			3	240770 ± 490			
4	242607 ± 492			4	241890 ± 492			
1	241501 ± 491	241565 ± 418 σ = 722 ~ .3%	1st rotation	1	240567 ± 490	240456 ± 351 σ = 600 ~ .25%	1st rotation	3×10^{-8} A
2	242322 ± 492		2nd rotation	2	239802 ± 490		2nd rotation	
3	240878 ± 491			3	241003 ± 491			

target at different energies and different current of proton beam and on several similar targets. A considerable improvement has been observed in the yield measurement after modifications for the beam current measurement in the system. These experimental uncertainties could be considered also for the measurements on several similar biological targets.

CHAPTER FIVE

TARGET PREPARATION AND STANDARDISATION TECHNIQUES

5.1. INTRODUCTION

In PIXE analysis, homogeneity and uniformity of the target materials are very important factors and in case of non-homogeneous bulk materials, the use of an appropriate target preparation method is necessary to produce uniform and homogeneous targets.

J.L. Campbell et al (CamJ 1977) pointed out the suitability of wet digestion technique to prepare the homogeneous target out of non-homogeneous materials. Wet digestion refers to the breakage of cell structure of the sample material by using a chemical solution. Several methods of target preparation have been summarised by R.K.Jolly (JolR 1971),N.F. Mangelson et al (ManN 1977) and J.L. Campbell (CamJ 1977), and several experimenters (UmbC 73, WalR 1974, HidK 1974, MurL, ValV 1973, RudH 1972, HasI 1977, ValV 1974, JohT 1970, ManN 1977, and WalR 1977) , have used these methods successfully to prepare the target specimen of biological and bioenvironmental nature. Thin target deposits or films are usually prepared for qualitative and quantitative analysis to overcome the difficulties of inhomogeneity in unprepared samples.

Since thin target deposits of biological nature are fragile and non-self supportive, backing materials or supporting foils of high mechanical strength are used.

A.W. Harman et al (HerA 1973), R. Walter et al (WalR 1974) , V. Valkovic et al (ValV 1974) and H. Kaji et al (KajH 1977) studied the effect on sensitivity of the backing materials available commercially. Hideo Kubo (HidK 1974) reported a method

to prepare backing foil (collodion foil) spreading collodion dissolved in anilacetate over distilled water. N.F. Mangelson (ManN 77) summarised the characteristics of various backing materials and also reported a basic agent for wet ashing technique. Similar technique has been employed in the present work. Target deposits on Nuclepore filter and pure aluminium foil of thicknesses between 1 mg/cm^2 to 3 mg/cm^2 have been prepared. Their thicknesses were estimated using a microscope and an electronic balance. The reproducibility of the target deposits has been observed as 14%.

5.2. TARGET PREPARATION METHOD

The ideal target sample for irradiation should have the following characteristics:

1. Homogeneity and stability (non fragility);
2. High electrical conductance and heat dissipation;
3. Surface uniformity;
4. Minimum contamination and minimum sample handling.

Most of the homogeneous liquid materials like water can be deposited directly on a clean thin supporting material and metallic foils can be prepared using evaporation chamber methods. Such techniques are reported by E.H. Kobisk et al (KobE 1973) to prepare thin targets both supported and self-supported of most of the elements in the periodic chart. R.K. Jolly et al (JolR 1971) and N.F. Mangelson et al (ManN 1977) summarised the following methods to prepare thin targets of biological and environmental nature:

1. Slicing the frozen tissue by microtome;

2. Animal tissue, plants, etc., are slowly frozen to rupture their cells, followed by mixing them in a high speed mixer to change into liquidized form (JolR 71);
3. Blood, milk and similar other liquids are directly sonicated with an ultrasonic probe to break up the individual cells and deposited directly on the backing foils;
4. Environmental materials are ground using a tungsten carbide mortar and a pestle or a micronising mill;
5. Homogenisation and digestion (wet ashing) of the biological samples;
6. Homogenisation and dry ashing of the biological samples and using diluted glue to deposit the diluted ash on the backing materials.

Most of these methods are reported in PIXE analysis (SanH 1971, HasI 1977, WalR 1974, ManN 1977). Dry ashing of biological materials and the deposition of digested samples on thin backing material of low atomic number is reported (CamJ 77) to be the most sensitive method in PIXE analysis, provided the ashing procedure is free from contaminations. A few volatile elements may not be seen, but the matrix is reduced significantly because of oxidation, thereby resulting in increased sensitivity. Wet ashing or digestion with the use of acid or basic digestive agent such as tetra-methyl-ammonium-hydroxide (TMAH) is reported to be suitable (MurL, HasI 77, WalR 74, ManN 1977) with the use of internal standard. The amount of doped element should be such as not to change the volume of the

matrix by more than 1%. Wet digestion is also preferable in case of non-homogeneous biological materials and environmental specimens and the volatile elements may also be seen, although the sensitivity is less than compared to the dry ash method.

i) Homogenisation of the biological materials

Since most of the biological materials are non-homogeneous they were homogenised with deionised water using a tissue hand grinder (homogeniser). This process helps digesting the tissue completely at a later stage, when the digestive solution is added to the homogenate. In case of homogeneous material, the homogenisation process helps to transform the solid or powdered material to a homogeneous liquid form, therefore the process is very important in the target preparation for both homogeneous and non-homogeneous biological target material.

ii) Choice of digestive solution

I. Hasselmann et al (HasI 1977) and Laila Murthy (MurL) have reported a basic digestive agent for tissue digestion which is T.M.A.H. Although the use of acids at various concentrations is common to digest the biological material, but the material digested in acids reacts strongly with the backing materials. Therefore several digestive solutions were tested on aluminium foils and nuclepore filters to observe the reaction with the foils. It was found that all the tested digestive solutions reacted with the aluminium except tetra-n-butyl ammonium hydroxide in tolune/methanol (B. D. H.). This is a laboratory reagent, generally used as a non-aqueous titrant for weak organic acids which are insoluble in water (B. D. H. A.). It is available in various concentrations of tolune/methanol. Further tests for

tissue digestion show that 0.1N normality of tolune/methonol in tetra-n-butyl ammonium hydroxide $(CH_3(CH_2)_3)_4$ NaoH., was suitable tissue digestive solution and had no chemical reaction with aluminium foils or Nuclepore filters.

iii) Digestion and deposition of target

Wet sample materials were obtained in chunks and washed with deionised water three times and dried for an hour in petri dishes to remove the excess water. One gram pieces of each were taken on ready to use clean glass slides and were covered in petri dishes to avoid air contaminations. In case of dry solid or powdered form, one gram of sample was taken directly from the bulk material without washing it.

One gram of either dry or wet material was collected in a tissue hand grinder with the help of clean forceps and a suitable amount of deionised water was used to homogenise the materials. A dozen or more strokes of the pestle were enough to homogenise the liver tissue and a reddish milky homogenate was achieved. One ml. of homogenate was taken in 5 ml weighing bottle using Oxford samplers (BoeL) and disposable tips. A known small amount of standard solution of known concentration of standard element was used at this stage. The internal standardisation or internal doping can also be done at an earlier stage if required. 1 ml. of digestive solution was used to digest 1 ml. homogenate. Typical quantities in all the process are shown in Table 5.1. for various quantities along with the nature of the thickness of the target deposited with 50 µl. of the digestive homogenate.

The digestive homogenate aliquot of known volume, usually 0.2 ml, 0.1 ml and 0.05 ml and known density, could be deposited on

the backing materials, using the Oxford samplers. Several targets were deposited by dropping the aliquots of digestive homogenate on the backing materials placed on a smooth level surface in petri dishes. Clean paper with holes was used to grip the backing materials during the deposition and evaporation of the aliquots, which usually dried overnight easily at room temperature in petri dishes. This period could be minimised to 1 - 2 hours using a non-contaminated jar with a 60 watt bulb.

5.3. THICKNESS DETERMINATION OF THE DEPOSITS

The area and the weight of the deposit aliquots were measured with the help of a microscope provided with a millimeter grid and with an electronic balance respectively. The area was measured by adding all the squares of the grid, which covered the target deposit on the backing material.

Gravimetric thicknesses of several target deposits were determined by dividing their weights with their areas. The whole procedure of target preparation was found to be suitable for homogeneous and non-homogeneous biological materials.

It was found that the method could be used when the specimen was in minute quantity like biopsy samples. The various component and chemicals used in target preparation method are shown in the photographic plate (figure 5.1.) The thickness of the evaporated deposits were made to range from 1 mg/cm^2 to 3 mg/cm^2 by changing either the amount of deionised water during the process of homogenisation or the volume of the aliquot. Thicker deposits were achieved for "salajeet" than the tissue and other biological materials, due to the nature of the sample.

FIGURE 5·1

TABLE 5.1.

NO.	SAMPLE MATERIAL	VOLUME OR MASS	VOLUME OF DEIONISED WATER	VOLUME OF THE HOMOGENATE	VOLUME OF THE STANDARD SOLUTION	VOLUME OF THE DIGESTIVE SOLUTION	TARGET THICKNESS
1	FLUID:						
	a: Milk	1 ml	1 ml	1 ml	0.1 ml	1 ml	Thin
	b: Blood	1 ml	1 ml	1 ml	0.1 ml	1 ml	Thin
2	SOLID:						
	Dried Frozen Blood	0.1 ml	10 ml	1 ml	0.1 ml	1 ml	Thin
3	POWDER:						
	Bioenvironmental specimen "Salajeet"	1 gram	10 ml	1 ml	0.1 ml	1 ml	Semi-thick
4	POWDER:						
	NBS-SRM.1577 Bovine Liver	1 gram	10 ml	1 ml	0.1 ml	1 ml	Semi-thick
5	Wet Kidney	1 gram	2.5 ml	1 ml	0.1 ml	1 ml	Thin
6	Wet Sheep's						
	a : Liver	1 gram	5 ml	1 ml	0.1 ml	1 ml	Thin
	b : Tissue	1 gram	5 ml	1 ml	0.1 ml	1 ml	Thin

TABLE 5.2.

Sample Material	Thicknesses of the different volumes of the digestive homogenate deposited in mg/cm^2.		
	50 μl	100 μl	200 μl
Sheeps liver	1.34	1.91	2.787
deposited on	1.31	2.04	2.807
Aluminium	1.33	2.00	2.788
Mean Value	1.328 ± 0.0153	1.983 ± .066	2.822 ± .036
	~1.1%	~ 3.3%	~ 1.3%
NBS - 1577	1.81	2.90	3.37
Bovine liver	1.78	2.78	3.29
deposited on	1.72	3.1	3.28
Aluminium	1.89	2.83	3.30
Mean Value	1.800 ± 0.07	2.902 ± 0.071	3.310 ± 0.04
	~ 3.9%	~ 2.4%	~ 1.2%
Sheep's kidney	1.38	2.60	-
deposited on	1.41	2.50	-
Aluminium	1.45	2.32	-
Mean Value	1.413 ± 0.035	2.466 ± 0.082	
	~ 2.5%	~ 3.3%	

All the deposited aliquots on backing materials were sandwiched between the target holding frames and made ready for irradiation. Target deposits from liquid and solid biological materials are shown in figure 5.2. Disposable hand gloves were used during the process of target preparation to avoid hand contaminations to the targets and to safeguard the hands from contamination by the chemicals.

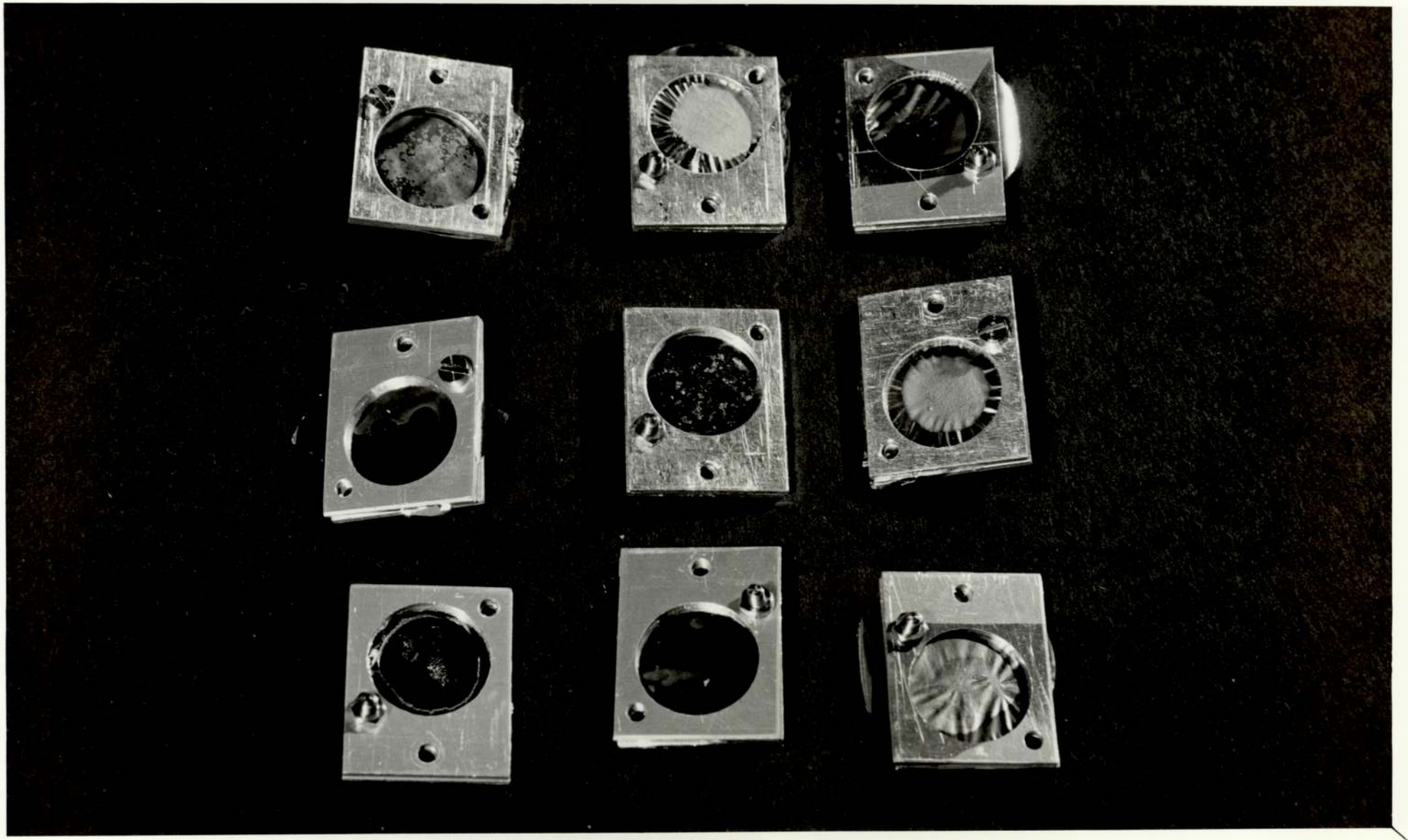

FIGURE 5-2

5.4. REPRODUCIBILITY OF THE TARGET DEPOSITS

Ten target deposits, each of 50 $\mu\ell$ and 100 $\mu\ell$ and seven target deposits of 200 $\mu\ell$ aliquots were deposited on aluminium foils of 12.5μm thickness of equal weights. These target deposits were prepared from sheep's wet liver and kidney and a standard biological material (NBS-1577), bovine liver in dry powder form, and the thicknesses of different amounts of the target aliquot are tabulated in table 5.2., along with their mean values. The variation of the thickness versus volume was determined for different samples.

Accuracy of the area measurements was 12% based on the number of incomplete squares near the edges of the deposit and the number of complete squares. An accuracy of 4% was observed in weighing nine similar 12.5μm thick commercial aluminium foils using the electronic balance. The standard deviations on the mean values of several deposits of equal volumes each for three target materials at different volumes of deposit aliquots are shown in table 5.2. They were between 3.9% and 1.1% on their respective mean values. An accuracy of 1% is reported on the volumetric transformation using Oxford samplers and a reproducibility of 99% is given for the disposable tips used in these transformations. Both of them were used at least five times during the processes of homogenisation, standardisation, digestion and deposition of the target material. This gives a composite error of $\backsim$ 3.2% quadratically on the use of the sampler and the disposable tips. Adding all the errors quadratically, i.e. 12%, 4%, 3.9% and 3.2%, a maximum error of 14% is estimated for the target preparation.

5.5. BACKING MATERIALS

Since thin target films of biological materials are fragile and non-self supporting (WilR 1977) , they are required to be deposited on a backing material. A suitable choice of backing material is therefore necessary with respect to the target material. A.W. Herman et al (HerA 1973) and J.L. Campbell et al (CamJ 1977) pointed out the following criteria for a suitable backing material:

1. Non-stretching and good adherence to the target deposits;
2. Inertness with the chemicals and other composits of the deposits;
3. Ability to withstand the proton bombardment of a sufficient beam current to acquire the required data;
4. Capable of conducting heat and reducing the build-up of charge;
5. Mechanical strength or stability in handling and processing with the target preparation;
6. Light matrix to achieve a high peak-to-background ratio;
7. Purity to achieve the best analytical results.

Johansson et al (JohT 1970) used commercial 20 and 40 mg/cm^2 carbon foils, and found a large quantity of impurities and they are fragile in spite of their good heat and charge conduction. Flocchini et al (FloR 1972) studied the background spectra generated from the ion bombardment on the organic backing material (Mylar, Kapton and teflon) of thickness ranging from 700 to 1000 mg/cm^2. Gordon et al (GorB 1972) used 1-250 nA proton beam of 3.2 - 3.5 MeV energy in an effort to compare the brems-strahlung from various backing materials, i.e. aluminium, Kapton, thick target reactor grade graphite and 50 mg/cm^2 carbon foil.

Formvar has been examined by many of the workers (WalR 1974, HidK 1974, and WilR 1977) using PIXE analysis. J.L. Campbell (CamJ 1977) has reported the successful preparation of Formvar film by Grader et al (GraR 1971) and Bearse et al (BeaR 1974) and their use in PIXE analysis by Walter et al (WalR 1974). He also mentioned that Formvar dominates the other backing material regarding its use in PIXE analysis. He described various methods to improve the Formvar's ability to withstand proton beam of 20 n A.

H. Kaji et al (KajH 1977) studied the production of bremsstrahlung at different angle to proton beam of 3.5 MeV energy using Mylar film and other commercial backing materials. The uses of polystyrene and collodion solutions are reported by Hideo Kibo et al (HidK 1974) to make backing films on the surface of deionised water. Nuclepore filter is also reported (WalR 1974 and NieK 1976) as one of the strong and low bremsstrahlung generating material. The porosity of Nuclepore acts as an adhesive for the target deposits, resulting in a stable target backing configuration. It also provides a good backing especially to homogenised liquid deposits and to emulsified materials (CamJ 1977).

From the above review, the target material can be categorised into three groups:

1. organic backing materials;
2. aluminium and carbon foils;
3. Nuclepore filters.

Carbon and Formvar are low bremsstrahlung generating materials but carbon foil is fragile and its use is not suitable because of

trace impurities. Formvar is unstable against proton beams above 1.5 n A / m^2. It is non-heat conductive and reactant to chemicals, and it is non-fragile. Other organic materials are similar to Formvar in their characteristics, but they are fragile relative to Formvar and Nuclepore filters and basically depend on their preparation methods.

Aluminium foils are good for heat conduction and are mechanically stronger than carbon and some organic backing materials, but they generate a high bremsstrahlung (HerA 1973). They are available commercially in ready to use spectroscopic pure form, but only in limited sizes. They withstand high beam currents up to several miliamperes. They are not attacked as much by chemicals as organic backing materials.

Nuclepore filters are low bremsstrahlung generating backing materials and have lower impurities than carbon and aluminium foils, but they stretch on the deposition of target material and get contaminated from atmospheric air due to their porosity. They are however preferable to other organic backing films. Semi-thick Nuclepore filters are available commercially. Trace elemental impurities and a few characteristics of most of the backing materials used in PIXE analysis are summarised in table 5.3.

Commercial aluminium foils of 12.5 μm thickness and 8 μm thick Nuclepore filters were used as backing materials in the present work. Both types have different matrix and each was irradiated with the protons of 2.4 MeV energy. Their observed x-ray yields/μC were compared as they were irradiated under the same experimental conditions, (table 5.4.). Their spectra are shown in

TABLE 5.3.

NO.	CHARACTERISTICS	CARBON FOILS	FORMVAR	POLYSTYRENE	COLLODION	NUCLEPORE	ALUMINIUM FOILS
1	Purity/ Impurities in p.p.m.	Variable/ High	Excellent/ Low	Subject to preparatory methods	Subject to preparatory methods	Excellent/ Low	Acceptable/ Variable
2	Mechanical strength	Fragile	Good	High Breakage Rate	High Breakage Rate	Good	Good
3	Acid/Alkaline Resistance	Excellent	Poor	Poor	Poor	Acceptable	Acceptable
4	Beam Tolerance	Excellent	Poor	Poor	Poor	Acceptable	Excellent
5	Adherence	Excellent	Poor	Poor	Poor	Good	Poor
6	Bremsstrahlung Generation	Low	Low	Low	Low	Low	High

figures 6.14 and 6.15 respectively. The comparison of x-ray yields shows that the aluminium foil produces 4.5 times higher bremsstrahlung than Nuclepore filters, in spite of its being thin and low energy loss of proton through it.

TABLE 5.4.

Backing Material	Thickness in μm	Energy loss keV	Irradiation time	Counts /μc	Mean
Nuclepore filter cellulose ($C_6H_{10}O_5$)	8	1.64	¾ hour	1343 ± 37	1416 ±65
			900 sec	1522 ± 39	
			½ hour	1382 ± 37	
Aluminium foils	12.5	32.09	900 sec	6246 ± 79	6100 ±136
			900 sec	5853 ± 77	
			1 hour	6200 ± 79	

The results show quite a wide variation, because they were taken for different aluminium foils and Nuclepore filters.

5.6. STANDARDISATION OF THE TARGETS

Standard solutions were prepared to standardise (dope) biological materials and a standard reference material (NBS-1577) in homogeneous powdered form. Targets of doped standard material were irradiated in order to establish internal standard (dopant) and the trace elemental measurements. Two laboratory compounds i.e. yttrium nitrate ($Y(NO_3)_3 6.H_2O$) and cadmium sulphate ($3\ Cd.SO_4.8H_2O$) were used to prepare standard solution with distilled water. They were chosen to be used as suitable dopants, because they are very rare in biological materials. The standard

solutions were introduced into the homogenate samples of the target materials in such an amount so as to make the required concentration of yttrium and cadmium in the target deposits.

5.6.1. Concentrations of dopants in the standard solutions in terms of weight

The molecular weight of both of the compounds respectively are 384.04 and 769.53 g/mole. 2.133 gram of yttrium nitrate and 1.13 gram of cadmium sulphate were used with distilled water to make 100 ml of standard solutions respectively to achieve the following concentrations:

A. Amount of yttrium in 1 ml $= \frac{88.9 \times 0.02133}{384.04} = 4.94$ mg/ml

B. Amount of cadmium in 1 ml $= \frac{112.4 \times 3 \times 0.0113}{769.53} = 4.95$ mg/ml

Since densities of the standard solutions are necessary to calculate the concentrations of the dopants in P.P.m. by weight, they were determined practically using 5 ml weighing bottles and tabulated in the table 5.5, along with the concentration of dopants in P.P.m.

TABLE 5.5.

No.	Concentration	Dopant	Densities	Dopant concentration in P.P.m.
1.	4.94 mg/ml	Y	1.019 g/cc	4805
2.	4.95 "	Cd	1.022 "	4805
3.	0.988 "	Y	1.014 "	969
4.	0.99 "	Cd	1.015 "	969
5.	0.0988 "	Y	1.009 "	97
6.	0.099 "	Cd	1.010 "	97

5.6.2. Concentrations of dopants in terms of atoms in standard solutions

A. Yttrium nitrate:

($Y(NO_3)_3 6.H_2O$) 1 ml of this compound contained 0.02133 g. of yttrium nitrate when

384.04 gram contains $31 \times 6.02 \times 10^{23}$ atoms (1)

Therefore 0.02133 gram contains $\frac{31 \times 6.02 \times 10^{23} \times 0.02133}{384.04}$

$= 0.010365 \times 10^{23}$ atoms

and 0.02133 gram contains y $\frac{6.02 \times 10^{23} \times 0.02133}{384.04}$ atoms

$= 0.000334 \times 10^{23}$ y atoms

since 1.019 g/ml is the density of the yttrium nitrate solution of 4.94 mg/ml concentration, 1 ml. of st. solution contains (1.019 - 0.02133) = 0.99767 g of water and

18.016 grams of water contains $3 \times 6.02 \times 10^{23}$ atoms (2)

therefore 0.99767 g of water contains $\frac{3 \times 6.02 \times 10^{23} \times 0.99767}{18.016}$

$= 1.0001 \times 10^{23}$ atoms.

Total number of atoms in 1 ml of standard solution = 1.01047×10^{23} atoms

Therefore concentration of yttrium atoms in the standard solution

$= \frac{.000334 \times 10^{23}}{1.01047 \times 10^{23}}$ = 330 P.P.m.

B. Similarly, the concentration of Cd. atoms was calculated in its solution to be 260 P.P.m.

5.6.3. Concentration of Dopants in the target deposits

i) 0.1 ml of yttrium nitrate and cadmium sulphate were introduced into 1 ml of the homogenate separately and each mixture was digested with 1 ml of the digestive solution. The quantities are shown in table 5.1. The densities of the standardised digestive homogenate samples were determined gravimetrically to be 0.9338 g/cm^3 and 0.9401 g/cm^3 respectively. The masses of the homogenate were 1.961g and 1.97 g respectively. The volume of each of the standardised digestive homogenate was 2.1 ml after standardisation and contained 494 mg yttrium and 495 mg of cadium respectively. Hence the concentration of yttrium and cadmium in 1 gram of each standard digestive homogenate was 494/1.961 = 252 P.P.m. and 495/1.974 = 250 P.P.m.

ii) 0.05 ml of each of the standard solutions was used together to standardise 1 ml of the biological homogenate which was digested with 1 ml of the digestive solution and the density of the standardised digestive homogenate was determined to be 0.934 g/ml. The volume of the standardised digestive homogenate was 2.1 ml and it contained 247 mg and 248 mg of yttrium and cadmium. Therefore the concentrations of yttrium and cadmium by weight was calculated to be $\frac{247}{2.1 \times 0.934}$ = 126 P.P.m. and $\frac{248}{2.1 \times 0.934}$ = 126 P.P.m. respectively.

TABLE 5.6.

Run	Observed FeKα x-ray yield/100 μc	Observed Y Kα x-ray yield/100 μc	Observed Cd-Kα yield/100 μc	Standardised Target Material
A	23278 ± 152	9840 ± 99	1068 ± 33	Target
B	25529 ± 160	10376 ± 102	1178 ± 34	OKD01
C	24629 ± 157	9910 ± 99	1049 ± 32	NBS-1577
D	25300 ± 159	11327 ± 106	1155 ± 34	Yttrium
E	24762 ± 157	9850 ± 999	1070 ± 33	& cadmium
F	24350 ± 156	10178 ±1101	1086 ± 33	concentra-
weighted mean ± st. error	24613 ± 325 ~1.3%	10221 ± 231 ~2.3%	1096 ± 22 ~2%	tions 125
st.dev. (σ)	728 ~ 3%	520 ~ 5%	48 ~ 4.4%	p.p.m.
A	25178 ± 159	9780 ± 99	1120 ± 33	Target
B	25141 ± 158	9778 ± 99	1140 ± 34	deposit
C	24990 ± 158	9701 ± 95	1149 ± 34	OKD02
D	25227 ± 159	9760 ± 99	1137 ± 34	NBS-1577
E	23909 ± 155	9270 ± 96	1068 ± 33	Yttrium
weighted mean ± st. error	24878 ± 247 ~ 1%	9530 ± 117 ~1.2%	1123 ± 15 ~1.3%	& cadmium
st.dev. (σ)	496 ~ 2%	196 ~ 2%	28 ~ 2.5%	concentra-
				tions 125
				p.p.m.

TABLE 5.7.

Run	Fe Kα/Y Kα	Fe Kα/Cd Kα	YKα/Cd Kα	Target Deposit
A	2.36 ± 0.03	21.79 ± 0.67	9.22 ± 0.29	
B	2.46 ± 0.03	21.67 ± 0.73	8.81 ± 0.28	
C	2.48 ± 0.03	23.47 ± 0.74	9.44 ± 0.30	125 P.P.m.
D	2.23 ± 0.03	21.90 ± 0.66	9.8 ± 0.30	Cd and Y
E	2.51 ± 0.03	23.14 ± 0.71	9.19 ± 0.28	
F	2.39 ± 0.03	22.42 ± 0.69	9.37 ± 0.29	
weighted mean	2.41 ± 0.04 ~ 1.7%	22.46 ± 0.30 ~1.3%	9.32 ± 0.14 ~1.5%	
st.dev. (σ)	0.09 ~ 3.7%	0.69 ~ 3%	0.3 ~ 3.2%	

TABLE 5.7. (continued)

Run	Fe K_α/Y K_α	Fe K_α/Cd K_α	YK_α/Cd K_α	Target Deposit
A	2.57 ± 0.03	22.48 ± 0.68	8.73 ± 0.27	
B	2.57 ± 0.03	22.05 ± 0.76	8.58 ± 0.27	125 P.P.m.
C	2.57 ± 0.03	21.75 ± 0.66	8.44 ± 0.27	Cd and Y
D	2.57 ± 0.03	22.18 ± 0.67	8.15 ± 0.25	
E	2.58 ± 0.03	22.38 ± 0.67	8.48 ± 0.27	
weighted mean	2.57 ± 0.002 ∽ .08%	22.15 ± 0.12 ∽ .5%	8.49 ± 0.09 ∽ 1.1%	
st.dev. (σ)	.004 ∽ .15%	.26 ∽ 1.2%	.19 ∽ 2.2%	

5.6.4. Reproducibility of the concentrations of the dopants in the targets

A known amount (5-1000 P.P.m.) of yttrium and cadmium were introduced to the digestive homogenate of a standard biological material (NBS-1577) to establish a test on the internal standards (dopants) by scaling their observed K_α x-ray yields/100 μc with the yield of iron K_α x-ray in the standard material. The x-ray yields for iron, yttrium and cadmium are tabulated in table 5.6 for the two similar targets OKD01 and OKD02 in which similar aluminium foils were used as backing material. Each target was irradiated several times (A, B, C ....) under the same experimental conditions with protons of 2.5 MeV energy. Weighted means on several irradiations on each target for iron and the dopants with their respective standard errors were also calculated as shown in the table 5.6. The standard deviation on the measurements for each of the three elements was observed ± 3%, ± 5% and 4.4% respectively for the first target and ± 2.0%, 2.0% and 2.5% respectively for the second target. Most of the sets of

measurements are consistent within 95% confidence limit, using S^2/σ^{-2} criterion (HerH 78), where S is the estimated standard deviation of n measurements and σ^{-2} is the variance of the counting distribution function. Comparing the x-ray yield/100μc of the two targets for Fe, Y and Cd respectively, it was observed that the yields agreed for each element by 80 per cent confidence, after applying t-distribution and corresponding test procedures. The values of t(n) were 0.43, 1.24 and 0.49 using the formula (MulR 72) for the comparison.

$$t(n) = \frac{x' - x}{\sqrt{(\sigma_{x'}^2 + \sigma_x^2)}} \qquad (5.1)$$

where t(n) is the value of the t-distribution for n measurements

x' and x are two mean values of n measurements and

$\sigma_{x'}$ and σ_x are the standard deviation on the values.

The relative yields of Fe K_α to Y K_α, Fe K_α to Cd K_α and Y K_α to CD K_α, x-rays were also calculated for each target for consistency checks and are tabulated in table 5.7. Weighted means on the relative yields for each target was calculated with their standard deviations using x-ray yields (table 5.6.). The errors on each relative yield depends on the statistical errors on the K_α x-ray yields of two elements and are added quadratically to give the composite errors. Standard deviation on the relative measurements show that the relative yield is fairly consistent within the statistical errors mentioned.

CHAPTER SIX

ANALYSIS OF THE BIOLOGICAL MATERIALS

6.1. INTRODUCTION

The observed x-ray yield/μc for the irradiated metallic foils (Chapter 4) and the measurements on the doped targets of a standard material NBS-SRM 1577 in Chapter 5, are important in order to establish the reliability of the target mounting design and the reproducibility of the measurements.

In addition, a number of biological standardised thin and semi-thick targets of different concentration of standard have been irradiated and the linearity of the concentrations versus observed x-ray yield determined.

Several doped and undoped targets of biological and bio-environmental nature were also irradiated and identifications were made for the detectable elements. A comparison was made between the elements detected and the ones known to be present. The trace elements detected in case of salajeet and other biological materials are briefly discussed indicating their dietary and clinical significances. Quantitative measurements have been made for the standard reference biological material using iron as reference element and the recovery of internal standards was determined. The elemental concentrations were calculated relative to iron using observed x-ray yields, x-ray production cross sections and their atomic masses. The determined values of trace elements were compared with the latest quantitative analysis of bovine liver (CooJ 73, WilR 74, JolR 78).

6.2. LINEARITY OF INTERNAL STANDARDS

The use of internal standards has been discussed by various

authors (NobA 76, CamJ 77). It is a convenient method to normalise the x-ray yields in the targets of thick and intermediate thicknesses and particularly useful in the thin target technique, where the exact target thickness is difficult to determine (NobA 76).

In order to establish the internal standards for the measurements, eighteen doped targets of known amount of standard ranging from (5 - 1000 P.P.m.) and three undoped targets of various biological materials were prepared by depositing 50 μl and 100 μl of their standard digestive homogenate on pure Al foil and Nuclepore filters respectively. They were irradiated with 2.4 MeV protons and the results in x-ray yield/10 μC are tabulated in table 6.1. and 6.2. for 50 μl and 100 μl target deposits respectively. Ratios of iron Kα to copper Kα observed x-ray yields were evaluated in order to characterise the target materials and are tabulated along with the results in a separate column. Due to a lower level of copper content in salajeet, a ratio of iron Kα to titanium Kα x-ray counts was used.

A reproducibility of not less than 85% in the observed x-ray yields was observed for yttrium standard within the targets of the same concentration.

This was perhaps expected within the different target materials, because of the slight change in their target thicknesses due to unequal fluidity of their digestive homogenates.

Since an average value of observed x-ray yields of yttrium at the deposits of different materials at the same concentration could represent its yield, the weighted means on the yields were calculated for each set of measurements for a particular yttrium concentration. The mean values for 1000, 250 and 5 P.P.m. at 50 μl

TABLE 6.1.

Target Number	Target Material	Backing Material	Concentration of yttrium p.p.m.	Fe/Cu K_α x-rays	Fe/Ti K_α x-rays	Observed γ counts/10μc	Weighted means ± standard error	Volume of the target aliquots
1	Salajeet	Nuclepore	1000	-	10.56±0.04	5163±72		
2	Salajeet	Aluminium	1000	-	10.93±.05	4754 ± 69		
3	NBS-1577	Nuclepore	1000	2.6 ± 0.02	-	5557 ± 75	5097 ± 171 ≃ 3.4%	
4	NBS-1577	Aluminium	1000	2.8 ± 0.1	-	4969 ± 70	σ = 295	
5	Whole blood	Aluminium	250	14.2 ± 0.1	-	1253 ± 35		50 μl
6	NBS-1577	Aluminium	250	3.1 ± .08	-	1222 ± 35		
7	NBS-1577	Aluminium	250	3.1 ± .08	-	1325 ± 36	1238 ± 39 ≃ 3.2%	
8	Milk	Nuclepore	250	5.5 ± 0.36	-	1225 ± 35	σ = 44	
9	S.kidney	Aluminium	250	5.8 ± 0.2	-	1195 ± 35		
10	Whole blood	Aluminium	5	15.4 ± .23	-	31 ± 7		
11	NBS-1577	Aluminium	5	3.0 ± 0.2	-	32 ± 6	31 ± 6	
12	NBS-1577	Aluminium	0	2.4 ± 0.1	-	0	0	

TABLE 6.2.

Target Number	Target Material	Backing Material	Concentration of yttrium p.p.m.	Fe/Cu K_α x-rays	Fe/Ti K_α x-rays	Observed γ counts/10 μc	Weighted means ± standard error	Volume of the target aliquots
1	S.kidney	Nuclepore	250	6.0 ± 0.5	-	2007 ± 45		
2	Salajeet	Nuclepore	250	-	9.9 ± 0.5	2201 ± 47		
3	Salajeet	Nuclepore	250	-	10.7 ± 0.7	2145 ± 46	2091 ± 53	
4	Salajeet	Nuclepore	250	-	10.8 ± 0.9	2000 ± 45	∫ 2.5%	
							σ = 87	
5A	NBS-1577	Nuclepore	125	1.9 ± 0.09	-	1181 ± 34		
B	NBS-1577	Nuclepore	125	1.9 ± 0.08	-	1120 ± 33		100 μl
C	NBS-1577	Nuclepore	125	1.9 ± 0.06	-	1152 ± 34		
D	NBS-1577	Nuclepore	125	1.9 ± 0.04	-	1148 ± 34	1150 ± 8	
							∫ 0.5%	
							σ = 16	
E	NBS-1577	Nuclepore	125	1.9 ± 0.03	-	1163 ± 34		
F	NBS-1577	Nuclepore	125	1.9 ± 0.02	-	1142 ± 34		
G	NBS-1577	Nuclepore	125	1.9 ± 0.02	-	1130 ± 33		
6	S.kidney	Aluminium	5	6.4 ± 0.4	-	48 ± 7	46 ± 2	
7	S.kidney	Aluminium	5	5.4 ± 0.4	-	44 ± 7		
8	NBS-1577	Aluminium	0	2.2 ± 0.09	-	0		
9	NBS-1577	Aluminium	0	2.2 ± 0.09	-	0	0	

deposits and 250, 125 and 5 P.P.m. at 100 μl deposits are also shown in the tables 6.1. and 6.2. These values were plotted against their concentrations for 50 μl and 100 μl deposits as shown in figures 6.1. and 6.2. The error bars shown to the points for the mean x-ray yields in the figures are the standard errors on the weighted means.

The graphs in figure 6.1 and figure 6.2 show a reasonable linearity of the yields of the dopant to its concentration respectively in twenty-one targets of 50 μl and 100 μl deposits of various biological and bioenvironmental materials.

It was noticed that the target deposits at the same concentration and the same volume of the deposited aliquot of the same target material show a significant ∽ 10% variation in x-ray yield/10 μC (table 6.1.) therefore a further study was made to see the effect on the x-ray yields due to the thickness variation of the target deposits of the same material and at the same yttrium concentration.

6.3. THICKNESS VARIATION AND ITS EFFECT ON X-RAY YIELDS

Four target deposits of standard material (NBS-1577) were doped with 125 P.P.m. Y. and irradiated several times with the protons of 2.5 MeV energy. Their observed YK_{α} x-ray yield/10 μC were recorded and the results are tabulated in table 6.3.

The relative x-ray yields of iron K_{α} to CuK_{α} were calculated from the measurements to determine the effect of the variation of the target thickness. They are also shown in the table 6.3. The weighted mean and the mean relative yield was calculated for the set of measurements on each target (table 6.3.).

Fig. 6.1

Linearity of internal standard

E_p; 2.5 MeV

50 µl Wet deposits

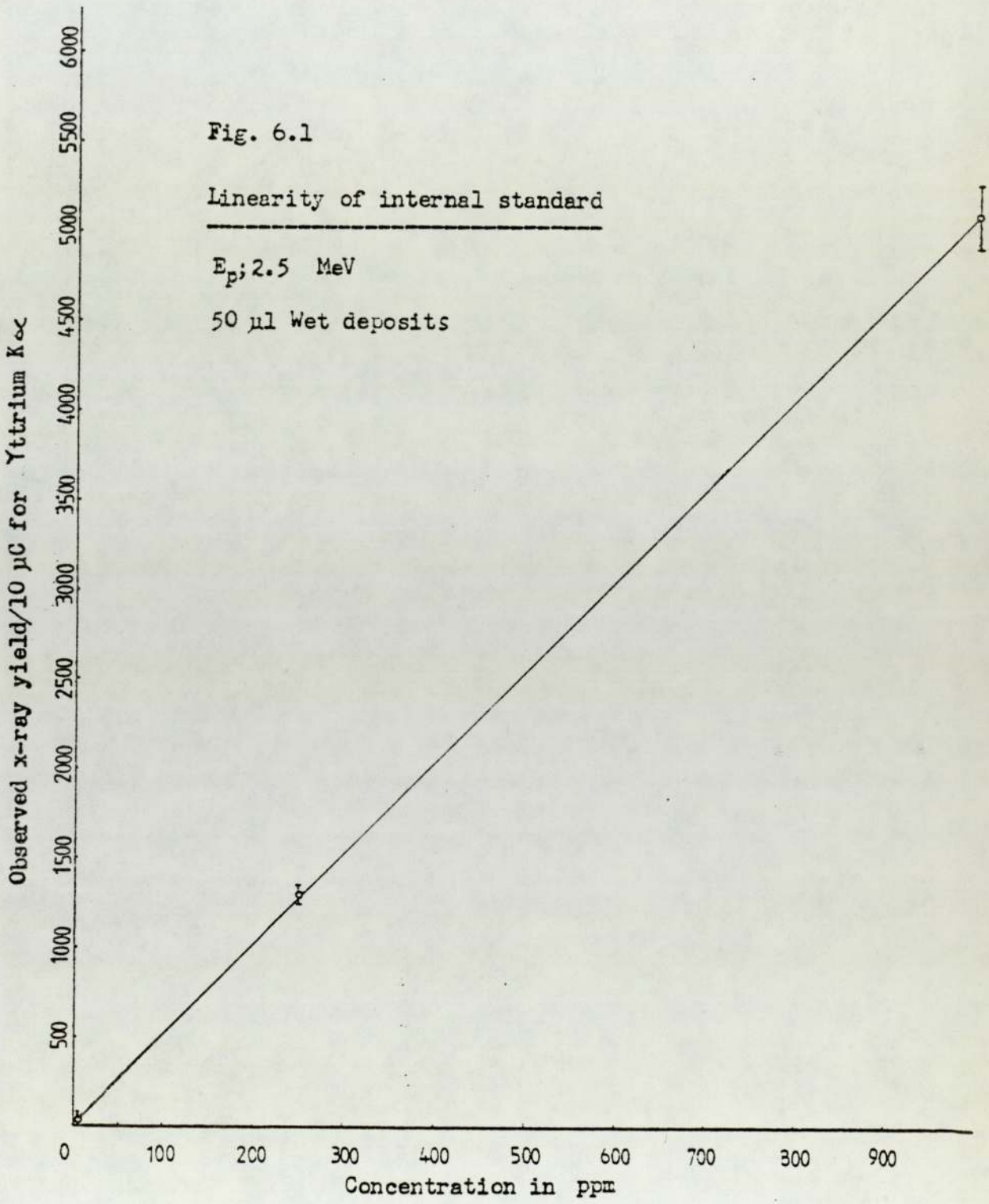

Fig. 6.2

Linearity of internal standard

E_p; 2.4 MeV

100 µl Wet deposits

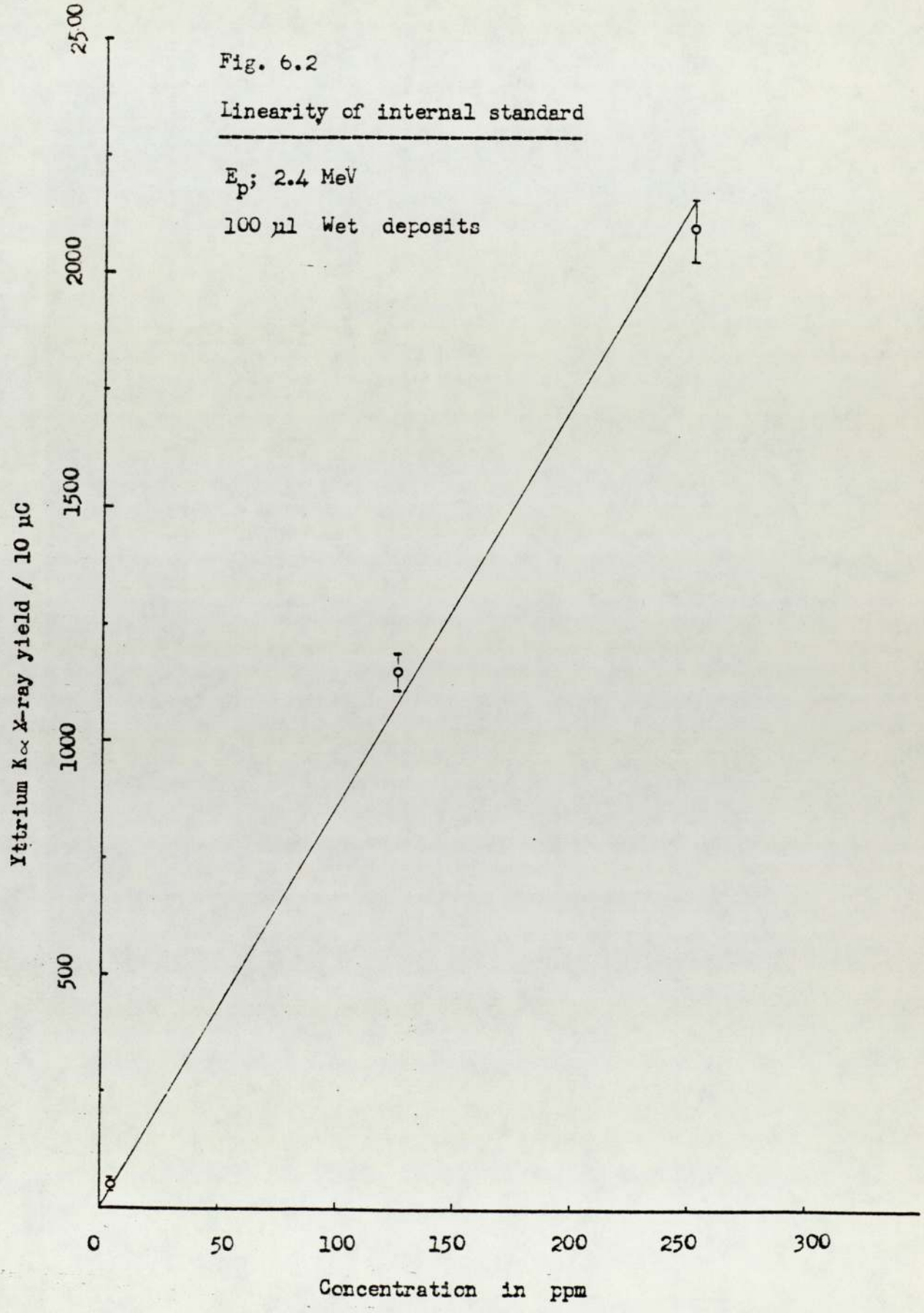

TABLE 6.3.

Target thickness in g/cm^2	Target Run	Yttrium observed x-ray yield/10 μC ± statistical error	Weighted mean ± standard error	Relative yield ± St.error FeK_α/CuK_α	Mean value for the rel.yield FeK_α/CuK_α
	A	978 ± 31		2.9 ± 0.06	
	B	978 ± 31		2.9 ± .08	
1.8	C	970 ± 31	962 ± 14 ~1.4%	2.9 ± .07	2.9 ± .15
(50 μl)	D	977 ± 31		2.9 ± .07	
target	E	909 ± 30	σ = 34 ~3.5%	2.9 ± .06	
aliquot					
1.9	A	986 ± 31		2.5 ± .05	
	B	1008 ± 32	1000 ± 8 ~.7%	2.5 ± .05	2.5 ± .10
(50 μl)	C	991 ± 31		2.6 ± .05	
target	D	1017 ± 32	σ = 13 ~1.3%	2.5 ± .05	
aliquot					
2.26		1110 ± 33	1110 ± 33	2.2 ± .05	2.2 ± .05
(100 μl)					
	A	1294 ± 36		1.9 ± 0.09	
	B	1236 ± 35		1.9 ± 0.08	
2.61	C	1262 ± 35	1258 ± 8 ~ 0.5%	1.9 ± 0.06	
	D	1258 ± 35		1.9 ± 0.04	1.9 ± .15
(100 μl)	E	1274 ± 36		1.9 ± 0.03	
target	F	1251 ± 35	σ = 19 ~1.5%	1.9 ± 0.02	
aliquot	G	1249 ± 35		1.9 ± 0.02	

Fig. 6.3

Linearity of internal standard and the relative yield

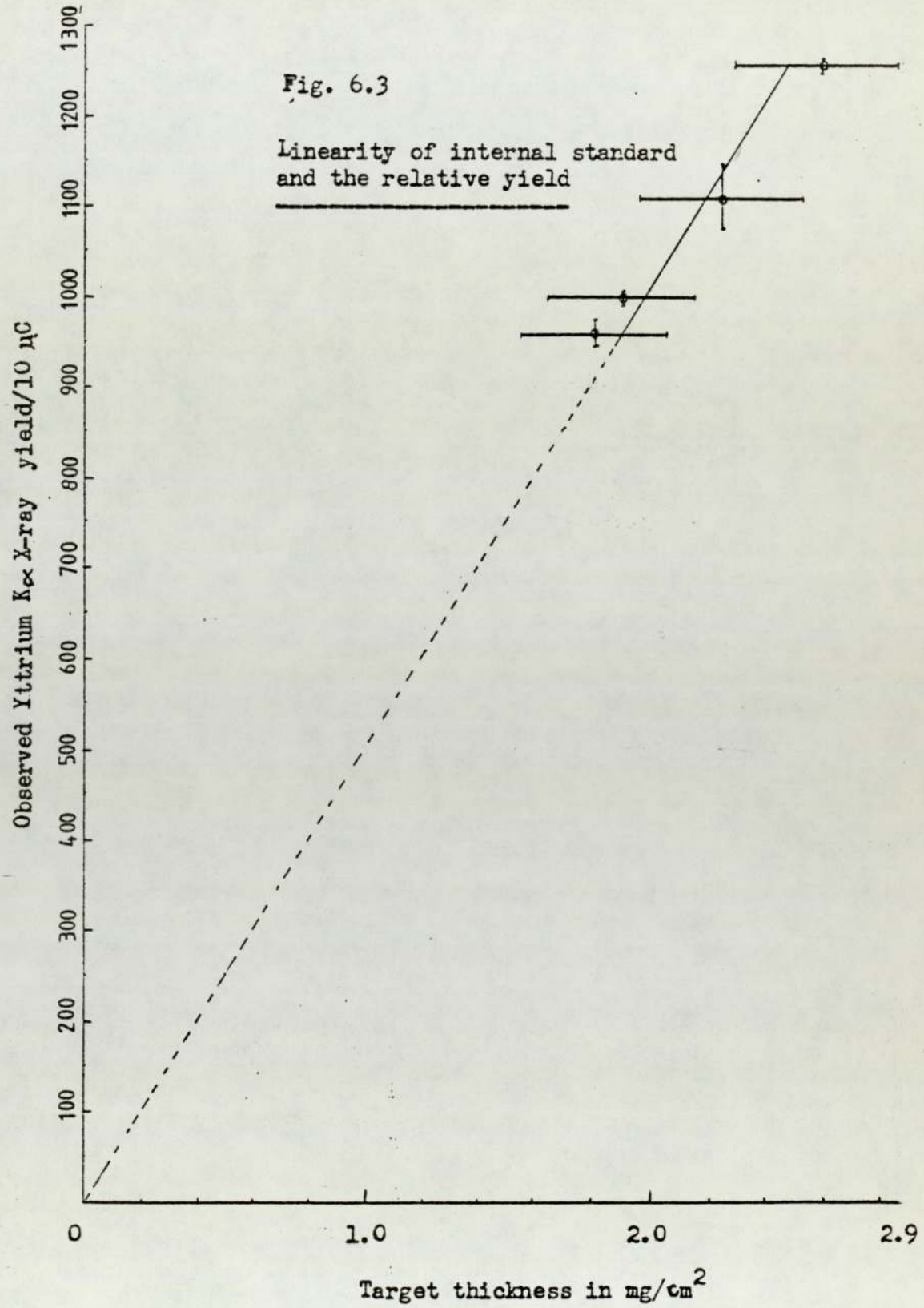

The weighted means were plotted against the thicknesses of the target deposits in mg/cm^2, as shown in figure 6.3., and a linear relationship was observed, because the absorption of yttrium K_α x-rays in the targets is negligible. The error bars shown are the standard errors on the weighted means and on the target thickness. The mean values on the relative yields Fe/Cu for the four targets were also plotted versus the thickness of the respective targets as shown (curve) in the figure 6.4.A The curve indicates that the iron K_α to copper K_α relative x-ray yield decreases on increasing the target thickness, which may be possible due to the fact that iron x-rays, being lower energy x-rays, are absorbed more in the target matrix than the copper x-rays, during their passage. Absorption of x-rays was therefore studied to account the variation in the figure. The major constituent elements of biological specimens are hydrogen, carbon, nitrogen and oxygen (BowH 74) and wet human tissue has $\backsim$ 70% of water in it (ICRP 59), therefore carbon, nitrogen and oxygen remained the major constituents on dry basis. Since the major elements of bovine liver were not exactly known except nitrogen, which is 10.6% (NBS), carbon concentration $\backsim$ 88.4% were used with 10.6% concentration of nitrogen to calculate the absorption of characteristic x-rays due to the target matrix. J.L. Campbell et al pointed out that the carbon can be used as a representative target matrix for dried biological specimens. Data values from Storm and Israel (StoI 70) were used to calculate the percentage absorption of x-rays for the target of different thicknesses, of dry ashed prepared biological deposits.The values at different x-ray energies for various thicknesses are shown in table 6.4. These values were also plotted versus their respective x-ray energies as shown in figure 6.4. from which the variation

in the relative yield measurements (figure 6.4.A) as a function of target thickness was determined. The Fe K_{α} to Cu K_{α} relative yield calculated from equation 6.11 was calculated to be 2.4 for a very thin target deposit of Bovine liver. Using this value, the relative yields were calculated for the four target deposits of similar thicknesses as those of our experimental ones, taking into account the absorption of Fe and Cu K_{α} x-rays. The variation in the relative yields was found to be only $\backsim$ 0.7% to 1.1% compared with the variation of 30% in the relative yield found experimentally.

This discrepancy may possibly be due to target contamination and/or the loss of trace elements during the target preparation process and its deposition.

Subsequent measurements in section 6.5 shows an improvement in the variation of the relative yield due to a more careful target preparation technique.

Table 6.4.

Energy of x-rays (keV)	mass absorption co-efficient in cm^2/g C 88.4% + N 10.6%	% Absorption of x-ray at different energies for various thicknesses			
		1.8 mg/cm^2	1.9 mg/cm^2	2.26 mg/cm^2	2.61 mg/cm^2
3	93.29	15.46	16.24	19.00	21.61
4	39.896	6.90	7.30	8.62	9.89
5	20.17	3.56	3.76	4.46	5.13
6	11.488	2.05	2.16	2.56	2.95
8	4.52	0.81	0.86	1.01	1.17
10	2.311	0.41	0.44	0.52	0.60
15	0.806	0.15	0.15	0.18	0.21
20	0.443	0.08	0.082	0.1	0.12

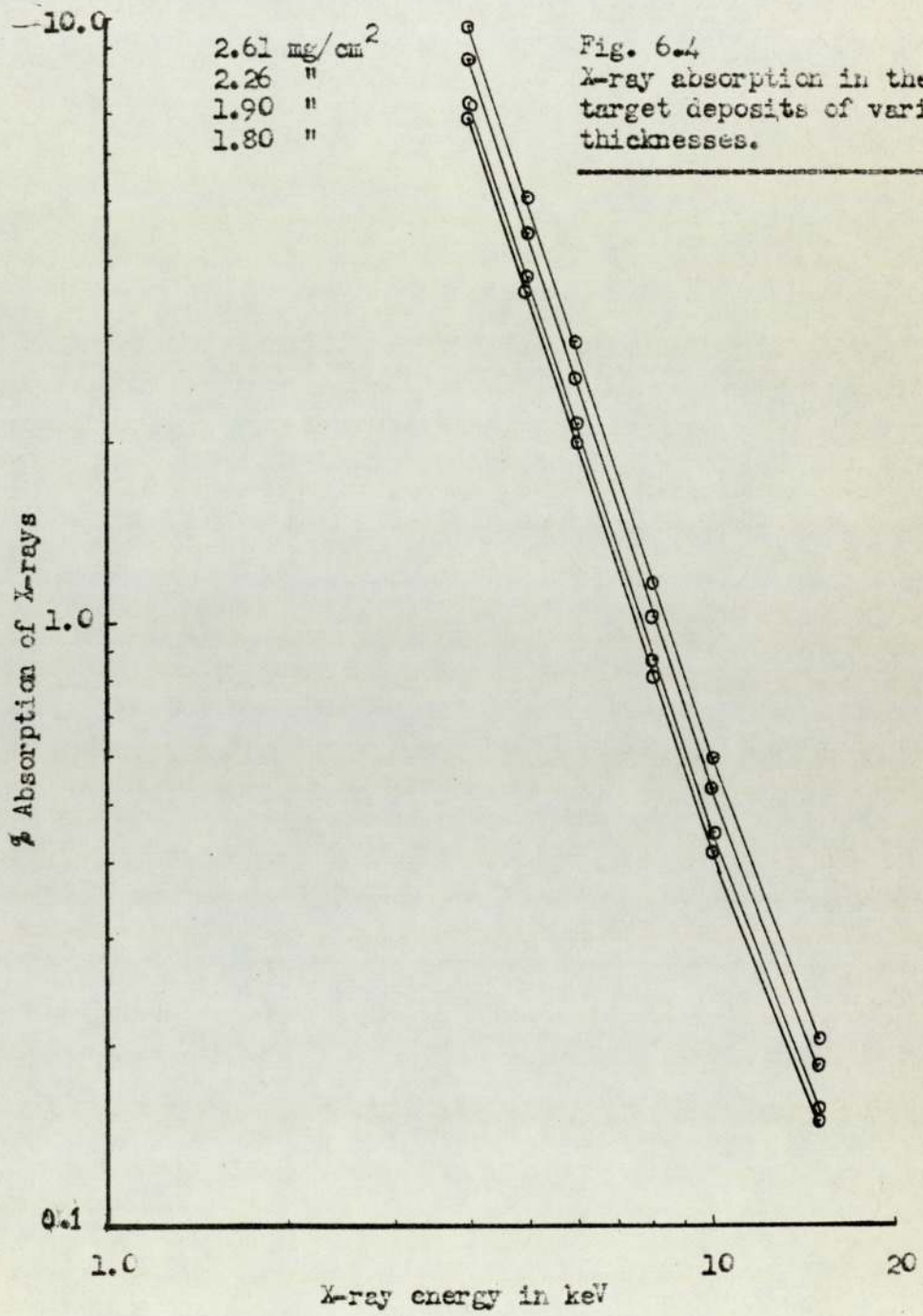

Fig. 6.4
X-ray absorption in the target deposits of various thicknesses.

Fig. 6.4.A

Variation of relative x-ray yield of the targets as a function of their thicknesses.

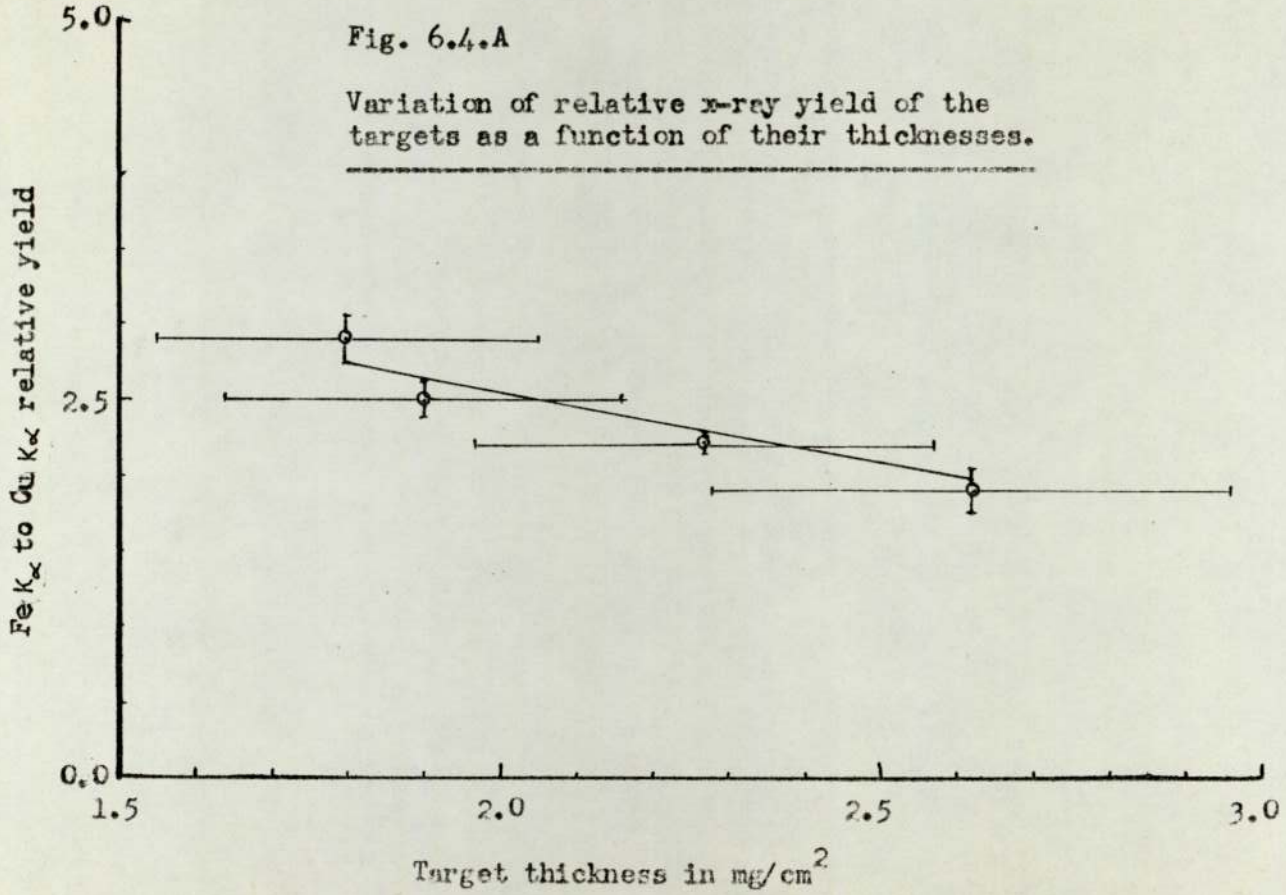

6.4. QUALITATIVE ANALYSIS OF VARIOUS BIOLOGICAL AND BIOENVIRONMENTAL SPECIMENS

According to J.E. Underwood there are three groups in which trace elements can be classified; 1) dietary essentials, 2) possible essentials, 3) non-essentials, including toxic elements. Analysis of biological materials may be used to draw conclusions about their nature as classified.

It was a matter of interest to study the potential of proton induced x-ray analysis for making qualitative analysis of the samples reported in section 6.1. and others to identify the trace elements present.

Figures 6.5. and 6.6. show the spectra obtained from the irradiation of 50 µl deposits of yttrium doped salajeet on spectroscopic pure aluminium and Nuclepore filter respectively. The elements detected were K, Ca, Ti, Mn, Fe, Zn, As and Rb in both of the spectra. yttrium peaks were also seen. Figure 6.6. is shown in log representation.

The presence of Ti and As indicates that the irradiated material "salajeet" is a soil and biosphere material (UndJ 71). Arsenic occurs in normal soil at the levels ranging from less than 1 P.P.m. to 4 P.P.m. and is absorbed by plants in extremely low amounts (GreJ 35). According to Schroeder et al (SchH 66), arsenic content is less than 0.5 P.P.m. and rarely 1 P.P.m. in most of the foods on the fresh basis, though arsenic is identified with poison, but a dose of 1 µg or less per day has been suggested (UndJ 71) to be essential trace element in the diet for mammals. Sonjo (SonK 34) has reported As as a stimulant for the growth of tissue cultures.

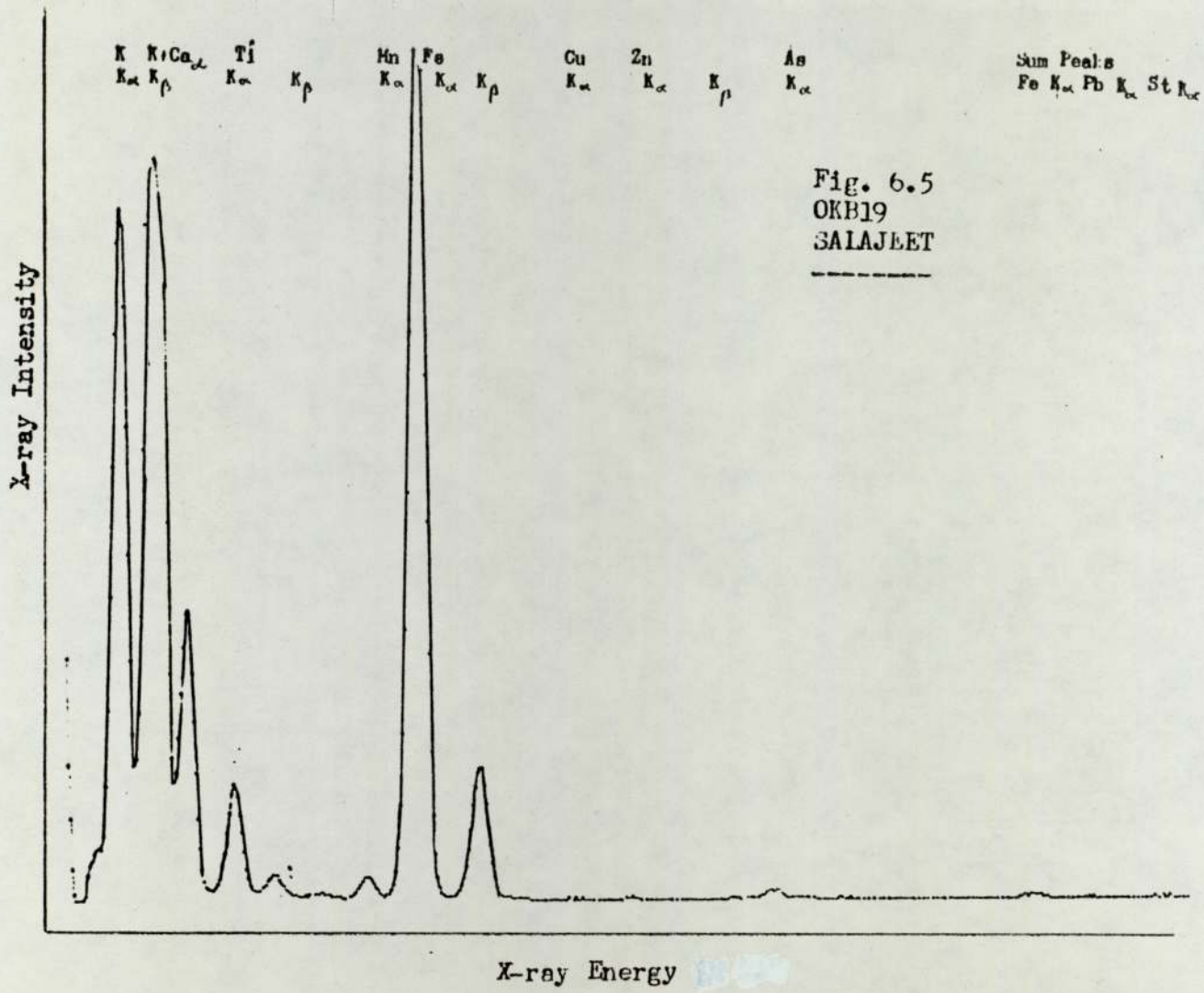

Fig. 6.5
OKB19
SALAJEET

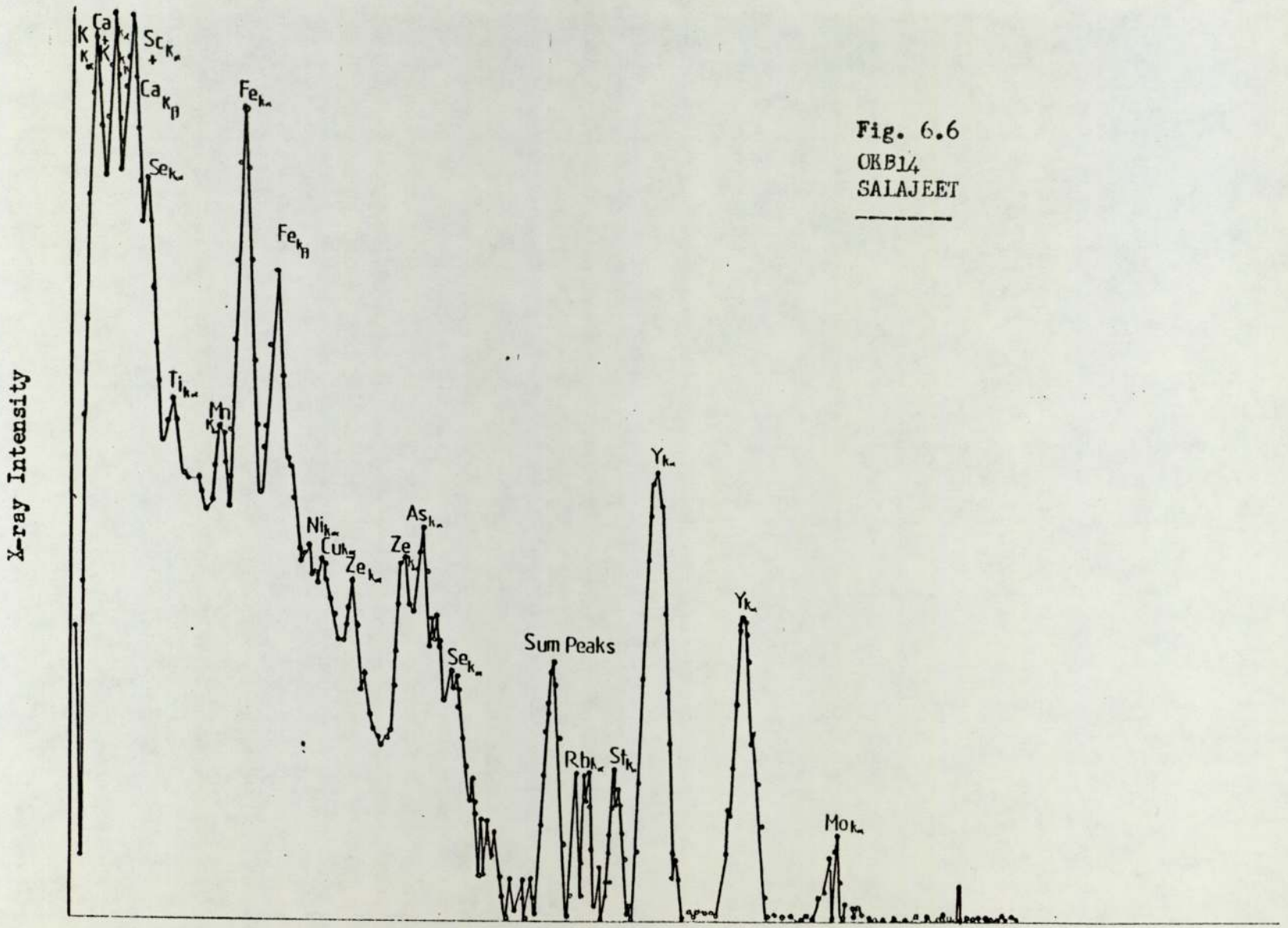

Fig. 6.6
OKB14
SALAJEET

Figures 6.7. and 6.8. show the trace elemental peaks in the characteristic x-ray spectra of the standard biological material (NBS-SRM 1577) on the target deposits of 50 μl wet aliquots on the aluminium foils, such that one target was doped with known amount of yttrium and cadmium and the other was undoped. The undoped target was irradiated to study the extent of impurities introduced into the matrix of the standard by the dopant. The same trace elemental peaks Mn, Fe, Cu, Zn, As, Se, Rb and strontium were observed, and no contaminations were seen by doping the targets. Two target deposits, each of the same materials, were irradiated to test stringently the reproducibility of trace elemental analysis.

Figures 6.9., 6.10. and 6.11. respectively show the spectra obtained from the samples of sheep's liver and kidney and a specimen of pasturised milk. They were irradiated in an attempt to see the selenium presence in the body tissue and fluid, because the disorder responsive to selenium in the body is responsive to Vitamin E (UndJ 71). Dickson et al (DicR 67) have examined an adult autopsy specimen of liver, skin and muscles and found mean ranges of 0.44, 0.27 and 0.37 P.P.m. of Se presence respectively. Analysis of a wider range of tissue for an infant and an adult revealed that the kidney and thyroid have the highest Se concentration and fat the lowest. At the higher toxic (10 - 1000 times the normal) intake, its concentration rises steadily and reached the levels of 5 - 7 P.P.m. in liver and kidney and 1 - 2 P.P.m. in the body tissue. Andrew et al (AndE 68) have suggested that the lower levels of Selenium ∽ 0.25 P.P.m. in kidney indicate its deficiency. Selenium was observed in the irradiated kidney sample in a very small peak with Fe, Cu, Zn and the internal standard (Yttrium).

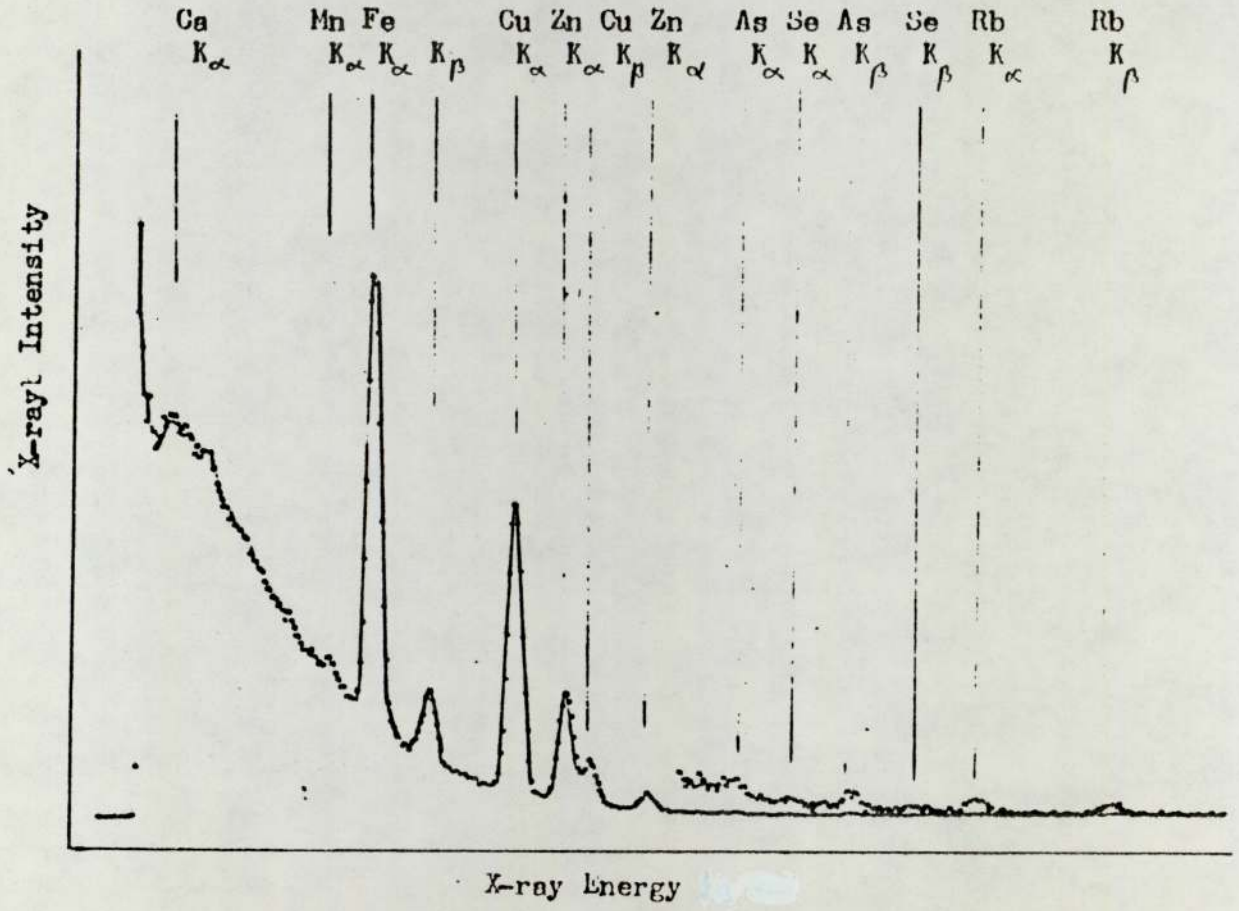

Fig. 6.7

OKD3K

"Bovine liver"

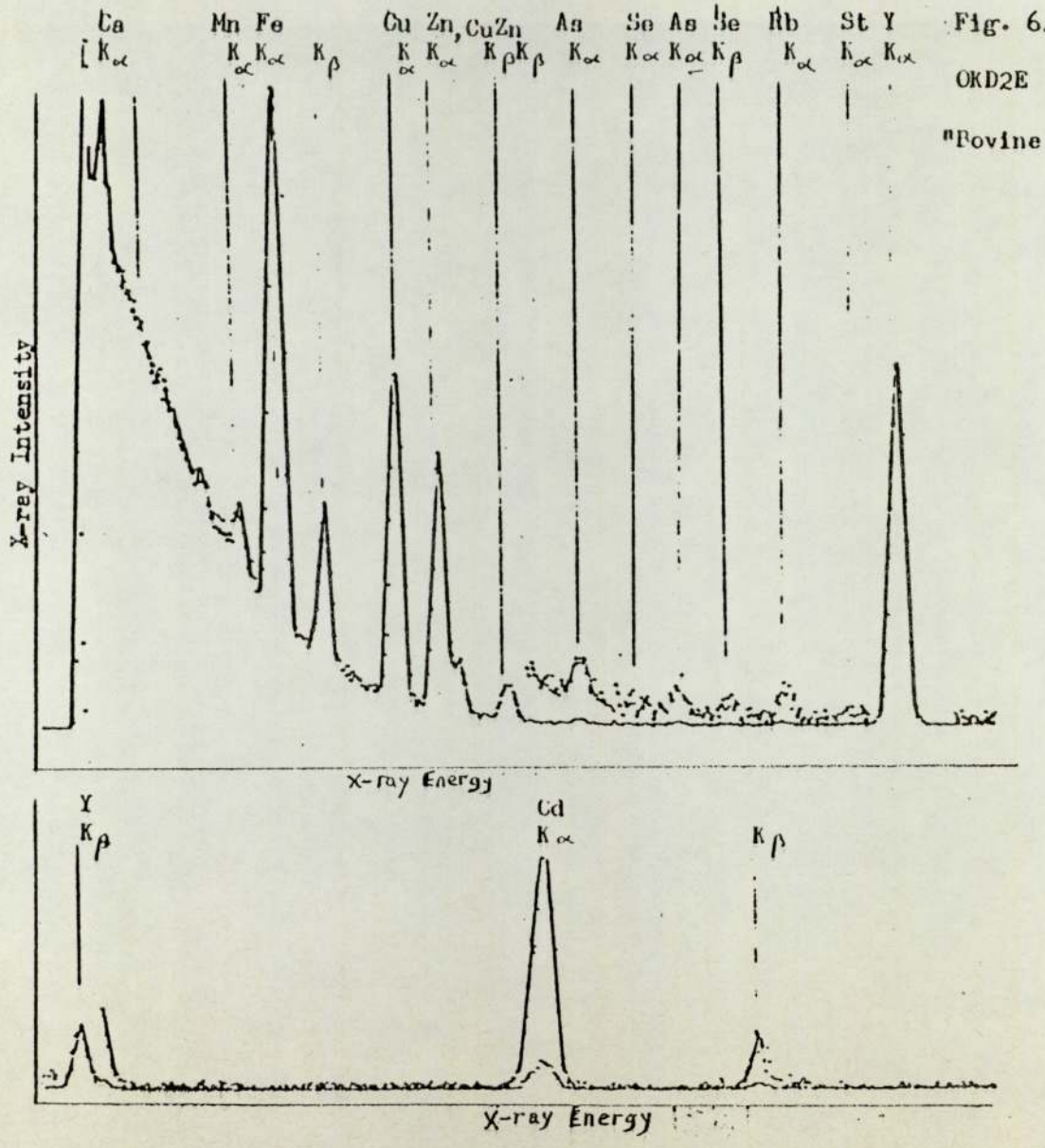

Fig. 6.8

OKD2E

"Bovine liver"

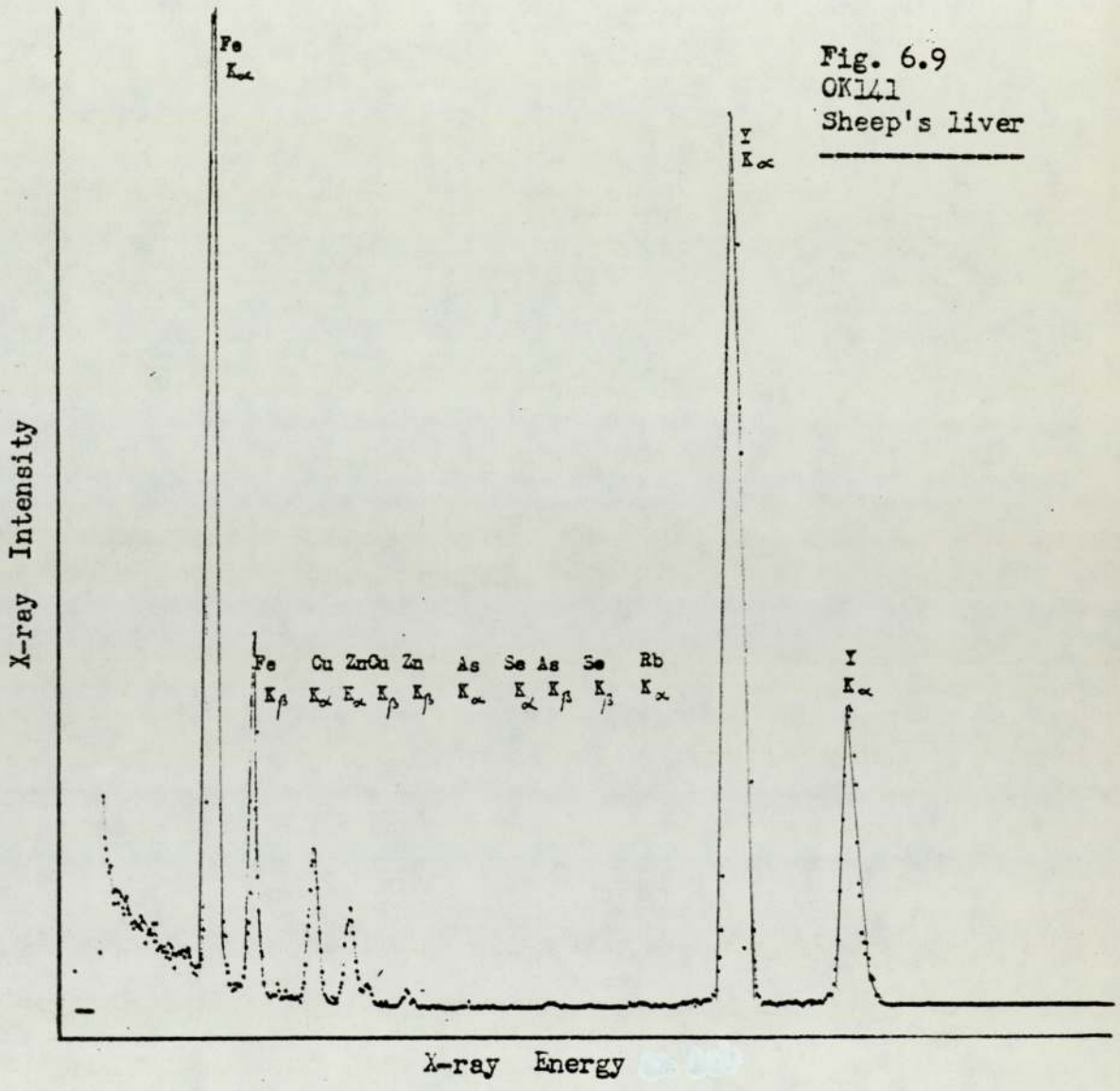

Fig. 6.9
OK141
Sheep's liver

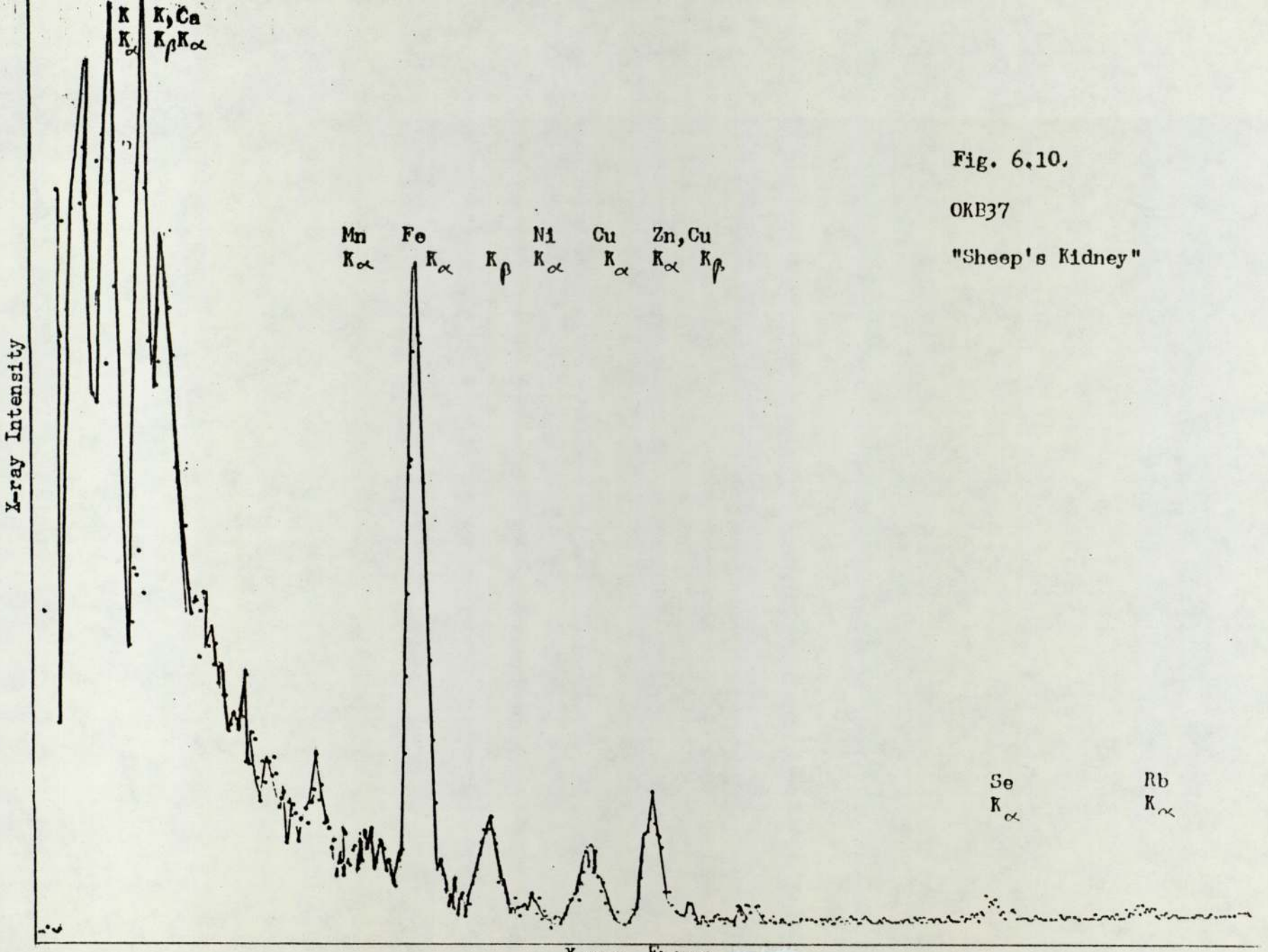

Fig. 6.10.

OKB37

"Sheep's Kidney"

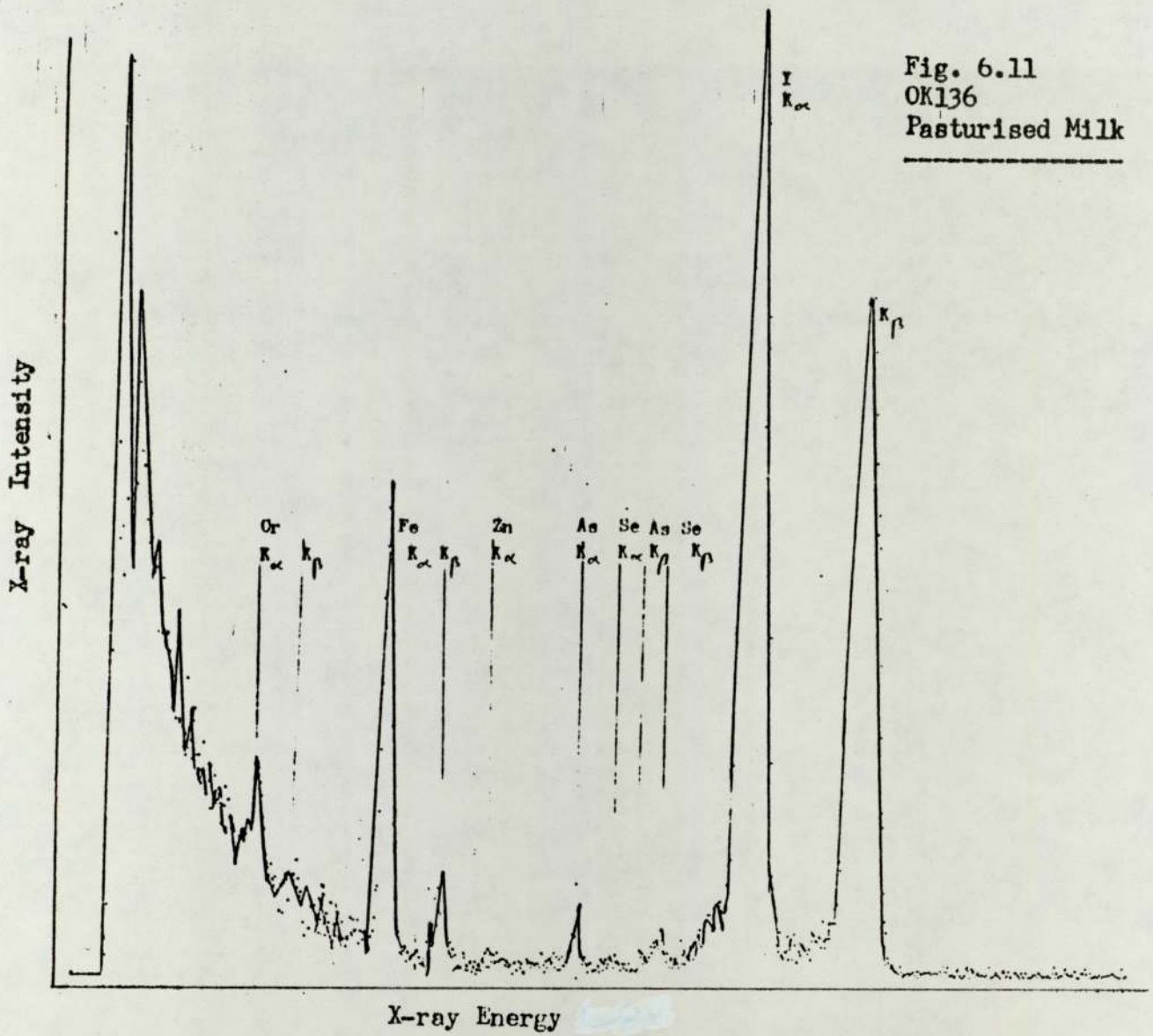

Fig. 6.11
OK136
Pasturised Milk

Target deposits of sheep's muscle, which were prepared in the early stage of this study, were also irradiated and the presence of a small chromium peak was noticed. Chromium levels in body tissue decline with age (TipI 60) until they remained extremely low and in variable concentrations ∽ (0.02 to 0.04 P.P.m.) on dry basis. Human stillborn and infant tissues carry chromium concentrations several times higher than those of adults. Kidney and liver are the only organs in which its concentrations decline in the second decade of the human body. It is reported to be a growth stimulant to the living organism in presence of free oxygen (aerobacter aerogenes) (PenD 45). Schroeder et al (SchH 62) suggested that the chromium levels are higher in the tissues of animals than those of the same tissues of most adult humans. Chromium was also observed in milk and sheep's kidney specimens in the targets reported, while it was not detected at all in sheep's liver specimen deposit. Figure 6.12. shows several trace elemental peaks in the characteristic x-ray spectrum of a target deposit of sheep's muscle.

Figure 6.13. shows the spectrum from a human whole blood target deposit which was deposited on an aluminium foil. Mn, Fe, Cu and Zn were observed in the spectrum. Aluminium foil and Nuclepore filter used as backing materials for thin and semi-thick targets were also irradiated. Figure 6.14. and 6.15. shows the impurities respectively for Al and Nuclepore backing material which were substracted from the spectra from the target deposits in quantitative analysis. Iron and copper were observed in both of the backing materials, but very small in Nuclepore filter. Figure 6.16. shows a spectrum from a similar aluminium foil having 20 μl mixture

Fig. 6.12

OK113

"Sheep's Tissue"

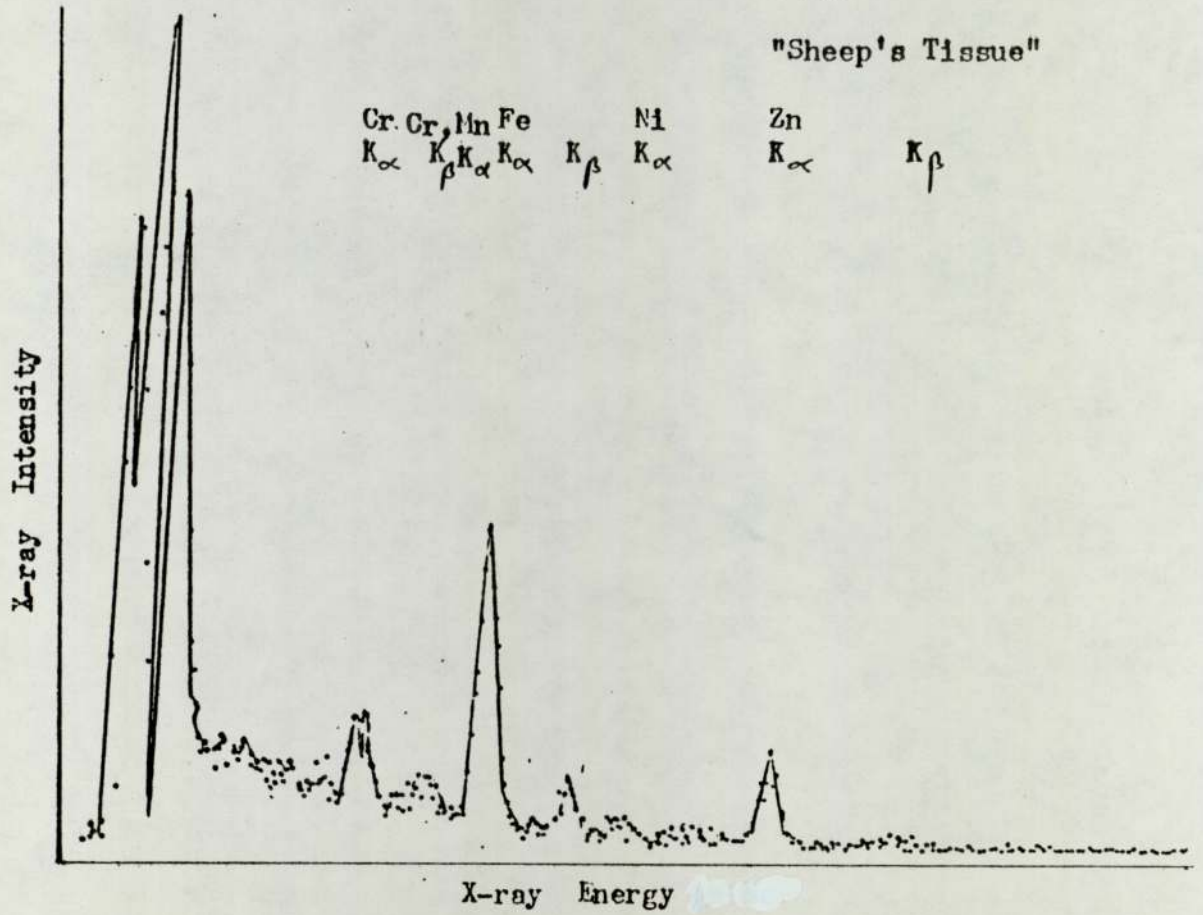

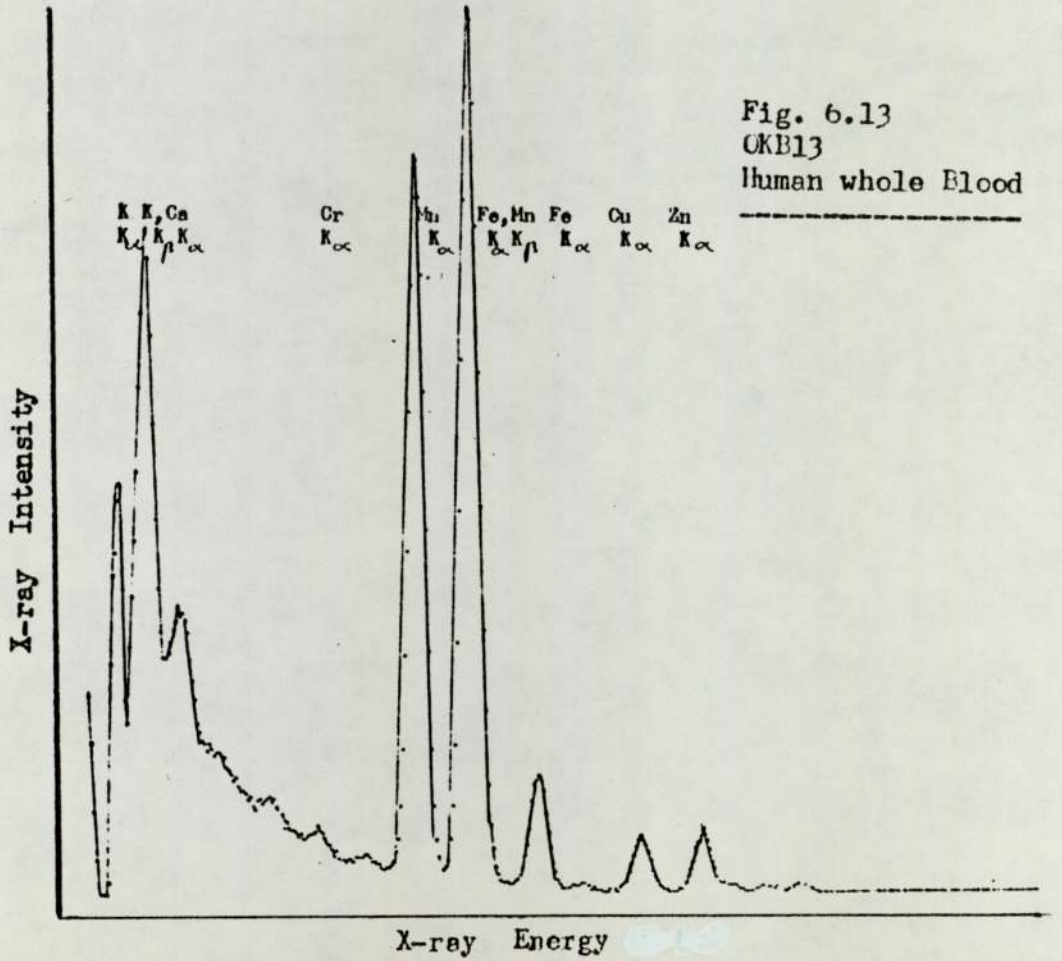

Fig. 6.13
OKB13
Human whole Blood

Fig. 6.14

OKBO2

Aluminium Foil

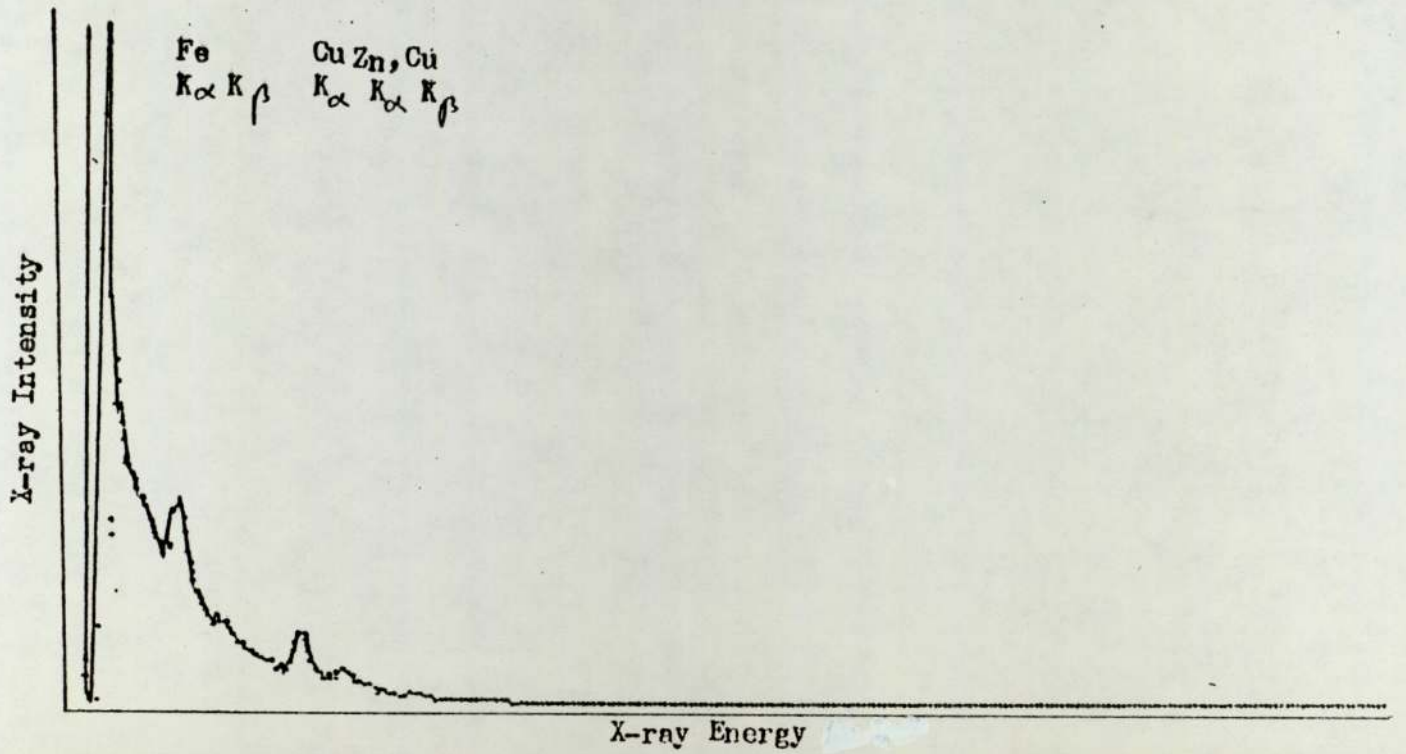

Fig. 6.15

OKB31

Nuclepore Filter

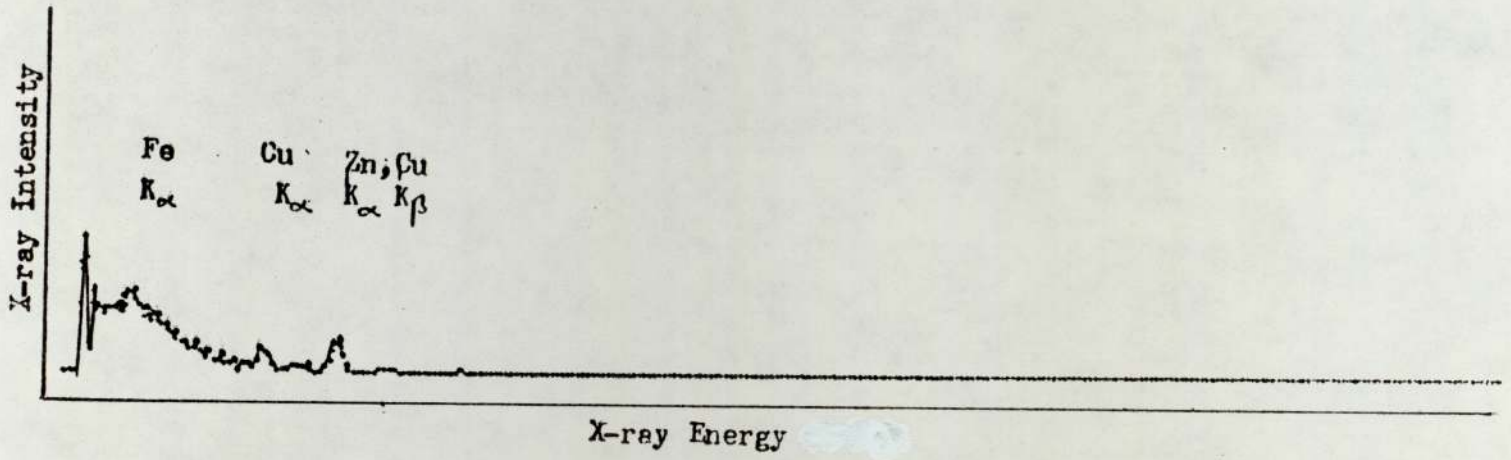

of digestive solution and standard solutions. No impurities were observed for the chemicals and distilled water used during the preparations of target deposits.

All of the target deposits were prepared using the target preparation technique discussed in Chapter 5 and were irradiated using target mounting and rotary assembly described in Chapter 4. Several anticipated trace elements were identified. The yields from the elements of medium to high atomic number $30 < Z > 70$ were lower than the yields from the elements of low atomic number $Z < 30$ in all the spectra, because K x-ray production cross sections decrease rapidly as atomic number (z) of the bombarded element increases at $Z > 30$ and L x-ray production cross section are greater than K x-rays as shown in the figure 6.17 (WalR 74). Since L x-rays have low energy and cannot be detected with the detector used for the elements of atomic number $Z < 50$, K x-ray peaks were observed in the characteristic x-ray spectrum. These peaks may not be resolved at low energy end of the spectrum because of very small difference of energies and our detection limits. Table 6.5. shows a comparison of the elements detected to the ones known to be present. (UndJ 71, BowH 74, HasI 77, RinH 77, WilR 77, LubM 72, N.B.S., I.C.R.P. 59).

Fig. 6.16
OK108
Al. foil with Digestive
and Standard solutions

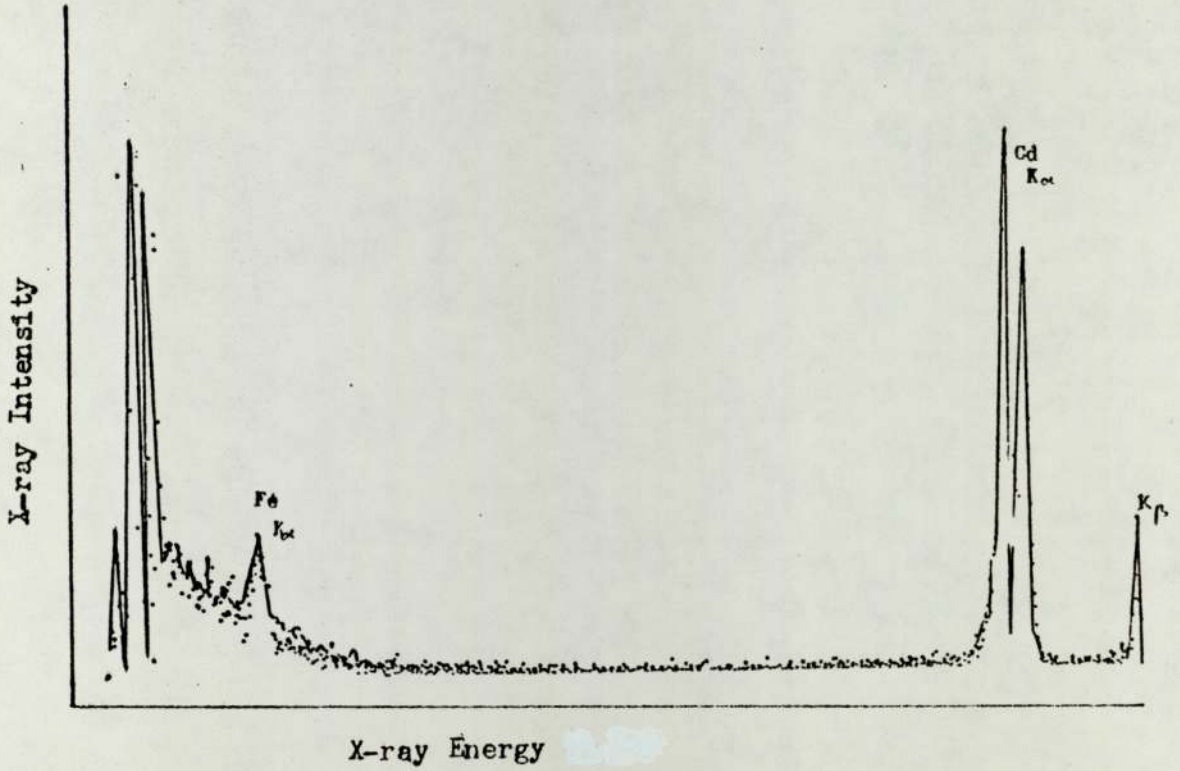

Fig. 6.17

Proton induced x-ray production cross sections for 3 MeV energy

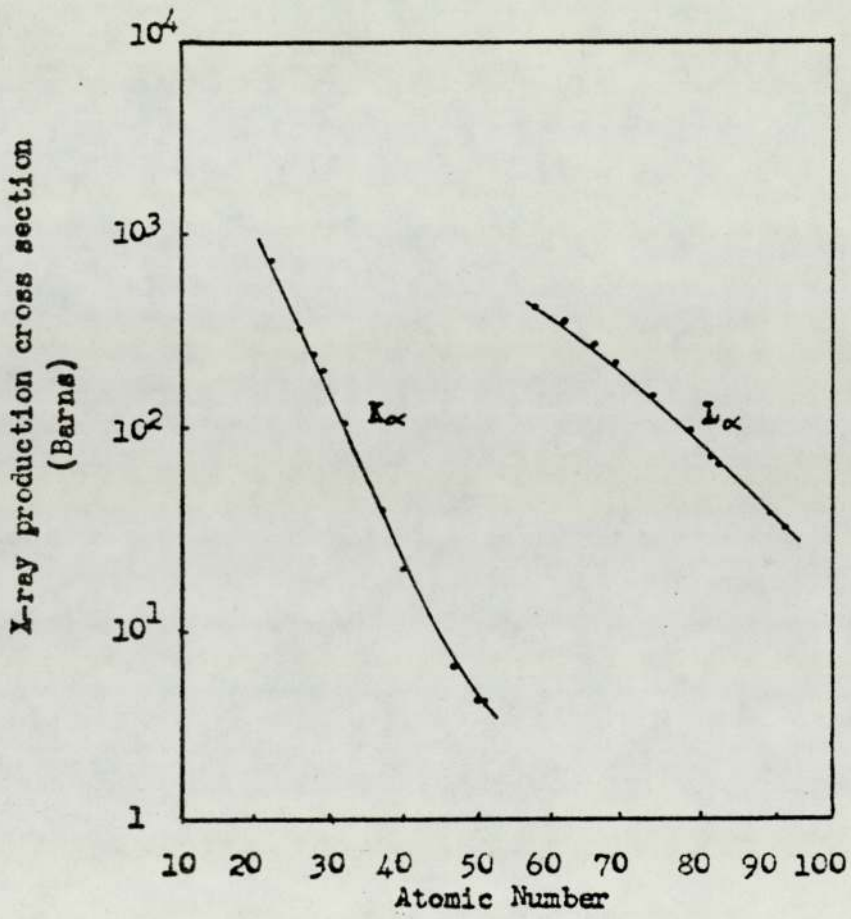

TABLE 6.5.

Target Specimen	Elements known ⩾1 P.P.m. w/w	Elements known ⩽1 P.P.m. w/w	Elements detected by various workers	Elements detected in present work	Dopant recovered
NBS-1577	N, K, Na, Ca, Cl, Mg, Fe, Cu, Zn, Rb, Mn, Se, Mo, (NBS)	Pb, Cd, Hg, Co, As, Ag, St, Th, U (139)	K, Ca, Mn, Fe, Cu, Zn, Rb, Mo, (CooJ 73, RinH 77) Mn, Fe, Cu, Zn, (WilR 77)	K, Ca, Co, Mn, Fe, Cu, Zn.	Y&Cd
Salajeet	-	-	-	K, Ca, Ti, Mn, Fe, Cu, Ni, Zn, As, Rb, St.	Y
Human whole blood	K, Ca, Cl, Na, Mg, P, S, Si, Cu, Fe, Zn, Br, Rb, (BowH 74,ICRP 59)	Al, Pb, Mn, As, Se (BowH 74)	Cl, Ar, K, Ca, Fe, Ni, Cu, Zn, W, As, Br, Rb, Mo, (LubM 72)	K, Ca, Mn, Fe, Cu, Zn, Cr, Ni, Co.	-
	to Human kidney				
Sheep's kidney	P, S, K, Cl, Na, Ca, Mg, Fe, Cu, Zn, Pb, Rb, Si, Te (ICRP 59).	Mn, Cr (ICRP 59) Cd, Pb, Te, Hg, Se, (UndJ 71)	K, Ca, Ti, Ba, Cr, Mn, Fe, Cu, Zn, Pb, Se, Br, Rb, Sr, Mo (ManN 77)	K, Ca, Mn, Fe, Ni, Cu, Zn, Se, As, Rb.	-
Sheep's liver	Human liver Ca, Cl, Cu, Fe, K, Co, Zn (ICRP 59) Mg, Mn, Mo, Na, P, Cd, Pb,(RinI 77) Rb, Zn, Si, Te, (ICRP 59)		Rat liver P, S, Cl, K, Ca, Mn, Fe, Ni, Cu, Zn, Rb, Sr, Mo, Se, Br, Sr, (HasI 77) Pima Indian liver K, Ca, Mn, Fe, Cu, Zn, Pb, Br, Mo, Cd. (RinH 77)	K, Ca, Mn, Fe, Cu, Zn, Se, Rb,	Y

TABLE 6.5. (continued)

Sheep's muscle	Human muscle Br, Cl, Si, (ICRP 59).	F, I, (ICRP 59)	-	K, Ca, Cr, Mn, Fe, Ni, Cu, Zn, Se, Rb.	-
Pasturised milk	Br, Bo, Fl, Fe, Rb, Zn. (UndJ 71)	Al, Cd, Cr, Co, Cu, I, Mn, Pb, Mo, N, Se, Si, St, V (Biol.)	-	Cr, Mn, Fe, Ni, Cu, Zn, Se, Rb.	Y

6.5. QUANTITATIVE ANALYSIS OF BOVINE LIVER (NBS-SRM 1577)

In case of thin biological target deposits and thin metallic foils in which the energy loss of the incident particles, during its passage through the target, is negligible, the analysis is simpler than the thick targets, where the energy of incident protons is completely absorbed. The x-ray production cross section for K_α radiation for a sample element (Sp) in a thin target can be derived by the expression:

$$\sigma_{K(Sp)}\ (Ep) = (4\pi \cdot Y_K(Sp) \cdot X_e(Sp)) / (np \cdot Nsp \cdot t) \qquad (6.1.)$$

where Y_K = observed K_α x-ray yield

np = number of protons

Nsp = number of atoms of the element/c.c.

t = thickness of the target observed by proton beam

x_e = total correction factor for K x-rays including the matrix effect and the efficiency of the detector such that: $X_e = Cair \cdot C_{TCW} \cdot Cdw \cdot Cm / de \cdot G$ (6.2)

where G = geometrical factor = A/d^2, d being the distance from target to the detector collimation and A is its Area.

Cair = correction factor for air = $e^{x_1 \cdot \mu m_1 \cdot \rho_1}$ (6.3)

C_{TCW} = correction factor for target chambers window = $e^{x_2 \cdot \mu m_2 \cdot \rho_2}$ (6.4)

Cdw = correction factor for detector's window = $e^{x_3 \cdot \mu m_3 \cdot \rho_3}$ (6.5)

de = correction factor for detector's efficiency = $1 - e^{-x_4 \cdot \mu m_4 \cdot \rho_4}$ (6.6)

where x_1, x_2, x_3, x_4, μm_1, μm_2, μm_3, μm_4 and ρ_1, ρ_2 ρ_3 and ρ_4 are respectively the thicknesses, mass absorption coefficient at a particular energy of x-rays and the density of the

air path, target chamber's window, Beryllium window and detector.

$$\text{The density of Air } \rho_1 = \frac{0.001293}{1 + 0.00367\ t} \times \frac{H}{70} \qquad (6.7)$$

(Hand Book Phy. & Chemistry),

where H is the pressure in mm

t is the temperature in centigrade

and C_{T_m} = correction for target matrix =

$$e^{t} \cdot \mu_{T_m} \cdot \rho_{T_m} \qquad (6.8)$$

where t is the thickness of the target matrix observed by proton beam

μ_{T_m} = mass absorption co-efficient of target matrix

ρ_{T_m} = density of the target matrix.

The observed K x-ray yield of an element of a known quantity "S_t" (a standard) may be compared with the x-ray yield of an element from a similar target provided that the sample target and the standard target are irradiated under the same experimental condition and have the same matrix and thickness.

The target specimen may also be doped with a known amount of "S_t" internally prior to the bombardment. The quantity of the standard (S_t) must be small enough not to change the matrix significantly.

In this way, both external and internal standard may be used to find the unknown quantity of an element, and for both the cases equation (6.1) can be used for the standard material "S_t".

$$\sigma_{K(S_t)}(Ep) = (4\pi \cdot Y_K(S_t) \cdot X_e(S_t)) / (np \cdot N_{(S_t)} \cdot t) \qquad (6.1.A)$$

Dividing equation (6.1) by (6.1.A.), we have:

$$\sigma K(Sp)/\ \sigma K(S_t) = \frac{4\pi.YK(Sp).X_e(Sp)/np.N(Sp).t}{4\pi.YK(S_t).x_e(S_t)/np.N(S_t).t}$$

$$\frac{\sigma K(Sp)}{\sigma K(S_t)} = \frac{YK(Sp).x_e(Sp).N(S_t)}{YK(S_t).x_e(S_t).N(Sp)} \qquad (6.1.B)$$

Rearranging $N(Sp) = N(S_t).(\sigma K(S_t)/\sigma K(Sp)).(Y(Sp).X_e(Sp)/YK(S_t).X_e(S_t))$ (6.9.)

Concentrations in number of atoms/c.c. can be changed to the concentration in weight (w/w) or vice versa, using Avogadro number "N_A" , the atomic weight "A" and the density "ρ" such that:-

$$\text{concentration of standard in gram "CSt"} = \frac{A(S_t)}{N_A.\rho_{St}}.N(S_t)$$

$$\text{concentration of specimen element in gram"CSp"} = \frac{A(Sp)}{N_A.\rho_{Sp}}.N(Sp) \qquad (6.10)$$

Expression 6.9 can be written using expression (6.10)

$$C(Sp) = C(S_t)\ \frac{YK(Sp).X_e(Sp)}{YK(S_t).X_e(S_t)}\ .\ \frac{\sigma K(S_t)}{\sigma K(Sp)}\ .\ \frac{A(Sp)}{A(S_t)}\ .\ \frac{\rho_{St}}{\rho_{Sp}} \qquad (6.11)$$

The intensities of the x-rays of an element of a known amount (standard) and the unknown (specimen) measured from a doped target can be compared simply, because certain parameters such as dead time correction factor, number of protons and geometrical factor cancel out together with their uncertainties. Absorption corrections, including the matrix effect, must be calculated for a particular experimental arrangement for both standard and specimen

elements with respect to the energies of their x-rays. In order to calculate the concentration of an element using either equation (6.9) or equation (6.11), it is necessary to know the appropriate x-ray production cross section at a particular energy of proton and absorption correction factors for standard and specimen. X-ray production cross section can be obtained from the following formula:

$$\sigma_K (Ep) = W_K \sigma_i(Ep) \qquad (6.12)$$

where W_K is the fluorescence yield for K-shell and $\sigma_i(Ep)$ is the ionisation cross section at Ep. For K_α x-rays, equation (6.12) will be

$$\sigma_{K_\alpha}(Ep) = R_{K_\alpha} W_K \sigma_i (Ep) \qquad (6.13)$$

where R_{K_α} is the K_α/K x-ray intensity ratio. The values of R_{K_α} and W_K were obtained from the data by W. Bambynek et al and Storm and Israel (StoI 70). Ionisation cross section " σ_i (Ep)" was calculated from the emperical formula (2.19) mentioned previously in Chapter 2. The calculated ionisation cross sections using equation (2.19) and K_α x-ray production cross sections using equation 6.13 for different elements from atomic numbers (Z) 22 to 50 , are shown in table 6.6. Total absorption correction factor including air detector window, target chamber window and detector efficiency was also calculated at various x-ray energies and the values were fitted to a six order polynomial using a standard programme. Interpolated and calculated values are shown in table 6.7. The computer programmes for these calculations were designed by A. Hopkin (HopA).

TABLE 6.6.

Atomic No	Ionisation Cross Section	Fluorescence Yield	K_α / K	K_α x-ray Cross Section
19	2788.374	0.138	0.912	351.588
20	2059.200	0.163	0.907	304.434
21	1522.821	0.190	0.902	261.010
22	1128.264	0.219	0.898	222.0843
23	837.802	0.250	0.898	188.212
24	623.677	0.282	0.896	157.621
25	465.536	0.314	0.894	130.757
26	348.487	0.347	0.893	108.022
27	261.638	0.381	0.892	88.959
28	197.031	0.414	0.891	72.729
29	148.833	0.445	0.890	58.998
30	112.778	0.478	0.889	48.065
31	85.715	0.510	0.888	38.854
32	65.350	0.540	0.887	31.316
33	49.977	0.567	0.885	25.104
34	30.336	0.596	0.884	20.201
35	29.495	0.622	0.882	16.182
36	22.761	0.646	0.879	12.936
37	17.615	0.669	0.877	10.340
38	13.672	0.691	0.874	8.264
39	10.642	0.711	0.869	6.616
40	8.306	0.730	0.867	5.395
41	6.501	0.748	0.864	4.314
42	5.101	0.764	0.862	3.449
43	4.014	0.779	0.860	2.759
44	3.166	0.793	0.858	2.209
45	2.504	0.807	0.854	1.734
46	1.985	0.819	0.853	1.390
47	1.577	0.830	0.851	1.173
48	1.257	0.840	0.849	0.899

TABLE 6.7.

CALCULATED VALUES OF ABSORPTION CORRECTION AT VARIOUS X-RAY ENERGY

Energy of x-ray (keV)	Total Absorption Correction Factor
1.000	2.119×10^{10}
1.500	3.928×10^{4}
2.000	1.708×10^{2}
3.000	4.619
4.000	1.804
5.000	1.323
6.000	1.169
8.000	1.070
10.000	1.039
20.000	1.004
30.000	1.003
40.000	1.065
50.000	1.823
60.000	3.648
Interpolated values using Least square fit	
12.000	1.025
15.000	1.013
25.000	1.002
35.000	1.009
45.000	1.401
55.000	1.516
58.000	1.664

Target matrix absorption correction factors C_{TM} at different thicknesses were calculated using equation 6.8, and plotted against their corresponding x-ray energies, as shown in the figure 6.18. Correction factors due to iron and copper impurities from aluminium foil were also estimated and were taken into account in the calculations. Four doped targets of 50 μl of wet digestive aliquots of the bovine liver were irradiated several times at the same energy of proton (2.5 MeV) for the quantitative analysis. The iron concentration in this material was used to calculate the concentration of other elements and the dopants. An undoped target deposit of 50 μl digestive homogenate of bovine liver was also irradiated at the same energy of proton. Target thickness was also determined for each target.

Relative yields of iron to various major trace elements and dopants were calculated for each measurement and are tabulated in table 6.8 with the random error. The values of the weighted mean on each of the several measurements on a target deposit were also given along with the standard deviations.

The reproducibility of the relative yields was fairly consistent 3.0% for each of the targets, except for iron to rubidium yield, because of low x-ray counts from rubidium. The reproducibility of the relative yields was not less than 93% for the rest of the target deposits. It was also noticed that the Fe/γ yield was very consistent (more than 97%) for each of the five target deposits.

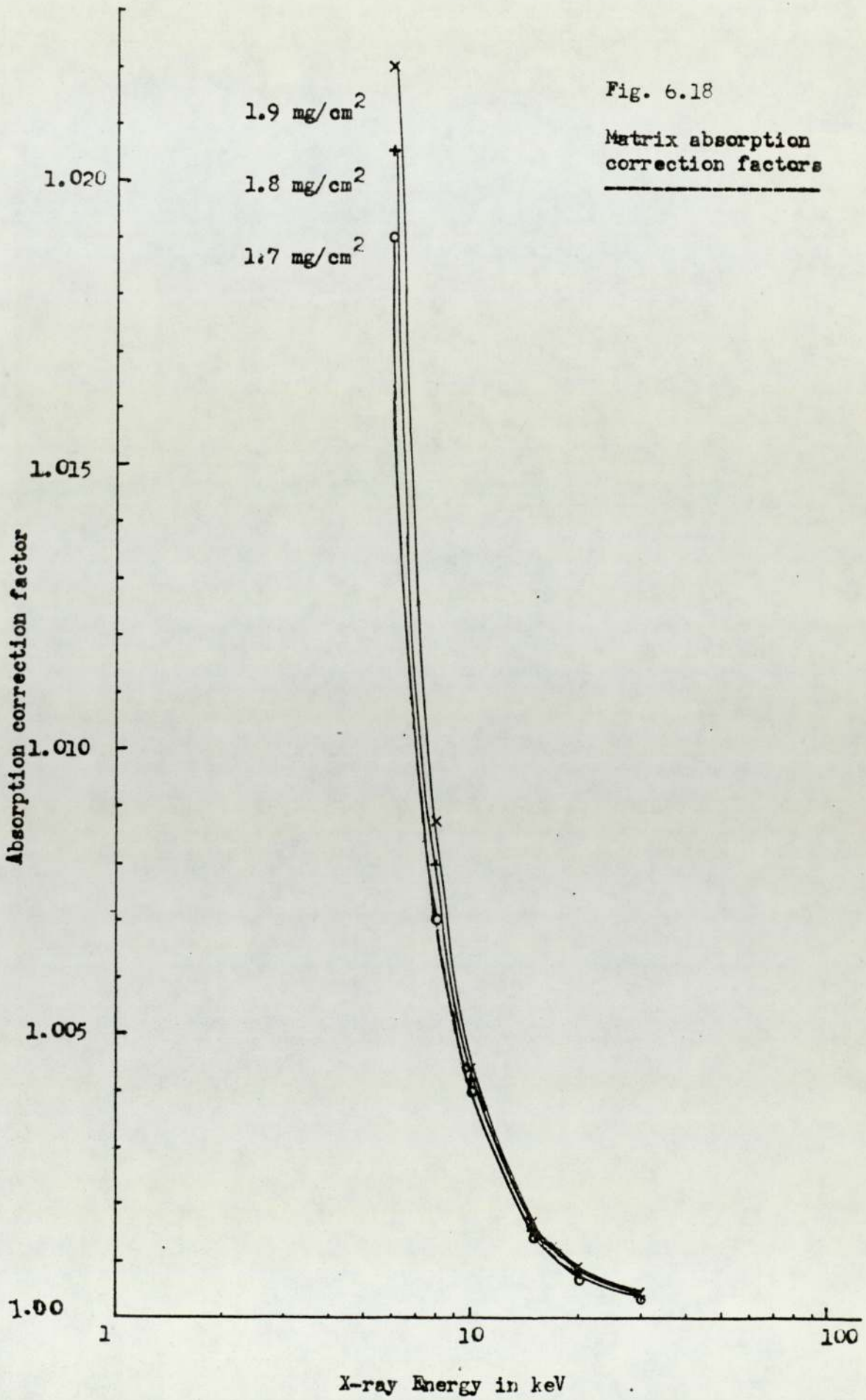

Fig. 6.18

Matrix absorption correction factors

TABLE 6.8.

Target Material NBS-1577		Target Deposit Thickness in mg/cm^2	Relative yields of observed K_α peak area				
			Fe/Cu	Fe/Zn	Fe/γ 125 P.P.m. γ dopant	Fe/Cd 125 P.P.m. Cd. dopant	Fe/Rb
1	A		2.49 ± 0.15	4.60 ± 0.28	2.36 ± 0.05	21.77 ± 1.3	127.16 ± 21.19
	B		2.60 ± 0.15	4.52 ± 0.28	2.45 ± 0.05	21.67 ± 1.3	126.74 ± 22.45
	C	1.9	2.59 ± 0.15	4.22 ± 0.22	2.46 ± 0.04	23.10 ± 0.92	121.07 ± 11.94
	D		2.60 ± 0.08	4.37 ± 0.22	2.51 ± 0.03	23.12 ± 0.69	141.05 ± 11.98
	E		2.50 ± 0.08	4.45 ± 0.23	2.38 ± 0.03	22.5 ± 0.86	122.15 ± 11.15
	F		2.52 ± 0.05	4.56 ± 0.23	2.39 ± 0.02	22.41 ± 0.45	143.63 ± 9.34
	G		2.62 ± 0.10	4.4 ± 0.22	2.23 ± 0.02	21.9 ± 0.88	143.0 ± 17.09
		W. Mean	2.54 ± 0.09	4.4 ± 0.2	2.39 ± 0.02	22.15 ± 0.45	133.39 ± 4.33
		st.dev(σ)	.05 ~ 2%	.12 ~ 2.7%	.08 ~ 3.3%	.21 ~ 1%	9.3 ~ 7%
2	A		2.98 ± 0.09	4.60 ± 0.23	2.68 ± 0.04	22.18 ± 0.7	138.24 ± 12.58
	B		3.00 ± 0.06	4.66 ± 0.24	2.68 ± 0.03	22.2 ± 0.54	148.72 ± 12.09
	C	1.8	2.96 ± 0.06	4.48 ± 0.23	2.51 ± 0.03	20.87 ± 0.49	149.85 ± 16.66
	D		3.04 ± 0.1	4.59 ± 0.23	2.69 ± 0.02	22.37 ± 0.47	148.57 ± 7.98
	E		3.02 ± 0.1	4.64 ± 0.24	2.68 ± 0.02	22.65 ± 0.46	145.77 ± 7.23
		W. Mean	2.99 ± 0.014	4.59 ± 0.03	2.66 ± 0.02	22.06 ± 0.32	146.4 ± 6.04
		st.dev(σ)	.028 ~ 1%	.062 ~ 15%	.069 ~ 2.6%	.61 ~ 2.8%	4.24 ~ 2.9%
3	A		2.86 ± 0.11	4.71 ± 0.24	2.57 ± 0.04	22.47 ± 0.96	133.76 ± 14.98
	B		2.88 ± 0.09	4.79 ± 0.24	2.57 ± 0.03	22.04 ± 0.70	145.13 ± 11.91
	C	1.8	2.93 ± 0.06	4.73 ± 0.24	2.58 ± 0.03	21.76 ± 0.46	144.63 ± 9.72
	D		2.93 ± 0.06	4.71 ± 0.24	2.58 ± 0.02	21.85 ± 0.44	142.34 ± 8.15
	E		2.90 ± 0.03	4.76 ± 0.24	2.58 ± 0.02	22.37 ± 0.45	144.83 ± 7.53
		W. Mean	2.90 ± .0044	4.74 ± 0.03	2.57 ± 0.02	22.03 ± 0.42	143.24 ± 5.96
		st.dev(σ)	.027 ~ 1%	.03 ~ .6%	.005 ~ .2%	.28 ~ 1.3%	4.3 ~ 3%

TABLE 6.8. (continued)

4	A		3.07 ± 0.18	4.79 ± 0.26	1.20 ± 0.05
	B	1.71	3.17 ± 0.19	4.54 ± 0.23	1.18 ± 0.04
	C		3.13 ± 0.19	4.43 ± 0.23	1.19 ± 0.03
	D		3.08 ± 0.15	4.33 ± 0.22	1.18 ± 0.03
		W. Mean	3.10 ± 0.1	4.42 ± 0.14	* 1.19 ± .013
		st.dev(σ)	.04 ~ 1.3%	.17 ~ 3.8%	.008 ~ .7%
5	A		2.47 ± 0.07	4.84 ± 0.26	
	B	1.9	2.57 ± 0.05	4.88 ± 0.25	
		Mean	2.53 ± 0.048	4.86 ± 0.2	

* This value is at different concentration of yttrium dopant (250 p.p.m.)

Target five was irradiated twice only its mean value of the relative yields was compared with the values of the weighted mean of target 1 for Fe/Cu and Fe/Zn ratios. The Fe/Cu yields are consistent within 1% and Fe to Zn and Fe to Rb ratios differ by 9.9%. The relative yields of Fe to Y and Fe to Cd are fairly consistent at the same concentration. The values of weighted mean of the several measurements were used in equation 6.11 and 6.9 for the quantitative analysis of the dopants and the major trace elements (i.e. $>$ 1 P.P.m.) except manganese.

Equation 6.11 was used for the calculations of trace concentration in gravimetric basis (in grams) and equation 6.9 was used to calculate the amount of doping elements. Since 1 gram of the material was homogenised with deionised water to give 10 ml of the homogenate sample, a tenth factor of the calculated value of the dopant's amount was its concentration in the target deposit.

The concentrations of the doped element and their recovered amount were tabulated with the concentration of the major trace elements except manganese in the target deposits as shown in the table 6.9. The values determined are shown with the values determined by the other workers (CooJ 73, WilR 77, JolR 78) along with the certified values.

All the concentrations are shown with their uncertainties due to the total composite error in the measurements. Since the errors related to other factors in equation (6.11) and (6.9) were almost constant, the errors estimated including the statistical error were close to each other depending upon the concentration of the trace elements or the dopants.

Combining the errors on ionisation cross section $\backsim$ 15% (KhaM), fluorescence yield $\backsim$ 4% K_{α} to K x-ray intensity ratios

TABLE 6.9.

Thickness of the target	Measurement on one target	Backing Material	w/w concentration of Elements in p.p.m.			Elements doped in p.p.m.		Dopants recovered in p.p.m.	
			Cu	Zn	Rb	Y	Cd	Y	Cd
$1.9_m g/cm^2$	7	Aluminium	176 ± 33	141 ± 26	23 ± 4	126	126	133 ± 25	103 ± 20
$1.8_m g/cm^2$	5	Aluminium	148 ± 27	133 ± 25	22 ± 4	126	126	121 ± 22	105 ± 20
$1.8_m g/cm^2$	5	Aluminium	157 ± 29	130 ± 24	24 ± 4	126	126	125 ± 23	105 ± 20
$1.71_m g/cm^2$	4	Aluminium	147 ± 28	141 ± 26	22 ± 4	250	-	269 ± 50	-
$1.9_m g/cm^2$	2	Nuclepore	181 ± 34	122 ± 23	-	-	-	-	-
(WilR 77)		Fe concentrations determined							
Pellets (thick)	9	273 ± 8.5	186 ± 5.5	132 ± 3.3	16.8 ± 1.9	-	-	-	-
Deposits (thin)	8	293 ± 21	194 ± 13	144 ± 12	20.9 ± 2.5	-	-	-	-
(JolR 78)	-	271.5 ± 11.5	173.5 ± 13.9	125.7 ± 10.6	15.0 ± 2.5	-	-	-	-
(CooJ 73)	-	250	200	132	16	-	-	-	-
NBS values		270 ± 20	193 ± 10	130 ± 10	18.3 ± 1.0				

$\sim$ 5% (BamW 72) and absorption correction factors 8.5 $\sim$ 7.0% (StoI 70) including the matrix absorption correction, we estimate a composite error $\sim$ 18.5% on all the concentrations of the trace elements and the dopants, which must be added with the error due to statistical uncertainty estimated on the mean values for the relative yields in the table 6.8.

The concentration determined of trace elements in the target deposits agree with the NBS values except copper for the second and fourth target in the table 6.9., which differ by 5% from NBS value for copper concentration. This discrepancy might be due to the variation in thickness of either target deposit or the backing material, since Zn and Rb concentrations agree with the NBS values.

The values of copper, however, are not as consistent as those of other values of Zn and Rb, and on comparing these values with the values of copper concentrations obtained by R.D. Willis et al (WilR 77) and J.A. Cooper (CooJ 73), similar inconsistency was observed.

The values of Zn and rubidium are found in better agreement with NBS values than their values for Zn and Rb concentrations (WilR 77, CooJ 73).

Comparing the amount of doped elements with their recovery in the target deposits using NBS value for iron concentration (270 P.P.m.), it was noticed that yttrium recovery was better than cadmium, though the recovery of both of the dopants was fairly consistent. The recovered values for cadmium concentration must be high including the x-ray yield from the cadmium presence in the target material, since NBS value of cadmium concentration is

0.27 P.P.m. Contrarily, we obtained slightly lower values of cadmium concentration in the target deposits. However, the values agree within the experimental error.

6.6. PRECISION STUDY OF THE MEASUREMENTS ON THE BIOLOGICAL TARGETS

In general, the analytical precision is limited by the instrumental error and the method of target sample preparation (NieK 76). From the analysis of the mean relative yields reported in section 6.4., table 6.8., it was observed that the reproducibility of the measurements on a target was not less than 93%, which indicates the precision of the analysis due to measuring system including the statistical uncertainties. The comparison of the mean values on the relative yields of the five target deposits, which were prepared from equal volume of the target aliquot, i.e. 50 µl, shows a maximum variation from each other of ∽ 19.0%, which includes the error due to the measuring instrument and counting statistics. Therefore, a value of ∽ 17.6% is obtained for the sample preparation error when one substracts square of ∽ 7.0%, error due to measuring instrument and counting error for the biological samples. This error is certainly low compared with the variation of 30% of relative yield for the target deposits in section 6.3., and shows an improvement minimising the error due to the loss of trace elements and target contamination during its preparation.

CONCLUSIONS

6.7. Proton induced x-ray emission analysis (PIXE) is a useful analytical tool for the determination of elemental constituents in a wide range of materials. Several improvements which could be made in order to increase its sensitivity include improving the signal to background ratio by decreasing the production of background radiations from the target matrix and from the backing material. Therefore main work has been done on the preparation of thin and semi-thick target deposits, using the appropriate backing material. Wet ashing technique was successfully carried out to prepare the thin and semi-thick target deposits of biological nature and Nuclepore filter was found to be very suitable backing material for such target deposits.

It would have been very desirable to have had an automatic target changing system for the rapidity of analysis using thin and semi-thick targets in the existed target chamber at the end of proton beam line of the Dynamitron at Birmingham Radiation Centre. Therefore a thin target rotary system has been designed and constructed and reasonable reproducibility of the measurements has been achieved.

Certain factors were found very important to be noted in the analysis, such as measurement of accurate beam current, uniformity and homogeneity of the targets. Factors such as increased count time and high beam currents were not found to be very helpful in improving the sensitivity of the analysis, since the background radiation was increased with the signal increase, resulting almost the same peak to background ratio.

The applicability of PIXE on both qualitative and

quantitative analysis was observed using biological reference material. The preparation of standard biological target is an area which this work is potentially applicable, since internal standardisation of the biological materials were found effectively useful in the work.

The precision measured for the analysis depends mainly on the target preparation and it is certainly not as good as one would accept from a standard analytical technique.

Few areas such as target preparation, the target rotary system and data handling require more improvement and further work. Homogenisation may be done using the electric motor to achieve more homogeneous homogenate, the estimation of absolute thickness of the target deposits require their densities and the hinged block must be hinged tightly to achieve the reproducibility of the target positions. Appropriately, online computer programme could improve the rapidity of the analysis.

However, the work reported here indicates that PIXE has the desirable characteristics of small sample size and quantity, rapidity of analysis and multi-elemental and non-destructive nature for a variety of materials.

REFERENCES

AhlM 75 : M. Ahlberg, R. Akselsson, D. Brune and J. Lorenzen.
Nuclear Inst. and Methods, Vol. 123 (75), p. 385 - 393.

AksR 73: R. Akselsson, C. Orsini, D.L. Meinert, T.B. Johanson, R.E. Van Grieken, H.C. Kaufmann, K.R. Chapman, J.W. Nelson and T.W. Winchester.
Advances in X-ray Analysis, Vol. 18 (73) p. 588 - 597.

AldK 56: K. Alder, A. Bahr, T. Huus, B. Mottleson and A. Whither.
Review Mod. Physics, Vol. 28 (56) p. 432.

AndE 68: E.D. Andrews, W.J. Hartley and A.B. Grant.
N.Z. Vet. Journal, Vol. 16 (68) p. 3 - 18.

BamW 72: W. Bambynek.
Review Mod. Physics, Vol. 44, No. 4 (72) p. 716.

BarB 74: B.K. Barnes, R.M. Coleman, G.H.R. Kejal, P.W. Quinn and N.J. Rencrieca.
Adv. in X-ray Analysis, Vol. 18 (74) p. 343 - 352.

BasG 73: G. Basbas, W. Brandt and Laubert.
Physical Review, Vol. A7 (73) p. 983.

BauR 76: Rudy Baum and W.F. Gutkneckt, R.D. Willis and R.L. Walter.
Anal. Chiomica Acta, Vol. 85 (76) p. 323 - 329.

BeaR 74: R.C. Bearce, D.A. Close, J.J. Malanify and C.J. Umberger.
Anal. Chemistry, Vol. 46, No. 4 (74) p. 499.

BeaC : Nuclear Physics by Bearcham.

BioD : Biology Data Book.

BisG 70: G.A. Bissinger, J.M. Joyce, E.J. Ludwig, W.S. McFever and S.M. Shafroth.
Phys. Rev. A. Vol. 1, No. 3 (70) p. 841 - 847.

Boeh : The Boehinger Corporation (London) Ltd., Bell Lane, Lewes, East Sussex.

BonM 75: M.C. Bonnet, J.P. Thomas, H. Betuel, M. Fallavier and S. Marsund.
Proceeding 2nd International Conference on ion beam surface analysis, Plenum Press, New York (75), p. 785 - 793.

BorR 75: Ronald T. Bora and Sam J. Appala.
Nucl. Inst. and Methods, Vol. 131 (75) p. 343 - 352.

BowH 74: H.J.M. Bowen.
Journal of Radioanalytical Chemistry, Vol.19 (74), p. 215 - 226.

BreD 75: Dennis N. Breiter, M.L. Roush.
American Journal of Physics, Vol. 43, No. 7 (75), p. 569 - 572.

BDH : The British Drug Houses Ltd., (B.D.H.) Lab. Chemicals Division, Poole, England.

BDHA : Personal communication with Assistant Chief Analyst, BDH, dated 2nd June, 1977.

CahT 72: T.A. Cahill.
Bull. American Phys. Society, Vol. 17 (72), p. 505.

CaiJ 75: J.A. Cairns, A. Lurio and J.F. Ziegler.
Proceeding 2nd International Conference on ion beam surface analysis, p. 773 - 783.

CamJ 72: J.L. Campbell and L.A. McNelles.
Nucl. Inst. and Methods, Vol. 101 (72), p. 153 - 162.

CamJ 77: J.L. Campbell.
Nucl. Inst. and Methods, Vol. 142 (77), p. 263 - 273.

CarE 75: E. Caruso, C.I.S.E. - Segrate (Milano).
Energia Nuclaire, Vol. 22, No. 7 (75), p. 382.

CheJ 75: J.F. Chemin, J. Roturier, B. Saboya and G.T. Dieu.
Phys. Rev. A. Vol. 11, No. 3 (75), p. 549 - 555.

ChuF 74: F.H. Chung, A.J. Lentz and R.W. Scott.
X-Ray Spectrometry, Vol.3 (74), p. 172 - 175.

CleG 62: G.E. Cleit and W.D. Holland.
Analytical Chemistry, Vol. 34 (62), p. 1454.

CooJ 73: J.A. Cooper.
Nucl. Inst. and Methods, Vol. 106 (73), p. 525 - 538.

CurL 68: Lloyd A. Currie.
Analytical Chemistry, Vol. 40 (68), p. 586.

DawB 71: B.J. Dawson.
Extrait de la revive du Gams, Vol. 3 (71), p. 32.

DecG 75: G. Deconninck G. Demortier, F. Bodart.
Atomic Energy, Vol. 18, part II (75), p. 365 - 412.

DemG 74: G. Demortier.
Radiochem., Radioanalytical letters, Vol. 20, part III, (74), p. 197 - 305.

DicR 67: R.C. Dickson and R.H. Tomlinson.
Chin. Chem. Acta, Vol. 16 (67), p. 311.

DRG 74 : Target Mechanism and internal parts for x-ray target
Drawing No. 12401, Birmingham University, 7th Oct.74.

DugJ 72: J.L. Duggan, W.L. Beck, L. Albrecht, L. Meinz and J.D. Spaulding.
Advances in X-ray Analysis, Vol. 15 (72), p. 407 - 423.

FelE 72: E.J. Feldle, C.J. Umberger.
Nucl. Inst. and Methods, Vol. 103 (72), p. 341 - 343.

FelL 75: L.C. Feldman and P.J. Silverman.
Proceeding 2nd International Conference on ion beam surface analysis, p. 735 - 741. Plenum Press, Newyork 1975.

FloR 72: R.G. Flochini, P.J. Feeny, R.J. Sommerville and T.A. Cahill.
Nucl. Inst. and Methods, Vol. 100 (72), p. 397.

FolF 74:A F. Folkmann, C. Gaarde, T. Huus and K. Kemp.
Nucl. Inst. and Methods, Vol. 116 (74), p. 487 - 499.

FolF 74:B F. Folkmann, J. Borggreen and A. Kjeldgaard.
Nucl. Inst. and Methods, Vol. 119 (74), p. 117 - 123.

FolF 75:A F. Folkmann.
Proceeding 2nd International conference on ion beam surface analysis, p. 747 - 757. Plenum Press, Newyork 1975.

FolF 75:B F. Folkmann.
Proceeding 2nd International Conference on ion beam surface analysis, p. 695 - 717. Plenum Press, Newyork 1975.

GalM 76: M. Gallorini, N. Genova, E. Orvini, R. Stalle.
J. Radioanal. Chem., Vol. 34 (76), p. 135 - 139.

GarJ 70: J.D. Garcia.
Physical Review A, Vol. 1, No. 5 (70), p. 1402 - 1403.

GarJ 73: J.D. Garcia.
Physical Review A, Vol. 1, No. 2 (73), p. 280 - 285.

GerT 33: Gerthsen and C. Ruesse.
Physics Z., Vol. 34 (33), p. 378 - 482.

GliC 62: Chester E. Gliet and W.D. Holland.
Analyt. Chem., Vol. 34 (68).

GooF : Good Fellow Metals Ltd., Foils for research and development. Catalogue.

GorB 72: B.M. Gordon and H.W. Kramer.
Brookhaven National Lab., Report BNL.15931 (72).

GorT 59: T.J. Gorsuch.
Analytical Methods GmH., Vol. 34 (59), p. 135 - 147.

GouF 77: F.S. Goulding and J.M. Jaklevic.
Nuclear Inst. and Methods, Vol. 142 (77), p. 323 - 332.

GouF 69: F.S. Goulding, J. Walton and D. Malone.
Nucl. Inst. and Methods, Vol. 71 (69), p. 273.

GraR 71: R.J. Grader, R.W. Hill, C.W. McGoff, D.S. Salami.
Rev. Sci. Inst., Vol. 42 (71), p. 465.

GraT 73: Tom J. Gray and R. Lear, R.J. Dexter, F.N. Schwettmann and K.C. Wiemer.
Thin Solid Films, Vol. 19 (73), p. 103 - 119.

GreJ 35: J.E. Greaves.
Soil Biology, Vol. 38 (35), p. 355.

HanJ 73: J.S. Hansen, J.C. McGeorge, D. Nix, W.D. Schmidt - OTT, I. Uniss and R.W. Fink.
Nucl. Inst. and Methods, Vol. 106 (73), p. 365 - 379.

HanJ 73: J.S. Hansen.
Phys. Review, Vol. 8, No. 2 (73), p. 822.

HanJ 57: J.S. Hansteen and Messelt.
Nucl. Phy., Vol. 2 (56/57), p. 526 - 532.

HanJ 73: J.M. Hansteen and O.P. Mosebekk.
Nucl. Phys. A., Vol. 201 (73), p. 541.

HasI 77: I. Hasselmann, W. Koenig, F.W. Richter, V. Steiner, V. Watjen, J.C. Bode and W. Chta.
Nucl. Inst. and Methods, Vol. 142 (77), p. 163 - 169.

HatL 75: L.R. Hathaway and G.W. James.
Analy. Chemist, Vol. 47, No. 12 (75), p. 33- 36.

HenW 33: W. Henneberg.
Z. Physik, Vol. 86 (33), p. 592.

HerA 73: A.W. Herman, J.R. Menelles and J.L. Campbell.
Nucl. Inst. and Methods, Vol. 109 (73), p. 429 - 37.

HerH 78: H.K. Herglotz and L.S. Birks.
X-Ray Spectrometry, Vol. 2, p. 69 - 110.

HidK 74: Hideo Kibo.
Nucl. Inst. and Methods, Vol. 121 (74), p. 541 - 545.

HopA : Personal communication, A. Hopkin, P.G. Research Student, Dept. of Physics, The Univ. of Aston in Birmingham.

ICRP 59: ICPR - 2. Report of Committee II on Permissable dose for internal radiation (59), Table 7, p. 147 - 160.

JohT 70: T.B. Johansson, R. Akselsson and S.A.E. Johansson.
Nucl. Inst. and Methods, Vol. 84 (70), p. 141 - 143.

JohT 70: T.B. Johansson, R. Akselsson and S.A.E. Johansson.
Adv. in x-ray Analysis, Vol. 15, p. 373 - 387.

JolR 71: R.K. Jolly and H.B. White Junior.
Nucl. Inst. and Methods, Vol. 97 (71), p. 103 - 105.

JolR 78: R.K. Jolly et al.
Nucl. Inst. and Methods, Vol. 151 (78), p. 183 - 188.

JanJ 65: J.F. Janni.
Technical Report No. AFWL-TR-65-150.
Air Force Weapons Lab., Research and Technical Division, Air Force System Command, Kirtland Air Force Base, New Mexico.

JopR 62: R.C. Jopson, Hans Mark and C.D. Swift.
Physical Review, Vol. 127, No. 5 (62), p. 1612.

KajH 77: H. Kaji, T. Shokawa, K. Ishii, S. Morita, M. Kamiya, K. Sera and H. Twara.
Nucl. Inst. and Methods, Vol. 142 (77), p. 21 - 26.

KanK 69: K. Kandiah and A. Stirling.
Acad. Sci. Publication 15943 (National Academy of Sciences (69), p. 495.

KatA 76: A. Katsonos, Xenoulis, A. Hadjiantoniow and R.W. Fink.
Nucl. Inst. and Methods, Vol. 137 (76), p. 119 - 124.

KeiM 76: M.J. Keir, J.B. Dawson and D.J. Ellis.
Spectrochemia Acta, Vol. 32B (76), p. 59 - 69.

Keithley: Keithley electrometer manual - Radiation Centre, Birmingham.

Kevex 77: Kevex-ray Inst. manual Cryogen. Subsyst. 3000 Series (77).
Analy. Inst. Div., 898 Mahler Road, Burlingham, California 94010, U.S.A.

KhaJ 64: J.M. Khan and D.L. Potter.
Physical Review, Vol. 133, No. 3A (64), p. 890.

KhaM 76: a) M. Rashiduzzaman Khan, D. Crumpton and P.E. Francois.
J. Phys. B. Vol. 9, No. 3 (76), p. 455 - 461.
b) Ph.D. Thesis, Physics Department, The Univ. of Aston in Birmingham.

KhaM 77: M. Rashiduzzaman Khan, A.G. Hopkins, D. Crumpton and P.E. Francois.
X-Ray Spect., Vol. 6, No. 3 (77), p. 140 - 143.

KhaM : M. Rashiduzzaman Khan, A.G. Hopkins, D. Crumpton and P.E. Francois.
8th International Conference on x-ray optics and microanalysis, Boston, U.S.A, 1977.

KliJ 72: J.K. Kliver, J.J. Krausshaar, R.A. Rislinen, H. Rudolph and W.R. Smith.
Bull. Am. Physic. Society, Vol. 17 (72), p. 545.

KobE : E.H. Kobisk.
Conf. : 680411, Unclass. Oak Ridge Association 471P, p. 34 - 40.

LanD 71: D.A. Landis, F.S. Goulding, R.H. Phel and J.T. Walton.
I.E.E.E. transactions, Nucl. Science NS-18, No. 1 (71), p. 115.

LanD 72: D.A. Landis, F.S. Goulding and B.V. Jarret.
Nucl. Inst. and Methods, Vol. 101 (72), p. 127 - 135.

LeaR 73: R. Lear and Tom J. Gray.
Physical Review A, Vol. 8, No. 5 (73), p. 2469 - 2474.

LieR 73: R.B. Liebert, T. Zabel, D. Miljavic, H. Larson, V. Valkovic and C.G. Phillips.
Phys. Rev. A., Vol. 8, No. 5 (73), p. 2336 - 2341.

LinJ 72: Jong Lin, J.L. Duggan, R.G. Carlton.
Proceedings International Conference. Inner shell ionisation phenomena, 1769, 7F Conf. 720404.

LivM 37: M.S. Livingston and H.A. Bethe.
Rev. Mod. Phys. 9, (37), p. 245.

LubM 72: M.F. Lubozynski, R.J. Baglan, G.R. Dyer and A.B. Brill.
Int. Journal of Applied Radiation and Isotopes, Vol. 23 (72), p. 487 - 491.

MadD 74: D.H. Madison, A.B. Baskin, C.E. Busch and S.M. Shafroth.
Physical Review, Vol. A9 (74), p. 675.

ManN 77: N.F. Mangelson, M.W. Hill, K.K. Neilson and J.F. Ryder.
Nucl. Inst. and Methods, Vol. 142 (77), p. 133 - 142.

MarG 71: G.E. Marks and C.E. Moore.
Applied Spectroscopy, Vol. 26, No. 5 (71), p. 523 - 527.

McCJ 73: J.D. McCoy, J.L. Duggan, E.L. Robinson and C.J. Cippola.
I.A.E.A. - Vienna (73), Proceeding of symposium, p. 591 - 610.

MerE 57: E. Merzbacher and H.W. Lewis.
Handbuek der Physics, Vol. 34 (57), p. 166 - 192.

MesS 58: S. Messelt.
Nuclear Phy., Vol. 5 (58), p. 435 - 466.

MugA 72: A.H.F. Muggleton.
Nucl. Inst. and Methods, Vol. 101 (72), p. 113 - 125.

MurL 73: L. Murthy, E.E. Menden, P.M. Eller and H.G. Pestering.
Analy. Biochem., Vol. 53 (73), p. 365 - 372.

MusR 75: R.G. Musket and W. Bauer.
Thin Solid Film, Vol. 19 (75), p. 69 - 80.

MusR 73: R.G. Musket and W. Bauer.
Nucl. Inst. and Methods, Vol. 109 (73), p. 449 - 452.

N.B.S.C.72: N.B.S. Certificate of Analysis - SRM 1577 bovine liver. Washington D.C., 20234, 15th April, 1972.

NieK 76: K.K. Nielson, M.W. Hill, N.F. Mangelson and F.W. Nelson.
Anal. Chem., Vol. 42 (76), p. 1947.

NobA 76: Ann C. Noble, B.H. Orr, W.B. Cook and J.L. Campbell.
Jour. Agricul. Food Chemistry, Vol. 24, No. 3 (76), p. 532 - 535.

NorL 60: L.C. Northcliffe.
Physical Review, Vol. 120 (60), p. 1744.

Nucl : Nuclepore Corporation.

OgiW 64: W.T. Ogier, G.L. Lucas, J.S. Murray and J.E. Holzer.
Physical Review, Vol. 134, No. 4A (64), p. 1070 - 1072.

PalJ 68: J.M. Palms, P.V. Rao and R.E. Wood.
Nucl. Inst. and Methods, Vol. 64 (68), p. 310.

PenD 45: D. Penlman.
Jour. Bacteriology, Vol. 49 (45), p. 167.

PooD 68: D.M. Poole and J.L. Shaw.
Fifth Inter. Congress on x-ray optics and micro-analysis, p. 319 - 324, Springer-Verlag, Berlin.

RinH 77: H.A. van Rinsvelt, R.D. Lear and W.R. Adams.
Nucl. Inst. and Methods, Vol. 142 (77), p. 171 - 180.

RudH 72: H. Rudolph and J.K. Kliver.
I.S.A. AID 72439 (72), p. 151 - 156.

RudM 72: Rudolf O. Muler.
Spectrochemical Analysis by x-ray Fluorescence, (72) p. 112.

RydG 75: G. Ryding.
Patent Specification 13892 (75).

SamA 77: Allan Sampson.
Ph.D. thesis, Dept. of Physics, University of Birmingham, Birmingham.

SanH 71: H. Sanvi.
Anal. Biochemistry, Vol. 42 (71), p. 21 - 28.

SteA 67: A.A. Sterk.
Advances in x-ray analysis, Vol. 8 (67), p. 189 - 197.

SchP 72: P. Schramel.
Determination of light metals in the International Biological Stand by Flameless Atomic Absorption Spectrometry.

ShaL 73: L. Shabason, B.L. Cohen, G.H. Wedbert and K.C. Cohen.
Jour. Applied Physics, Vol. 44, No. 10 (73), p. 4749.

SchH 66: H.A. Schroeder and J.J. Balassa.
Jour. of Chronical Disease, Vol. 19 (66), p. 85 - 106.

SchH 62: H.A. Schroeder, J.J. Balassa and I.H. Tipton.
J. Chronical Disease, Vol. 15 (62), p. 941.

SidG : G. Siddall.
Proceed. Euro. Req. Conf. Electron Microscopy, Vol. 1, p. 584.

SonK 34: K. Sonjo.
Folia Pharmocology, Vol. 34 (34), p. 151.

StrA 69: A. Strasheim, F.T. Wybenga and M.P. Brandt.
Spectrochimica Acta, Vol. 24 B (67), p. 363 - 368.

Stor 70: Storm and Israel.
Nuclear Data Tables, Vol. A7 (70), p. 566.

StrO 75: O.P. Strausz.
Anal. Chemistry, Vol. 47, No. 12 (75).

ThoJ 56: J.P. Thomas, L. Porte, J. Engerran, J.C. Viala and J. Tousset.
Nucl. Inst. and Methods, Vol. 117 (74), p. 579 - 587.

TipI 63: I.H. Tipton and M.J. Cook.
Health Physics, Vol. 9, (63), pp. 85 - 101 and 103 - 145.

UmbC 73: C.J. Umberger, R.C. Bearce, D.A. Close and J.J. Malanify.
Adv. x-ray Analysis, Vol. 16 (73), p. 102 - 110.

UndJ 71: J.E. Underwood.
Trace Elements in Human and Animal Nutrition,
3rd edition, New York.

ValV 73: V. Valkovic.
Contemporary Physics, Vol. 14, No. 5 (73), p. 415 - 438.

VolV 74: V. Valkovic, R.B. Liebert, J. Zabel, H.T. Larson,
D. Miljanic, R.M. Wheelar and G.C. Phillips.
Nucl. Inst. and Methods, Vol. 114 (74), p. 573 - 579.

VisR 77: R.D. Vis, P.M.A., V.D. Kam and H. Verheul.
Nucl. Inst. and Methods, Vol. 142 (77), p. 159 - 162.

WalR 74: R.L. Walter and K.D. Willis, W.F. Gutknect and
J.M. Joyce.
Anal. Chemistry, Vol. 46 (74), p. 843.

WalR 77: R.L. Walter, R.D. Willis, W.F. Gutknect and R.W. Shaw Jnr.
Nucl. Inst. and Methods, Vol. 142 (77), p. 181 - 197.

WatR 71: R.L. Watson, J.R. Sjursth and R.W. Howard.
Nucl. Inst. and Methods, Vol. 93 (71), p. 69.

WatR 74: R.L. Watson, C.J. McNeil and F.E. Jenson.
Adv. x-ray Analysis, Vol. 16 (74), p. 288 - 299.

WeaD 74: D.R. Weaver.
Information for new users of the Dynamitron, Paper No.
B.R.C.-74/01, Birmingham University.

WebJ 73: J. Webb, W. Niedermeir and J.H. Griggs.
Applied Spectroscopy, Vol. 27,No. 5 (73), p. 342.

WilC 57 W. Whaling.
Handbuek der Physik, Vol. 34 (57), p. 13 - 217.

WheR 73: R.M. Wheelar.
Bull. American Physical Society, Vol. 18 (73), p. 634.

WhiH 34: H.E. White.
Introduction to Atomic Spectra, Edit. (34),
Berkley, California, U.S.A.

WilC 67: C.F. Williamson, J.P. Boujot and J. Picard.
Report CEA-R.3042 (67).

WilR 77: R.D. Willis, R.L. Walter, R.W. Shaw Jnr. and W.F. Gutknecht.
Nucl. Inst. and Methods, Vol. 142 (77), p. 67 - 77.

WolR 73: R. Woldseth.
All you ever wanted to know about x-ray energy spectrometry (X.E.S.).
Kevex Corporation, Burlinghame, California, U.S.A.

WooR 71: R.E. Wood, P.V. Rao, O.H. Duckett and J.M. Palms.
Nucl. Inst. and Methods, Vol. 94 (71), p. 245.

APPENDIX

Absorption Correction factors.

```
10   %**/**/**   PROGRAMME OKB02A/108
20   COM X (41),  Y (40), V (40), Z1, D9, M9, Y9, M, N
30   SELECT PRINT 015 (80)
40   IF D9 > 0  THEN 50 : INPUT "DATE", D9, M9, Y9
50   FOR I = 1 TO 5 : PRINT : NEXT I : PRINTUSING 10, D9, M9, Y9
60   GO SUB 580
70   PRINT "CALCULATION OF LINEAR ABSORPTION CO-EFFICIENTS,
     CORRECTION FACTORS" : PRINT "CORRECTED COUNTS"
80   GOSUB 580 : PRINT
90   DIM E(15), F(15), G(15), I(15), J(15), K(15), L(15), M(15),
     N(15), O(15), P(15), Q(15), S(15), T(15), U(15), V(15), Z(15),
     A(15), W(15)
100  INPUT "AIR SPACE" T1
110  INPUT "AIR PRES, TEMP", A1, A2
120  D1 = (0.001293 * (A1))/((1 + 0.00367 * (A2)) * 76)
130  D2 = 1.39 : D3 = 1.847 : D4 = 2.329 : T2 = 0.3 : T3 = 0.00127
     : T4 = .005004
140  PRINT "AIR PRES="; A1, "TEMP="; A2, "AIR SPACE="; T1
150  PRINT "AIR DENSITY="; D1 : GOSUB 570
160  F1 = 0.02144 : F2 = 0.05014 : F3 = 0.03764 : F4 = 0.04300 :
     F5 = 0.01508
170  F6 = 0.06683 : F7 = 0.5975 : F8 = (0.04161)/(4*(T1 + 5.6)↑2)
180  PRINT "GEOMETRY FAC =", F8 : PRINT : FOR R = 1 TO 15 : READ
     E(R) : NEXT R
190  DATA
200  FOR R = 1 TO 15 : READ F(R), G(R), H(R), I(R), J(R), K(R),
     L(R) : NEXT R
210  DATA
220  DATA
```

```
230   DATA
240   DATA
250   FOR R = 1 TO 15
260   M(R) = (D4) * (F1) * F(R)
270   N(R) = (F2) * G(R)
280   O(R) = (F3) * H(R)
290   P(R) = (F4) * I(R)
300   Q(R) = (F5) * J(R)
310   S(R) = (F6) * (D3) * K(R)
320   T(R) = (F7) * L(R)
330   U(R) = (D1) * ((78*P(R)) + (21*O(R)) + (Q(R)))/100
340   V(R) = (D2) * ((60*N(R)) + (34.29 * O(R)) + (5.71 * T(R)))/100
      : NEXT R
350   INPUT "DO YOU WISH TO PRINT ABS CO-EFFS", A$ : IFA$ = "NO"
      THEN 410 : IF A$ = "YES" THEN 350
360   PRINT "ENERGY"; "SILICON"; "BERRYL"; "AIR"; "MELINEX"
370   GOSUB 570 : PRINT : FOR R = 1 TO 15
380   PRINT USING 390, E(R), M(R), S(R), &(R), V(R)
390   %**.**  ******.****  ******.****  ******.****  ******.****
400   NEXT R
410   GOSUB 580 : PRINT
420   PRINT USING 430, "ENER KEV", "COR FOR AIR", "COR FOR BERRY",
      "COR FOR MEL", "EFFICIENCY", "ABSORP", "TOTAL CO-EFF"
430   % ********  ********  ********  ******  ********  *******  ******
440   FOR R = 1 TO 15
450   1F E(R) > 6  THEN 460
460   W(R) = EXP(T1 * U(R))
```

```
470   X(R) = (1-EXP(-T2 * M(R)))
480   Y(R) = EXP(T3 * S(R))
490   Z(R) = EXP(T4 * V(R))
500   A(R) = (W(R) * Y(R) * Z(R))/X(R)
510   GOSUB 570 : PRINT : PRINT USING 520, E(R), W(R), Y(R), Z(R),
      X(R), A(R), A(R)/F8 : W(R) = 1 : X(R) = E(R) : Y(R) = A(R)/F8
520   % **.***  *.***      **.****.***      **.***  ****     *.***
530   NEXT R : GOSUB 580 : PRINT
540   INPUT "DO YOU WISH TO LOAD POLYNOM 1", A$
550   IF A$ = "NO" THEN 50 : IF A$    "YES" THEN 540 : Z1 = 6 :
      INPUT "ORDER OF POLYNON", M : M = 15 : GOSUB 31
560   END
570   FOR J = 1 TO 75 : PRINT "-" : : NEXT J : RETURN
580   FOR J = 1 TO 75 : PRINT "=" : : NEXT J : RETURN
590   DEFFN 0 "NO"
600   DEFFN 1 : INPUT "NO OF B/SPACES", J : BACKSPACE JF : STOP
610   DEFFN 15 "YES"
620   DEFFN 30 "OKGO2"
630   DEFFN 31 : LOAD "POLYNOM 1"
```

Production Cross Section for Kα X-rays.

```
10   %**/**/** PROGRAMME OKB02B/101 CROSEC
20   SELECT PRINT 015
30   IF B9   0 THEN 60
40   INPUT "DATE", D9, M9, Y9
50   GOSUB 250 : PRINT : PRINTUSING 10, D9, M9, Y9 : PRINT
60   PRINT "DATE 23/9/77. CROSEC. KA. IONIS.AND X-RAY CROSS SECS AT
     2.4 MEV
70   GOSUB 250 : PRINT
80   DIM Z(30), W(30), O(30), X(30), R(30), J(30)
90   BO = 1.12 : B1 = 10.397 : B2 = -2.7452 : FOR I = 1 TO 30 :
     READ Z(I) : NEXT I
100  DATA
110  FOR I = 1 TO 30 : READ W(I) : NEXT I : DATA
120  FOR I = 1 TO 30 : READ R(I) : NEXT I : DATA
130  FOR I = 1 TO 30 : O(I) = EXP(BO + (B1 * LOG(Z(I))) +
    (B2 * (LOG (Z(I)))   2))
140  FOR X(I) = O(I) * W(I)
150  J(I) = X(I) * R(I)
160  NEXT I
170  PRINT "DATA USED FROM GARCIA FOR FLUOR YIELD USING EMP. FORMULA"
180  PRINT : GOSUB 250 : PRINT
190  PRINT USING 200, "ATOM NO";  "ION.OR.SEC";  "X-RAY CR.SEC.";
     "W(I);  "R(I)";  KA X-RAY CRS"
200  % *****  *********  **********  ******  ***********
210  GOSUB 250 : PRINT
220  FOR I = 1 TO 30 : PRINT USING 230, Z(I), O(I), X(I), W(I), R(I),
     J(I) : NEXT I
230  % ***  ***.***  *.***  *.***  ***.****
240  STOP
250  FOR J = 1 TO 60 : PRINT "-"; : NEXT J : RETURN
```